



Universidad de Oviedo

**Programa de Doctorado en Biomedicina y Oncología Molecular**

**New mouse models and in vivo interventions in  
progeria and aging**

**Doctoral Thesis**

Pablo Mayoral García

December, 2022



## RESUMEN DEL CONTENIDO DE TESIS DOCTORAL

1.- Título de la Tesis	
Español/Otro Idioma: Nuevos modelos murinos e intervenciones <i>in vivo</i> en progeria y envejecimiento	Inglés: New mouse models and <i>in vivo</i> interventions in progeria and aging
2.- Autor	
Nombre: PABLO MAYORAL GARCÍA	DNI/Pasaporte/NIE:
Programa de Doctorado: BIOMEDICINA Y ONCOLOGÍA MOLECULAR	
Órgano responsable: CENTRO INTERNACIONAL DE POSTGRADO	

### RESUMEN (en español)

El envejecimiento presenta una relevancia creciente como uno de los mayores retos de la investigación biológica. Su íntima relación con el cáncer y su papel en el desarrollo de enfermedades tan importantes como las alteraciones cardiovasculares, los defectos óseos o el síndrome metabólico, hacen de este proceso un factor determinante de la salud humana. En los últimos años, nuestro laboratorio ha abordado la definición de sus claves biológicas a través del estudio de enfermedades raras de envejecimiento acelerado. Estos síndromes poco comunes representan grandes oportunidades para desentrañar los mecanismos del envejecimiento fisiológico y, mediante el establecimiento de nuevos modelos de ratón, para desarrollar intervenciones terapéuticas dirigidas frente a las claves del envejecimiento normal y patológico.

En la presente Tesis Doctoral hemos contribuido al estudio del envejecimiento generando y caracterizando nuevos modelos murinos de envejecimiento prematuro, así como evaluando nuevas intervenciones metabólicas para retrasar su declive funcional. En primer lugar, generamos un nuevo modelo murino de NGPS que porta la mutación p.Ala12Thr en *BAF*, una proteína nuclear esencial implicada en la respuesta al daño del ADN, la segregación cromosómica y el reensamblaje de la envoltura nuclear tras la mitosis. A continuación, caracterizamos sus alteraciones óseas en animales envejecidos y sometidos a diferentes desafíos, como la inducción de osteoporosis por ovariectomía y el daño óseo por estrés oxidativo debido a una sobredosis de hierro. Finalmente, realizamos un análisis de RNAseq que evidenció un patrón de expresión que se asemeja al observado en una patología llamada Osteogénesis Imperfecta. De forma general, estas alteraciones validan el modelo de ratón NGPS como una herramienta útil para el estudio de la progeria y el envejecimiento óseo.

A continuación, exploramos una intervención metabólica para retrasar el declive fisiológico en la progeria, basada en el aumento de  $NAD^+$  con suplementos de NR y niacina en dos modelos murinos diferentes. La suplementación con ambos precursores prolongó la vida y retrasó el envejecimiento en el modelo *Zmpste24<sup>-/-</sup>*, pero no en los ratones *Lmna<sup>G609G/G609G</sup>*. Estos resultados abren la posibilidad de un tratamiento con  $NAD^+$  para algunas patologías relacionadas con el envejecimiento acelerado, aunque también pone de manifiesto la complejidad de la biología y el metabolismo de la progeria.

Finalmente, interesados en la implicación de las mitocondrias en la mayoría de las intervenciones metabólicas, hemos estudiado los efectos de la sobreexpresión de la proteasa mitocondrial LONP1 mediante la generación de un modelo murino transgénico de Lonp1. Estos ratones muestran una mayor mortalidad en un fondo deficiente en *Trp53*, así como algunas alteraciones histológicas y mejoras en la coordinación motora en ratones viejos. Sin embargo, no observamos grandes alteraciones en el metabolismo, la biología mitocondrial ni la longevidad de estos ratones en comparación con los animales control de la misma camada.



En resumen, en la presente Tesis Doctoral hemos desarrollado el modelo murino de NGPS, con implicaciones traslacionales relacionadas con el ensayo *in vivo* de posibles terapias frente a este síndrome y otros relacionados. Asimismo, hemos empleado abordajes de ciencia aplicada para el desarrollo de nuevas intervenciones metabólicas. Finalmente, hemos llevado a cabo trabajos de experimentación en ciencia básica, relacionados con el estudio del papel de LONP1 en la mitocondria y su relación con el envejecimiento.

### RESUMEN (en Inglés)

Aging is increasingly recognized as one of the biggest challenges in biology research. Its intimate relation with cancer and its role in major diseases such as cardiovascular alterations, bone defects or metabolic syndrome, makes of this process a major determinant of human health. Over the last years, our lab has addressed the hallmarks of aging through the study of rare diseases of accelerated aging. These uncommon syndromes represent great opportunities to unravel the mechanistic intricacies of the aging process and, through the generation of new mouse models, to develop molecularly tailored interventions that target physiological and pathological aging.

In the present Doctoral Thesis we have contributed to the study of aging by generating and characterizing new murine models of premature aging, as well as testing new metabolic interventions to delay their functional decline. First, we generated a new murine model of NGPS that carries the p.Ala12Thr mutation in *BAF*, an essential nuclear protein involved in DNA-damage response, chromosome segregation and the nuclear envelope re-assembly after mitosis. Then, we characterized the bone alterations in aged mice and under different challenges, as induction of osteoporosis by ovariectomy and oxidative stress bone damage by iron overdose. Finally, we performed an RNAseq analysis that evidenced an expression pattern reminiscent of a pathology called Osteogenesis Imperfecta. Overall, these alterations validate NGPS mouse model as a useful tool for the study of progeria and bone aging.

Next, we explored a metabolic intervention to delay physiological decline in progeria, based on the increase of NAD<sup>+</sup> with NR and niacin supplementation in two different progeria mouse models. Supplementation with both precursors extended lifespan and delayed aging in the *Zmpste24*<sup>-/-</sup> model, but not in the *Lmna*<sup>G609G/G609G</sup> mice. These results open the possibility of NAD<sup>+</sup> treatment for certain pathologies related to accelerated aging, although it also highlights the complexity of the biology and metabolism of progeria.

Finally, interested in the involvement of mitochondria in most metabolic interventions, we have studied the overexpression of the mitochondrial protease LONP1 through the generation of a transgenic murine model of *Lonp1*. These mice display greater mortality in *Trp53*-null background, together with some histological alterations and motor coordination improvements in old mice. However, we did not observe great alterations in the metabolism, mitochondrial biology nor longevity of these mice compared to control littermates.

In summary, in this PhD Thesis we have generated the murine model of NGPS, which might bear translational implications in the future such as the *in vivo* assay of different therapies for this syndrome and related conditions. Also, we have used applied science for the development of new metabolic interventions. Finally, we have performed basic science research related to the study of LONP1 and its role in mitochondria and its relation to aging.





# TABLE OF CONTENTS

<b>TABLE OF CONTENTS</b> .....	<b>1</b>
<b>ABSTRACT / RESUMEN</b> .....	<b>5</b>
ABSTRACT .....	7
RESUMEN .....	9
<b>ABBREVIATIONS</b> .....	<b>13</b>
<b>INTRODUCTION</b> .....	<b>19</b>
Aging .....	21
Progeria and other premature aging syndromes.....	23
Role of the <i>BANF1</i> p.Ala12Thr mutation in the Nestor-Guillermo progeria syndrome .....	24
Metabolic interventions in <i>Zmpste24</i> <sup>-/-</sup> y <i>Lmna</i> <sup>G609G/G609G</sup> progeroid mouse models .....	27
NAD <sup>+</sup> /NADH energy balance in aging .....	29
Dual role of mitochondrial fitness in aging and cancer.....	31
<b>OBJECTIVES</b> .....	<b>37</b>
<b>EXPERIMENTAL PROCEDURES</b> .....	<b>43</b>
Molecular Biology methods .....	45
Cell Biology methods .....	48
Animal model procedures / methods.....	50
Bioinformatic and Statistical methods .....	57
<b>RESULTS</b> .....	<b>61</b>
1. Development and characterization of genetically modified mouse models to investigate the involvement of nuclear envelope components in age-associated pathologies.....	63
1.1. Generation and characterization of <i>Banf1</i> -deficient and <i>Banf1</i> <sup>A12T</sup> knock-in mice as potential Néstor-Guillermo Progeria Syndrome mouse models.....	64

1.2. Study of BANF1 and LMNA interaction in double mutant <i>Banf1</i> <sup>A12T/A12T</sup> <i>Lmna</i> <sup>G609G/G609G</sup> mice .....	68
1.3. Physiological and transcriptional characterization of bone phenotype in the <i>Banf1</i> <sup>A12T/A12T</sup> NGPS mouse model .....	70
2. Evaluation of dietary interventions to counteract nutrient sensing deregulation associated to pathological aging. ....	76
2.1. Physiological characterization of NAD <sup>+</sup> boost through NR and niacin supplementation in <i>Zmpste24</i> <sup>-/-</sup> and <i>Lmna</i> <sup>G609G/G609G</sup> mice .....	77
2.2. Description of the transcriptomic profile in liver of <i>Zmpste24</i> <sup>-/-</sup> mice after NAD <sup>+</sup> supplementation .....	85
3. Analysis of the anti-aging potential of genetic approaches designed to counteract mitochondrial dysfunction based on overexpression of the LONP1 protease .....	87
3.1. Generation and description of the new transgenic <i>Lonp1</i> mouse model .....	88
3.2. Characterization of mitochondrial and systemic metabolism in <i>Lonp1</i> <sup>TG</sup> mice .....	92
3.3. Longevity and healthspan evaluation in <i>Lonp1</i> <sup>TG</sup> mice .....	96
<b>DISCUSSION</b> .....	<b>103</b>
<b>CONCLUSIONS</b> .....	<b>121</b>
<b>CONCLUSIONES</b> .....	<b>127</b>
<b>REFERENCES</b> .....	<b>133</b>
<b>APPENDIX: PUBLICATIONS</b> .....	<b>159</b>





# **ABSTRACT / RESUMEN**



## ABSTRACT

Aging is increasingly recognized as one of the biggest challenges in biology research. Its intimate relation with cancer and its role in major diseases such as cardiovascular alterations, bone defects or metabolic syndrome, makes of this process a major determinant of human health. Over the last years, our lab has addressed the hallmarks of aging through the study of rare diseases of accelerated aging. These uncommon syndromes represent great opportunities to unravel the mechanistic intricacies of the aging process and, through the generation of new mouse models, to develop molecularly tailored interventions that target physiological and pathological aging.

In the present Doctoral Thesis we have contributed to the study of aging by generating and characterizing new murine models of premature aging, as well as testing new metabolic interventions to delay their functional decline. First, we generated a new murine model of NGPS that carries the p.Ala12Thr mutation in BAF, an essential nuclear protein involved in DNA-damage response, chromosome segregation and the nuclear envelope re-assembly after mitosis. Then, we characterized the bone alterations in aged mice and under different challenges, as induction of osteoporosis by ovariectomy and oxidative stress bone damage by iron overdose. Finally, we performed an RNAseq analysis that evidenced an expression pattern reminiscent of a pathology called Osteogenesis Imperfecta. Overall, these alterations validate NGPS mouse model as a useful tool for the study of progeria and bone aging.

Next, we explored a metabolic intervention to delay physiological decline in progeria, based on the increase of NAD<sup>+</sup> with NR and niacin supplementation in two different progeria mouse models. Supplementation with both precursors extended lifespan and delayed aging in the *Zmpste24*<sup>-/-</sup> model, but not in the *Lmna*<sup>G609G/G609G</sup> mice. These results open the possibility of NAD<sup>+</sup> treatment for certain pathologies related to accelerated aging, although it also highlights the complexity of the biology and metabolism of progeria.

Finally, interested in the involvement of mitochondria in most metabolic interventions, we have studied the overexpression of the mitochondrial protease LONP1 through the generation of a transgenic murine model of *Lonp1*. These mice display greater

mortality in *Trp53*-null background, together with some histological alterations and motor coordination improvements in old mice. However, we did not observe great alterations in the metabolism, mitochondrial biology nor longevity of these mice compared to control littermates.

In summary, in this PhD Thesis we have generated the murine model of NGPS, which might bear translational implications in the future such as the *in vivo* assay of different therapies for this syndrome and related conditions. Also, we have used applied science for the development of new metabolic interventions. Finally, we have performed basic science research related to the study of LONP1 and its role in mitochondria and its relation to aging.

## RESUMEN

El envejecimiento presenta una relevancia creciente como uno de los mayores retos de la investigación biológica. Su íntima relación con el cáncer y su papel en el desarrollo de enfermedades tan importantes como las alteraciones cardiovasculares, los defectos óseos o el síndrome metabólico, hacen de este proceso un factor determinante de la salud humana. En los últimos años, nuestro laboratorio ha abordado la definición de sus claves biológicas a través del estudio de enfermedades raras de envejecimiento acelerado. Estos síndromes poco comunes representan grandes oportunidades para desentrañar los mecanismos del envejecimiento fisiológico y, mediante el establecimiento de nuevos modelos de ratón, para desarrollar intervenciones terapéuticas dirigidas frente a las claves del envejecimiento normal y patológico.

En la presente Tesis Doctoral hemos contribuido al estudio del envejecimiento generando y caracterizando nuevos modelos murinos de envejecimiento prematuro, así como evaluando nuevas intervenciones metabólicas para retrasar su declive funcional. En primer lugar, generamos un nuevo modelo murino de NGPS que porta la mutación p.Ala12Thr en *BAF*, una proteína nuclear esencial implicada en la respuesta al daño del ADN, la segregación cromosómica y el reensamblaje de la envoltura nuclear tras la mitosis. A continuación, caracterizamos sus alteraciones óseas en animales envejecidos y sometidos a diferentes desafíos, como la inducción de osteoporosis por ovariectomía y el daño óseo por estrés oxidativo debido a una sobredosis de hierro. Finalmente, realizamos un análisis de RNAseq que evidenció un patrón de expresión que se asemeja al observado en una patología llamada Osteogénesis Imperfecta. De forma general, estas alteraciones validan el modelo de ratón NGPS como una herramienta útil para el estudio de la progeria y el envejecimiento óseo.

A continuación, exploramos una intervención metabólica para retrasar el declive fisiológico en la progeria, basada en el aumento de NAD<sup>+</sup> con suplementos de NR y niacina en dos modelos murinos diferentes. La suplementación con ambos precursores prolongó la vida y retrasó el envejecimiento en el modelo *Zmpste24*<sup>-/-</sup>, pero no en los ratones *Lmna*<sup>G609G/G609G</sup>. Estos resultados abren la posibilidad de un

tratamiento con NAD<sup>+</sup> para algunas patologías relacionadas con el envejecimiento acelerado, aunque también pone de manifiesto la complejidad de la biología y el metabolismo de la progeria.

Finalmente, interesados en la implicación de las mitocondrias en la mayoría de las intervenciones metabólicas, hemos estudiado los efectos de la sobreexpresión de la proteasa mitocondrial LONP1 mediante la generación de un modelo murino transgénico de Lonp1. Estos ratones muestran una mayor mortalidad en un fondo deficiente en *Trp53*, así como algunas alteraciones histológicas y mejoras en la coordinación motora en ratones viejos. Sin embargo, no observamos grandes alteraciones en el metabolismo, la biología mitocondrial ni la longevidad de estos ratones en comparación con los animales control de la misma camada.

En resumen, en la presente Tesis Doctoral hemos desarrollado el modelo murino de NGPS, con implicaciones traslacionales relacionadas con el ensayo in vivo de posibles terapias frente a este síndrome y otros relacionados. Asimismo, hemos empleado abordajes de ciencia aplicada para el desarrollo de nuevas intervenciones metabólicas. Finalmente, hemos llevado a cabo trabajos de experimentación en ciencia básica, relacionados con el estudio del papel de LONP1 en la mitocondria y su relación con el envejecimiento.





# ABBREVIATIONS

3D	Three-Dimension
A12T	<i>Banf1<sup>A12T/A12T</sup></i>
AAA+	ATPases Associated with diverse cellular Activities
ALAS	5-Aminolevulinic Acid Synthase
ACO	Aconitase
AD	Autosomal Dominant
ADP	Adenosine Diphosphate
AR	Autosomal Recessive
ATP	Adenosine Triphosphate
BAC	Bacterial Artificial Chromosome
BAF	Barrier-to-Autointegration Factor
BANF1	BAF Nuclear Assembly Factor 1
BN-PAGE	Blue Native Polyacrylamide Gel Electrophoresis
BSA	Bovine Serum Albumin
BS/BV	Bone Surface and Bone Volume Relation
BMD	Bone Mineral Density
Bp	Base Pair
BV/TV	Bone and Tissue Volume relation
cDNA	complementary DNA
CI	Confidence Interval
Conn.Dn	Trabecular Connectivity
COX4-1	Cytochrome C Oxidase isoform 4 subunit 1
CSB	CS complementation group B
Ct.BV	Cortical Bone Volume
Ct.TV	Total Volume of Cortical Bone and Bone Marrow
CTRL	Control
CTX-I	Type I Collagen
DKI	Double KI ( <i>Banf1<sup>A12T/A12T</sup> Lmna<sup>G609G/G609G</sup></i> )
DMEM	Dulbecco's Modified Eagles's medium
DNA	Deoxyribonucleic Acid

DNA-PKcs	DNA-dependent Protein Kinase catalytic subunits
DSB	Double Strand Break
EDTA	Ethylenediaminetetraacetic Acid
FCCP	Trifluoromethoxy Carbonylcyanide Phenylhydrazone
FDR	False Discovery Rate
G609G	<i>Lmna</i> <sup>G609G/G609G</sup>
GH	Growth hormone
GO	Gene Ontology
GSEA	Gene-Set Enrichment Analysis
H&E	Hematoxylin and Eosin
Hemi A12T	<i>Banf1</i> <sup>A12T/-</sup>
HFD	High Fat Diet
HGPS	Hutchinson-Gilford Progeria Syndrome
HSD	High Sucrose Diet
Iron-OD	Iron-Overdose
KEGG	Kyoto Encyclopedia of Genes and Genomes
KI	Knock-In
KO	Knock-Out
LEM	LAP2-emerin-MAN1
LMNA	Lamin A
LONP	Lon Protease
LPS	Lipopolysaccharides
mRNA	Messenger Ribonucleic Acid
mtDNA	Mitochondrial DNA
MTT	3-(4,5-Dimethylthiazol-2-Yl)-2,5-Diphenyltetrazolium Bromide
mtUPR	Mitochondrial Unfolded Proteins Response
MUP	Major Urinary Protein
NA	Nicotinic Acid
NAD <sup>+</sup>	Nicotinamide Adenine Dinucleotide
NADH	Reduced Nicotinamide Adenine Dinucleotide
NAM	Nicotinamide
NaOH	Sodium Hydroxide
NE	Nuclear Envelope
NES	Normalized Enrichment Score

NF- $\kappa$ B	Nuclear Factor Kappa-light-chain-enhancer of activated B cells
NGPS	Néstor-Guillermo Progeria Syndrome
NHEJ	Non-Homologous End-Joining
NIA	Niacin
NMN	Nicotinamide Mononucleotide
NR	Nicotinamide Riboside
OCR	Oxygen Consumption Rate
OI	Osteogenesis Imperfecta
OVX	Ovariectomy
OXPHOS	Oxidative Phosphorylation
PCA	Principal Component Analysis
PCR	Polymerase Chain Reaction
PFA	Paraformaldehyde
PINP	Procollagen I N-terminal Propeptide
Po(op)	Open Porosity
Po(tot)	Total Porosity
qPCR	Quantitative Polymerase Chain Reaction
RNA	Ribonucleic Acid
RNAseq	RNA Sequencing
ROS	Reactive Oxygen Species
RT-PCR	Real-time PCR
SD	Standard Deviation
SDS	Sodium Dodecyl Sulphate
Tb.Pf	Trabecular connectivity (inverse)
Tb.N	Trabeculae number
Tb.Sp	Trabecular Distance or Separation
Tb.Th	Trabecular Thickness
TG	Transgenic ( <i>Lonp1<sup>TG</sup></i> )
Tris	Tris(hydroxymethyl)aminomethane
TV	Cortical Bone Volume with Pores
UV	Ultraviolet
VCO <sub>2</sub>	Volume of CO <sub>2</sub>
VO <sub>2</sub>	Volume of O <sub>2</sub>

WAT	White Adipose Tissue
WT	Wild-type
ZMPSTE24	Zinc Metallopeptidase STE24
μCT	Micro-Computed Tomography





# **INTRODUCTION**



Since its origin, the cultural evolution of *Homo sapiens* has been driven mainly by curiosity. Around the primordial campfire under a starry sky, human beings began to question the world around them. Over time, they focused their gaze on themselves and their fellows, and began to ask the questions that have accompanied us the rest of the way: where we come from, where we are going to and what is our purpose in life. This insatiable curiosity and desire to know how life works has fueled the study of biology. With the development of appropriate technologies, from the first microscopes in the 17th century <sup>1</sup> to modern genome sequencing techniques <sup>2</sup>, we have delved deeper and deeper into the most elemental mechanisms underlying life-associated processes.

## Aging

Most of the intrinsic processes of life are related to the maintenance of cellular structures, allowing the optimal physiology in the body systems that we know as health. When these cellular structures begin to fail, the delicate physiological balance is lost and living beings develop diseases that compromise health <sup>3</sup>. Fortunately, living beings have efficient surveillance systems that detect these common failures in the cellular machinery. Then, they activate repair systems that generally prevent the propagation of these failures from the cellular level to higher levels of organization such as tissues, organs, systems or organisms. As molecular activity in our cells is incessant, failures in the cellular machinery occur continuously and repair systems work so efficiently that they repair the vast majority of them, not without a great energy cost. However, errors eventually begin to accumulate and biological efficiency begins to decline, leading to energetic and physiological adaptations, the onset of disease and finally the death of the individual <sup>4</sup>.

This process of slow accumulation of errors and adaptations, known as aging, is shared by most living beings, although the speed at which it takes place varies greatly among species <sup>5,6</sup> and even sexes <sup>7,8</sup>. Mainly, longevity is influenced by genetic and environmental factors. Genetic factors include a specie's gene pool, the particular variants of each individual or the changes and mutations produced during life <sup>9,10</sup>. Environmental factors include variables such as diet <sup>11,12</sup>, sleep <sup>13,14</sup>, physical activity <sup>15,16</sup> or lifestyle <sup>17-20</sup>. Both types of variables condition the aging process, affecting the molecular and cellular level in very diverse ways, resulting in a multifactorial,

interconnected and tremendously complex process that must be approached holistically<sup>21</sup>. In 2013, the so-called hallmarks of aging were introduced, which defined 9 common denominators of aging. By definition, all these hallmarks had to meet 3 fundamental requirements: they must appear during normal aging, their intensification leads to accelerated aging, and their decrease delays aging, resulting in greater or healthier longevity. Using these criteria, the nine proposed keys to aging were: genomic instability, telomere attrition, epigenetic alterations, loss of proteostasis, deregulated nutrient sensing, mitochondrial dysfunction, cellular senescence, stem cell exhaustion and altered intercellular communication.

In turn, these hallmarks of aging can be divided into 3 subgroups according to the way in which they affect the process. Primary hallmarks are those that cause direct damage and are unequivocally negative. They are genomic instability, telomere attrition, epigenetic alterations and loss of proteostasis. In response to this primary damage, a variety of defense responses are elicited that have an initial positive effect. However, when these defensive responses become chronic or are exacerbated, they become deleterious to the organism. This subgroup includes mitochondrial dysfunction, cellular senescence and deregulated nutrient sensing. Finally, stem cell exhaustion and altered intercellular communication constitute the so-called integrative hallmarks. These are the result of the interaction of primary and antagonistic hallmarks and are responsible for the physiological decline associated with aging<sup>22</sup> (Figure 1).

In mammals, old age typically promotes the development of some diseases such as cardiovascular alterations<sup>23</sup>, diabetes<sup>24</sup>, Alzheimer's disease<sup>25</sup>, neurodegeneration<sup>26</sup> or cancer<sup>27</sup>. The study of aging-associated diseases is a field with enormous social and economic relevance since, in a world with increasingly aged societies, these diseases have a growing incidence<sup>28,29</sup>. The research on these diseases is carried out using animal and cellular models that are essential for the development of specific therapies for each disease. However, the management of the aging process as a catalyst of these diseases is much more effective in prevention than the individualized treatment of each disease<sup>30,31</sup>.

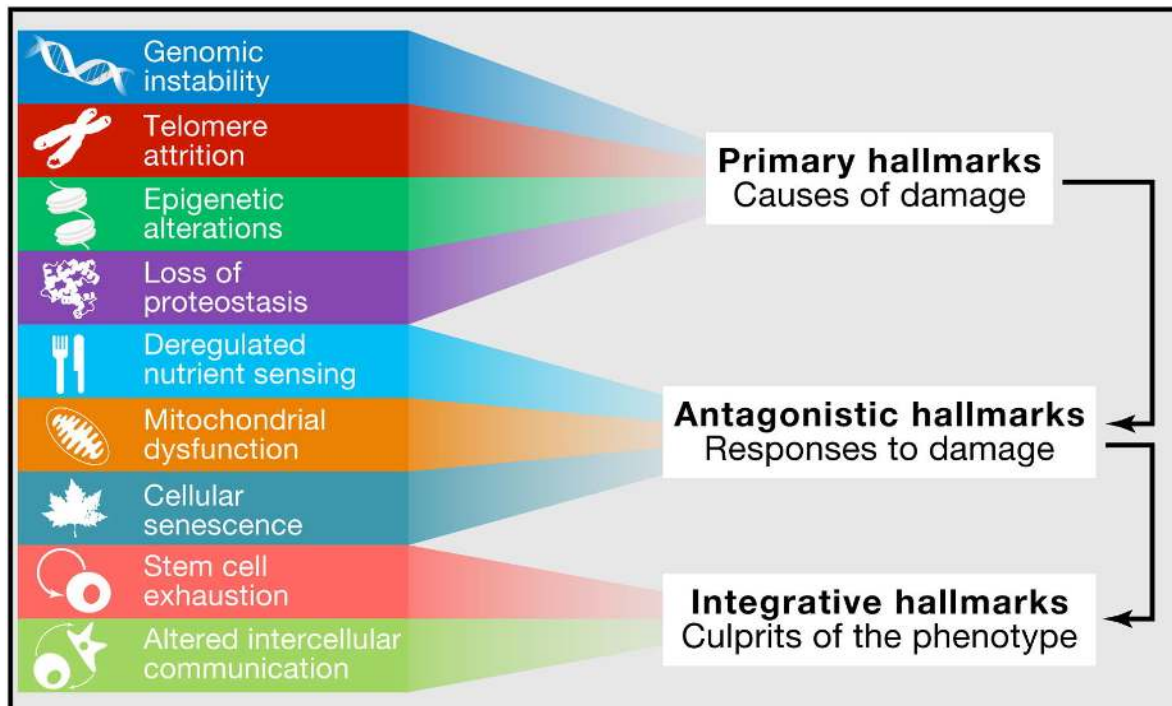


**Figure 1. Hallmarks of aging.** The nine hallmarks of aging categorized by their functional interconnections into primary, antagonistic or integrative hallmarks. Taken from López-Otín *et al.*, 2013.

## Progeria and other premature aging syndromes

Segmental progeroid syndromes constitute a group of human diseases characterized by premature aging, being rare or extremely rare pathologies with very low frequency. Some, such as Werner syndrome, can affect approximately 1 in 100,000 people, while others, such as Cockayne syndrome or Hutchinson-Gilford Progeria syndrome (HGPS), affect 1 in 2 and 4 million people, respectively<sup>32,33</sup>. As a result, it is challenging to correctly diagnose these diseases, especially in low-resource populations. Patients often have a long way to go before they can really know what their condition is and in many cases the diagnosis is their final step since the study of some rare diseases is very marginal<sup>34,35</sup>. Although these rare diseases have a very low incidence in the population, by compiling many of the characteristics of physiological aging they provide a unique opportunity to study not only pathological premature aging but also the physiological process<sup>36</sup>. Depending on the molecular cause, these syndromes can be classified into two groups<sup>37,38</sup>. The first of these includes those progeroid syndromes caused by defects in DNA repair genes such as Werner syndrome<sup>39</sup>, Bloom syndrome<sup>40</sup>, or Cockayne syndrome<sup>41</sup>. Due to alterations in genome repair genes, mutations accumulate at a much higher rate than normal,

and therefore these syndromes are characterized by the onset of aging in adult individuals at earlier ages and an increased incidence of cancers<sup>42</sup>. The second subgroup is formed by those syndromes caused by defects in components of the nuclear envelope. Among these, laminopathies constitute a group of diseases that are specifically characterized by mutations in genes encoding either components of the nuclear lamina or proteins involved in their processing, resulting in the accumulation of deleterious proteins that alter the nuclear structure. Examples of laminopathies include HGPS, Nestor-Guillermo progeria syndrome (NGPS) or Restrictive Dermopathy<sup>43,44</sup>.

HGPS, or simply progeria, is an ultra-rare human disorder with an incidence of approximately 1 in 4 million people. Children born with HGPS suffer an accelerated aging that causes a dramatic reduction in healthspan and lifespan, with a life expectancy of approximately 14 years. This disease recapitulates several aspects of physiological aging such as weight loss, alopecia, bone fragility and heart disease, which is the most common cause of death in these patients. HGPS is caused by the c.1824C>T dominant mutation in *LMNA* gene, which encodes the A-type lamins of the nuclear envelope. This point mutation interferes in the normal processing of lamin A and generates a toxic farnesylated protein called progerin<sup>45</sup>. This protein acts in a similar way as other aberrant prelamin A isoforms, accumulating in the nuclear lamina and disturbing the nuclear architecture and causing premature aging<sup>46–49</sup>. Importantly, progerin is also produced in small quantities during physiological aging, highlighting the potential benefits of progeria research for regular aging<sup>50</sup>.

### **Role of the *BANF1* p.Ala12Thr mutation in the Nestor-Guillermo progeria syndrome**

Nestor and Guillermo were two patients with clinical symptomatology compatible with an accelerated aging syndrome. Both presented a prematurely aged appearance similar to that of progeria with growth retardation, loss of subcutaneous fat, thin limbs and stiff joints. However, these patients had a remarkable longevity compared to the HGPS patients as they were 31 and 24 years old respectively at the time of the start of their study. Moreover, none of them showed signs of diabetes, hypertriglyceridemia or cardiovascular defects, which is particularly interesting as the latter are responsible for most of the mortality in HGPS. There was also a major bone

involvement, even greater than that observed in HGPS, which seemed to seriously compromise their quality of life and life expectancy<sup>51</sup> (Table 1). An exome analysis was performed in our laboratory and it was found that they did not present any mutation in *LMNA* or *ZMPSTE24*, denominating this new pathology as NGPS. After analyzing and filtering the possible variants causing their pathology, it was concluded that the genetic cause was the c.34G>A (p.Ala12Thr) mutation in homozygosis in the *BANF1* gene<sup>52</sup>. Supporting this, a young patient of Mexican origin has also been molecularly diagnosed with NGPS recently, carrying the same c.34G>A (p.Ala12Thr) mutation<sup>53</sup>.

**Table 1. Comparative analysis of molecular and clinical findings in NGPS patients and HGPS.** Adapted from Cabanillas *et al.*, 2011

Clinical findings	Patient 1 <sup>a</sup>	Patient 2 <sup>a</sup>	HGPS
Gene mutation	<i>BANF1</i>	<i>BANF1</i>	<i>LMNA</i>
Inheritance	AR	AR	AD
Prematurely aged appearance	+	+	+
Growth retardation	+	+	++
Delayed closure of anterior fontanel	+	+	+
Sparse scalp hair	+	+	-
Sparse eyebrows/lashes	+	+	-
Prominent eyes	+	+	+
Thin nose	+	+	+
Underdeveloped midface	++	++	+
Small chin	+	+	+
Premature loss of teeth	-	-	-
Decreased subcutaneous fat	++	++	+++
Patchy hyperpigmentation	+	+	+
Hypoplastic or absent clavicles	++	++	+
Thorax deformity	+++	++	+
Thin limbs	+	+	+
Stiff joints	+	+	+
Joint contractures	+	+	+
Acro-osteolysis	++	++	+
Osteoporosis	++	++	+
Hypertension	-	-	+
Premature arteriosclerosis	-	-	+
Metabolic complications	-	-	+
Hypogonadism	-	-	-

*BANF1* encodes a small protein of 89 amino acids called barrier-to-autointegration factor 1, or simply BAF, mainly located in the nucleus with a small cytoplasm fraction, whose functions are barely known<sup>52</sup> (Table 2). Its multiple cellular interactors include non-specific DNA, LEM-domain proteins, lamin A/C, histones and chromatin regulators and human transcription factors<sup>54</sup>. During interphase, BAF binds

to lamin A/C and other LEM-domain proteins having an important role in the nuclear envelope structure<sup>55</sup>. p.Ala12Thr mutation in BAF does not alter its dimerization or its binding to emerin, but reduces its affinity to DNA and lamin A/C generating nuclear abnormalities<sup>52,56,57</sup>. Contrary, in other progeroid syndromes as HGPS, where lamin A, progerin or farnesylated and unfarnesylated prelamin A accumulate in the nucleus, wild-type BAF is translocated to the nucleus due its great affinity to lamin forms<sup>58</sup>. Beyond its function in the nuclear envelope architecture, BAF seem to have roles in DNA double-strand breaks (DSB) repair pathways. In case of DNA DSB, a subpopulation of non-phosphorylated cytoplasmic BAF migrates to these ruptures at the nucleus, acting as a marker to the recruitment of LEM-domain proteins, lamin C, cGAS and other machinery repair systems<sup>59-61</sup>. Further, BAF regulates DNA DSB repair through the inhibition of PARP1 and DNA-PKcs<sup>62,63</sup>. In this sense, p.Ala12Thr mutation in BAF promotes its binding to PARP1, inhibiting its activity similar as in BAF overexpression and inducing a deficient oxidative lesions repair<sup>62</sup>. In contrast, the lack of wild-type BAF induces a faster repair and an increase in non-homologous end-joining (NHEJ) cascade while homologous recombination is decreased<sup>63</sup>. Also, BAF has an essential role in chromosome segregation and nuclear envelope assembly during mitosis. In S phase, BAF increases at nucleus being fundamental for lamin A migration to the nuclear envelope<sup>64</sup>. When mitosis begins, BAF is phosphorylated by VRK1 and loses its affinity to DNA, but not lamin A/C or emerin, being released from the chromatin and facilitating the rupture of nuclear envelope<sup>65-67</sup>. At the end of mitosis, during ana-telophase, PP2A dephosphorylates BAF, binding to chromatin and restoring the nuclear assembly<sup>67</sup>. In parallel, BAF binds to the core of chromosomes in the centromere region and recruits nuclear envelope proteins, as lamin A/C or emerin, and distant DNA regions, guiding membranes to reassemble the nucleus<sup>57,67,68</sup>. The p.Ala12Thr mutation in BAF, does not alter VRK1 3D conformation or phosphorylation status, but inhibits its union to lamin A/C and centromeres, producing mislocalization of emerin an lamins at the end of mitosis<sup>69</sup>. Further, although it does not inhibit nuclear envelope reparation, produces weak nuclear envelope structures that facilitates re-ruptures<sup>69</sup>. Despite these studies, the molecular basis of the progeroid phenotype observed in humans remains poorly understood. The lack of a mouse model of NGPS hampers the study of BAF function and the relationship of the p.Ala12Thr mutation with aging, as well as the comparative study with other progeroid syndromes.

**Table 2.** Description of BAF functions and the consequences of p.Ala12Thr mutation in BAF on the maintenance and repair of NE ruptures during interphase, DNA DSB repair and mitosis.

	<b>BAF</b>	<b>p.Ala12Thr BAF</b>
NE during interphase	Binding to LEM-domain proteins, DNA and lamin A/C	Loss affinity to DNA and lamin A/C
NE ruptures	Binding to DNA, acting as a marker for repair machinery recruitment	Loss affinity to lamin A/C, contributing to NE fragility
DNA DSB	Migration from NE to chromatin. Inhibition of PARP1/DNA-PKcs	Excessive inhibition of PARP1 and DNA-PKcs
Start of mitosis	Phosphorylation by VRK1, loss of affinity to DNA and mediation of NE rupture	Inhibition of lamin A/C binding
End of mitosis	Centromeres binding and NE proteins recruitment to nucleus re-assembly	Inhibition of centromeres binding and NE proteins mislocalization

## Metabolic interventions in *Zmpste24*<sup>-/-</sup> y *Lmna*<sup>G609G/G609G</sup> progeroid mouse models

Metabolism has an intimate role in aging and, in mammals, body size is linearly correlated with longevity, the species with higher metabolic rates usually having a shorter lifespan<sup>70,71</sup>. Beside this genetically programmed lifespan, aging is related with a metabolome shift and several metabolic changes such as insulin resistance and dyslipidemia that increase morbidity<sup>72,73</sup>. As discussed above, progeroid syndromes, and especially progeria, are pathologies that phenocopy most of the usual alterations in physiological aging<sup>36</sup>. In this sense, several animal models have been generated for its study, being *Zmpste24*<sup>-/-</sup> and *Lmna*<sup>G609G/G609G</sup> among the most validated and well-studied models<sup>74,75</sup>.

*Zmpste24*<sup>-/-</sup> mice are indistinguishable from their wild-type (WT) littermates until two months of age, when the knock-out (KO) animal begins to develop a premature aging phenotype. At that age, KO mice start to develop an up to 40% lower growth rate compared to WT animals, together with other metabolic alterations including decreased levels of glucose, triglycerides, aspartate aminotransferase, creatine kinase and glutamate dehydrogenases<sup>74</sup>. Also, *Zmpste24*<sup>-/-</sup> mice exhibit chronic

cardiac dysfunction and suffer a progressive aggravation of the accelerated aging phenotype with alopecia, lipodystrophy and lower weight, temperature and mobility than their WT littermates<sup>74</sup>. As in the case of human patients, they also present a clear bone affectation that, in addition to scoliosis, weakens their teeth and prevents them from gnawing normally. Consequently, the mice must be fed with powdered diets or softened pellets to prevent premature mortality caused by starvation. Finally, the life expectancy of KO mice varies between 6 and 10 months depending on the type of diet chosen<sup>76</sup>.

*Lmna*<sup>G609G/G609G</sup> mice, although infertile, develop normally during their first 3 months of life with slightly lower weight. As was the case in the *Zmpste24*<sup>-/-</sup> model, from that age onwards the mice develop an accelerated aging phenotype characterized by lower weight and size, cardiovascular alterations and impaired metabolism. Bone affectation is also manifested in scoliosis and dental weakness, which also forces us to maintain a powdered or softened diet to facilitate feeding and correctly evaluate their mortality, that places their life expectancy between 5 and 6 months of life<sup>75</sup>.

Despite their segmental progeroid molecular characteristics and the absence of some key aspects in physiological aging as neurodegeneration or dementia, *Zmpste24*<sup>-/-</sup> y *Lmna*<sup>G609G/G609G</sup> animal models represent unique tools to study the complexity of aging<sup>50,77</sup>. In this sense, many systemic interventions have been tested in *Zmpste24*<sup>-/-</sup> y *Lmna*<sup>G609G/G609G</sup> mice over the last years. Due to the nuclear aberrations and genomic instability, these mice exhibit a strong activation of NF-κB pathway that leads to chronic inflammation<sup>78</sup>, representing an extreme version of the chronic inflammation state observed in normal aging, also known as *inflammaging*<sup>79</sup>. Administration of anti-inflammatory drugs such as sodium salicylate mitigates this exacerbated activation in progeroid mice, leading to an improved appearance, partial recovery of weight and bone structure as well as increased lifespan<sup>78</sup>. Also, trophic pathways have been pointed out as central modulators of aging and mTOR inhibition has been widely tested for lifespan extension<sup>80</sup>. The easiness of direct approaches through diet interventions has boosted the development of many different strategies. Caloric restriction has been established as the most robust anti-aging strategy in mammals by lowering the insulin-like growth factor 1 (IGF-1) levels in serum<sup>81</sup>. Further, specific dietary restrictions, such as reduced protein or carbohydrate intake,

have also been tested in normal aging with the same aim <sup>82,83</sup>. Contrary, these progeroid mice display a dysregulation in the somatotrophic signaling with high growth hormone (GH) and decreased IGF-1 levels in serum. A recombinant IGF-1 treatment restores the somatotrophic signaling and GH/IGF-1 ratio, improving healthspan and extending lifespan <sup>84</sup>. On the other hand, a methionine restricted diet was positively tested in progeroid mice, with health benefits independent of IGF-1, as it was in fact decreased. Methionine restriction improved the lipid profile and changes bile acid levels and conjugation, also in WT mice. In addition, the transcriptome alterations in inflammation and DNA-damage response present in *Zmpste24*<sup>-/-</sup> y *Lmna*<sup>G609G/G609G</sup> mice were shown to be reversed upon methionine restriction, improving healthspan and extending lifespan <sup>76</sup>.

## NAD<sup>+</sup>/NADH energy balance in aging

Nicotinamide adenine dinucleotide (NAD<sup>+</sup>) metabolism has been closely related to the metabolic shift observed in aging due to its role in mitochondrial function and as energy-state marker among other reasons <sup>85,86</sup>. NAD<sup>+</sup> is an essential cofactor for NAD<sup>+</sup>-consuming proteins including sirtuins, CD38 and poly-ADP-ribose polymerases (PARPs), which regulate cell responses in high or low energy conditions <sup>87</sup>. A low NAD<sup>+</sup>/NADH ratio, which indicates a high-energy state, has been correlated with aging and the appearance of aging-related diseases <sup>88</sup>. On the other hand, high levels of NAD<sup>+</sup> induced by diet or exercise imply a low-energy state and trigger the activation of sirtuins and other pro-survival pathways that enhance lifespan and health <sup>89</sup>. Hence, NAD<sup>+</sup> metabolism has arisen as a promising therapeutic target to delay aging onset.

NAD<sup>+</sup> levels can be increased either by inhibiting NAD<sup>+</sup>-consuming proteins, activating NAD<sup>+</sup> biosynthetic enzymes or directly through diet supplementation with NAD<sup>+</sup> precursors <sup>90,91</sup> (Figure 2). PARP inhibitors increment NAD<sup>+</sup> levels and SIRT1 activity, and lead to metabolic improvement as seen in PARP knockout mice <sup>92</sup>. Similar results could be observed in CD38 knockout mice, displaying a protection against high-fat diet-induced obesity through the SIRT3-PGC1 $\alpha$  axis <sup>93,94</sup>. However, inhibiting sirtuins to raise NAD<sup>+</sup> levels is a problematic approach due to their roles as mediators of health improvement in calorie restriction and exercise, and most studies suggest the activation of specific sirtuins as a potential anti-aging therapy <sup>95–99</sup>. Overexpressing or maintaining the activity NAD<sup>+</sup> biosynthetic enzymes as NMAT3 through age could

also delay aging <sup>100–102</sup>. In any case, attempting to raise NAD<sup>+</sup> levels without a balanced physiological function of these NAD<sup>+</sup> consuming or producing proteins would imply serious risks, as undesired side-effects could overtake any potential metabolic benefits <sup>103,104</sup>. Recent studies have proven the beneficial effects of NAD<sup>+</sup> supplementation *in vivo* to treat several aging-related alterations in mice. NAD<sup>+</sup> precursors such as nicotinamide riboside (NR), nicotinamide (NAM), nicotinamide mononucleotide (NMN) and nicotinic acid or niacin (NA) have been used for the amelioration of diverse age-associated alterations as cardiovascular disease <sup>105–108</sup>, Alzheimer <sup>109,110</sup> or metabolic syndrome <sup>111–113</sup>. Further, diet supplementation with NAD<sup>+</sup> precursors appear to be safe and efficient both in mice and humans <sup>114–117</sup>.

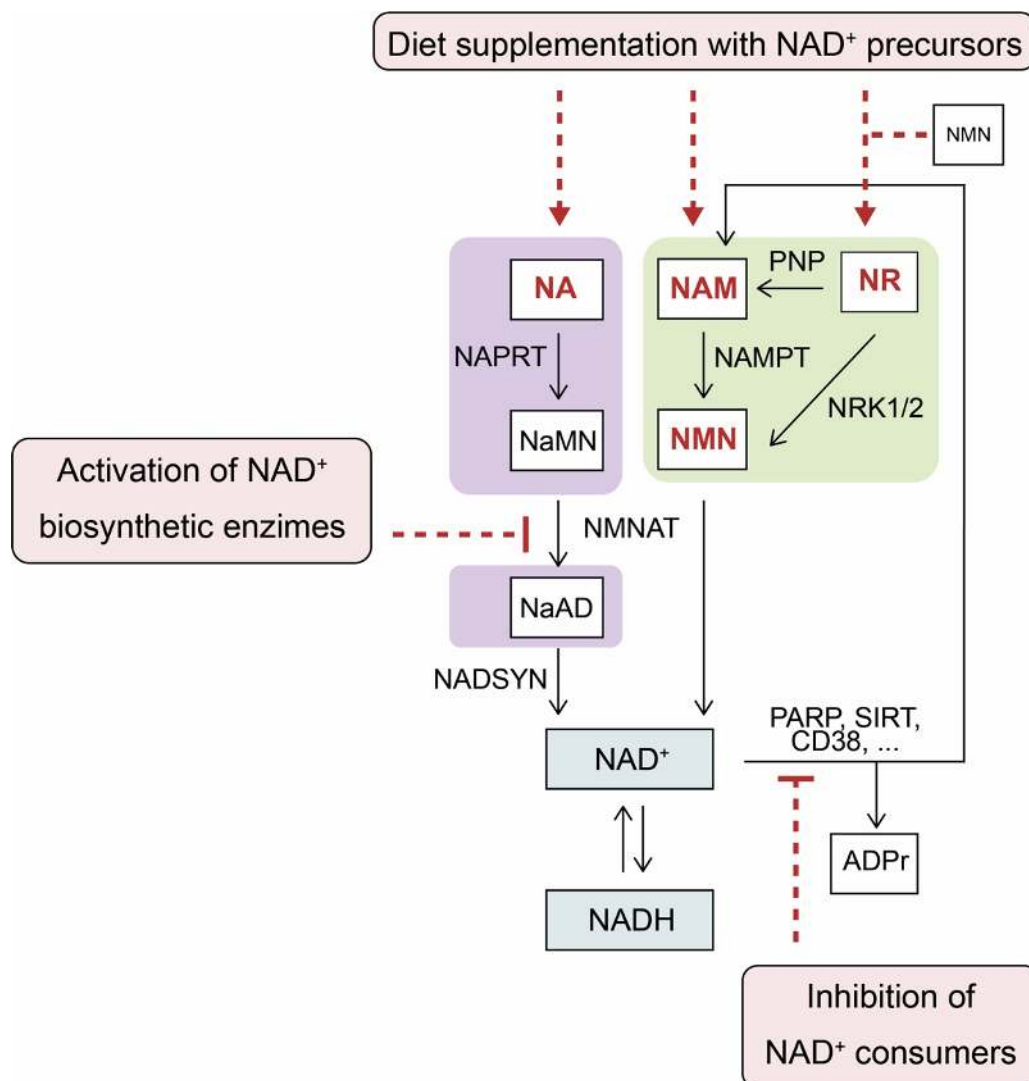


**Figure 2.** Review of NAD-boost strategies including activation of NAD<sup>+</sup> biosynthetic enzymes, inhibition of NAD<sup>+</sup>-consuming proteins and diet supplementation with NAD<sup>+</sup> precursors as NR, NAM, NMN or NA.

In this sense, premature aging syndromes usually present an aging-like metabolic shift with low NAD<sup>+</sup> levels and marked catabolism due to the overactivation of DNA-damage responses. In Werner syndrome, NR treatment has been reported to reestablish NAD<sup>+</sup> levels, restoring impaired mitophagy and fat metabolism and extending lifespan in a Werner syndrome worm model <sup>10</sup>. Likewise, NR supplementation in the Cockayne syndrome mouse model *Csb<sup>m/m</sup>* normalizes NAD<sup>+</sup> levels to wild-type and corrects the alterations in mitochondrial pathways <sup>119</sup>. Accordingly, increasing NAD<sup>+</sup> in *Zmpste24<sup>-/-</sup>* y *Lmna<sup>G609G/G609G</sup>* progeroid mice could represent a suitable strategy to delay premature aging onset.

## Dual role of mitochondrial fitness in aging and cancer

As seen, some interventions such as methionine restriction or NAD<sup>+</sup> boosting act at the systemic level to counteract the metabolic changes of aging. However, these systemic improvements depend on mitochondrial adaptations as responsible for the energy machinery and therefore the development of specific interventions on mitochondria that optimize their functionality could be beneficial even in normal aging <sup>120–123</sup>. Mitochondria may negatively influence aging mainly through ROS production or a dysfunctionality caused by mutations, altered proteostasis, mitophagy defects, impairments in energy homeostasis or mito-nuclear communication <sup>22,124</sup>. In this sense, mutations in the mtDNA polymerase POLG lead to the accumulation of mtDNA mutations, increased ROS, reduced mitophagy and accelerated aging <sup>125,126</sup>. Interestingly, the phenotype of POLG mutator mice could be partially rescued by metformin treatment or restoring NAD<sup>+</sup>/NADH balance with NR supplementation <sup>127,128</sup>. Likewise, disruption of mito-nuclear communication can activate defensive systems such as the mitochondrial response to unfolded proteins (mtUPR) <sup>129,130</sup>. Incorrect recycling of mitochondria through mitophagy can also cause the accumulation of errors in mitochondria that decrease their energy efficiency <sup>131–133</sup>, triggering aging-associated diseases such as cardiovascular alterations <sup>134</sup>, sarcopenia <sup>135</sup> or Alzheimer <sup>136</sup>. These alterations at the organelle and cellular level can be translated into systemic changes through molecular messengers such as mitokines. Different studies have shown how mitochondrial alterations in a single tissue can produce an increase in the mitokines FGF21 or GDF15, suppressing insulin

sensitivity and highlighting how specific tissue stresses can have a metabolic effect on the whole organism <sup>137–141</sup>.

To delay the mitochondrial function decline seen in aging is crucial the maintenance of proteostasis in mitochondria, which is sustained by the correct functioning of quality control systems for proteins <sup>124,142</sup>. This responsibility is assumed by mitoproteases and chaperones, and alterations in any of these systems could unbalance mitochondrial homeostasis, as it occurs in aging, where the levels and activity of some mitoproteases such as LONP1 are reduced <sup>143–145</sup>. Lon protease (LONP1) has an essential role in key processes of mitochondrial homeostasis and protein quality control <sup>132</sup>. This protein is located in the mitochondrial matrix and in the nucleus as recently described <sup>147</sup>, especially in response to heat shock. Catalytically classified as a serine protease, it belongs to the group of ATP-dependent peptidases (AAA+ protease) and is conserved from bacteria to eukaryotic cells <sup>148</sup>. The functions of LONP1 are varied and include the maintenance of proteostasis by degrading misfolded and damaged proteins, as well as the maintenance of mitochondrial functionality and cell viability under conditions of hypoxic, oxidative or endoplasmic reticulum stress <sup>149–152</sup>. In agreement with this diversity of functions, several substrates have been proposed in mammals, including a cytochrome C oxidase isoform (COX4-1) <sup>153</sup>, heat shock factor 1 (HSF1) <sup>147</sup>, aconitase (ACO) <sup>154,155</sup>, 5-aminolevulinic acid synthase (ALAS) <sup>156</sup> and steroidogenic acute regulatory protein (StAR) <sup>157,158</sup>. Interestingly, LONP1 also plays a role in the regulation of gene expression due to its binding to DNA <sup>159</sup>, and in the control of replication and transcription <sup>160</sup>. By binding to mitochondrial transcription factor A (TFAM), it causes its degradation, regulating mtDNA copy number and maintaining control over the TFAM/mtDNA ratio <sup>161,162</sup>. Taking into account its role in proteostasis, it is not surprising that changes in its expression can affect tumor development, which is highly dependent on the correct maintenance of homeostasis due to the high proliferative capacity of cancer cells <sup>150,163</sup>. Although the total absence of LONP1 is lethal in embryonic mice, mice with a heterozygous deletion are viable and show lower incidences of cancer and metastasis after chemical induction of skin and colon tumors, probably due to the reduced cell proliferation and altered tumor bioenergetics <sup>164</sup>. This metabolic adaptation occurs through remodeling of OXPHOS subunits, altering subunit abundance and organization, and resulting in decreased ATP levels and cellular oxygen consumption among other changes <sup>164</sup>. In contrast, increased LONP1 expression in humans

appears to increase the incidence and mortality of certain types of human cancers such as melanoma or colon cancer<sup>164</sup>. These results are consistent with the increased tumor volume and metastasis observed in animal experiments with tumor xenografts. Contrary to these observations in which decreased or increased LONP1 expression seems to have antagonistic results at the cellular level and *in vivo*, the mitochondrial adaptations in both cases seem to have similarities. As in the case of LONP1 knockdown, overexpression of LONP1 in cells appears to reduce oxygen consumption and increase glucose and lactate consumption and production levels. At the level of OXPHOS complexes, down-regulation of *Lonp1* reduces functional OXPHOS complexes by degradation, loss, and destabilization, while overexpression of this gene also results in the decrease of OXPHOS complexes by direct regulation instead<sup>165</sup>.

In summary, in this section we have tried to outline the relationship between aging and accelerated aging syndromes, and to discuss the development of animal models and metabolic interventions against normal and pathological aging based on systemic or mito-specific strategies. In this sense, during the present PhD Thesis we have characterized a new murine model of NGPS syndrome and studied the relationship of the p.Ala12Thr mutation in *BANF1* with the phenotype of patients under several bone stressing challenges. Using the most validated murine models of progeria *Zmpste24*<sup>-/-</sup> and *Lmna*<sup>G609G/G609G</sup>, we have studied the possibilities of dietary NAD<sup>+</sup> supplementation as a systemic metabolic intervention to delay premature aging. Finally, at the mitochondrial level, we have characterized a new transgenic murine model of *Lonp1* to evaluate the consequences of its overexpression in the bioenergetic framework and whether it could be used as a target for new interventions for healthy aging.







# **OBJECTIVES**



Aging is increasingly recognized as one of the biggest challenges in biology research. Its intimate relation with cancer and its role in major diseases such as cardiovascular alterations, bone defects or metabolic syndrome, makes of aging a major determinant of human health. Therefore, the demographic and economic consequences of our elderly modern societies highlight the importance of its research. Also, it is a heterogeneous and multifaceted problem whose study requires a holistic approach. In this regard, the characterization of aging development in nine different hallmarks has simplified its understanding. Over the last years, our research group has addressed these hallmarks through the study of rare diseases of accelerated aging. These uncommon syndromes represent great opportunities to establish new mouse models of accelerated aging, unravel the mechanistic intricacies of the process, and develop molecularly tailored interventions that target the physiological and pathological functional decline.

In this line, in the present Doctoral Thesis we have explored the hallmarks of aging by generating and characterizing the novel mouse models of NGPS and LONP1 overexpression, and by developing new metabolic interventions to delay premature aging. The specific objectives were:

1. Development and characterization of genetically modified mouse models to investigate the involvement of nuclear envelope components in age-associated pathologies
  - 1.1. Generation and characterization of *Banf1*-deficient and *Banf1*<sup>A12T</sup> knock-in mice as potential Néstor-Guillermo Progeria Syndrome mouse models
  - 1.2. Study of BANF1 and LMNA interaction in double mutant *Banf1*<sup>A12T/A12T</sup> *Lmna*<sup>G609G/G609G</sup> mice
  - 1.3. Physiological and transcriptional characterization of bone phenotype in the *Banf1*<sup>A12T/A12T</sup> NGPS mouse model
2. Evaluation of dietary interventions to counteract nutrient sensing deregulation associated to pathological aging.
  - 2.1. Physiological characterization of NAD<sup>+</sup> boost through NR and niacin supplementation in *Zmpste24*<sup>-/-</sup> and *Lmna*<sup>G609G/G609G</sup> mice
  - 2.2. Description of the transcriptomic profile in liver of *Zmpste24*<sup>-/-</sup> after NAD<sup>+</sup> supplementation

3. Analysis of the anti-aging potential of genetic approaches designed to counteract mitochondrial dysfunction, based on overexpression of the LONP1 protease
  - 3.1. Generation and description of the new transgenic *Lonp1* mouse model
  - 3.2. Characterization of mitochondrial and systemic metabolism in *Lonp1<sup>TG</sup>* mice
  - 3.3. Longevity and healthspan evaluation in *Lonp1<sup>TG</sup>* mice





# **EXPERIMENTAL PROCEDURES**



## Molecular Biology methods

### DNA genotyping

Genomic DNA was extracted from mouse tail biopsies by alkaline lysis buffer (NaOH 25 mM, EDTA 0.2 mM, pH=8) followed by 99 °C incubation for 90 min and sequential neutralization (Tris 40 mM, pH=7.4). In all cases, PCR was performed using Platinum™ Taq DNA polymerase (Invitrogen) under the following conditions: denaturalization at 95 °C for 30 s, annealing at 60 °C for 30 s and extension at 72 °C for 45 seconds, with 30 cycles of amplification. Mouse genotyping of *Banf1* mouse models was performed with the following oligonucleotides: 5'-CACCACTCCGCTTCTCAC-3', 5'-CAACTCTATGGCTCCGGGTA-3' and 5'-CGCGTCGAGAAGTTCCTATT-3'. The PCR fragment consisted of 122 base pairs (bp) from the knock-out allele, 421 bp from the knock-in mutated allele and 191 bp from the wild-type allele. *Lmna*<sup>G609G/G609G</sup> mice genotyping was performed with the following oligonucleotides: 5'-AAGGGGCTGGGAGGACAGAG-3', 5'-AGTAGAAGGTGGCGCGAAGG-3' and 5'-AGCATGCAATAGGGTGGGAAGGA-3'. The PCR fragment consisted of 340 bp from the knock-in mutated allele and 100 bp from the wild-type allele. For *Zmpste24*<sup>-/-</sup> mice, we used the following oligonucleotides: 5'-GCTGGCCTTGTTGCTGGAAT-3', 5'-GCTTCCTCCCTGAGCCAACC-3' and 5'-CTTCCGGAGCGGATCTCAAA-3'. The PCR fragment consisted of 303 bp from the knock-out allele and 520 bp from the wild-type allele. For *Lonp1*<sup>TG</sup> mice genotyping, the following oligonucleotides were used: 5'-TAATTGCTGGTGTGGCTTGA-3' and 5'-TTTATGCTTCCGGCTCGTAT-3'. The PCR fragment consisted of 439 bp from the transgenic allele.

### Genomic DNA extraction and qPCR analysis

Genomic DNA was extracted from liver, kidney, heart and colon for mtDNA copy number, mtDNA maintenance and telomere length experiments. Extraction was performed with a phenol-chloroform method. Then, samples were quantified using a NanoDrop ND-1000 spectrophotometer (NanoDrop Technologies) and evaluated for purity (260/280 nm ratio). Quantitative PCR analyses were performed using 4.5 ng of

DNA by triplicate for each sample in the Applied Biosystems 7300HT Real-Time PCR System. We used SYBR® green PCR Universal Master Mix (Applied Biosystems) and the following oligonucleotides for mtDNA copy number and maintenance analysis:

- HK2\_fwd (5'-GCCAGCCTCTCCTGATTTTAGTGT-3')
- HK2\_rev (5' GGGAACACAAAAGACCTCTTCTGG-3')
- ND1\_fw (5'-CTAGCAGAAACAAACCGGGC-3')
- ND1\_rev (5'-CCGGCTGCGTATTCTACGTT-3')
- ND4\_fwd (5'-AGCTCAATCTGCTTACGCCA-3')
- ND4\_rev (5'- TGCAATGACAAGTGCTATGTGG-3')

For telomere length measurements the following oligonucleotides were used:

- Tel\_fwd (5'-CGGTTTGTGGTTTGGGTTTGGGTTTGGGTTTGGGTTTGGGTT-3')
- Tel\_rev (5'- GGCTTGCCTTACCCTTACCCTTACCCTTACCCTTACCCT-3')
- 36B4\_fwd (5'-CAGCAAGTGGGAAGGTGTAATCC-3')
- 36B4\_rev (5'-CCCATTCTATCATCAACGGGTACAA-3')

### RNA preparation and quantitative real-time PCR

Collected tissues were homogenized in TRIzol reagent (Life Technologies) and RNA was extracted through alcohol precipitation or using the RNeasy Mini kit (QIAGEN) following the manufacturer's instructions. After extraction, samples were quantified using a NanoDrop ND-1000 spectrophotometer (NanoDrop Technologies) and evaluated for purity (260/280 nm ratio). cDNA was synthesized with the QuantiTect Reverse Transcription kit (QIAGEN) using 1 µg of total RNA and following the manufacturer's instructions. Quantitative RT-PCR analysis was performed in triplicate for each sample with 20 ng of cDNA using an Applied Biosystems 7300HT Real-Time PCR System. For *Lonp1* expression measurement we used the following oligonucleotides: *Lonp1\_fwd* (5'-ATGACCGTCCCGGATGTGT-3') and *Lonp1\_rev* (5'-CCTCCACGATCTTGATAAAGCG-3'). As internal control, gene expression was normalized to the *Gapdh* gene and relative expression was calculated using RQ values ( $RQ=2^{-\Delta\Delta Ct}$ )

### **RNA extraction for RNA-seq analysis**

After extractions, tissues were snap-frozen in dry ice and then stored at -80 °C until RNA extraction. Bones were homogenized using a mortar and a pestle with liquid nitrogen, taking special care to maintain the extreme-cold conditions at all times and previously cleaning all the material with RNaseZap (Invitrogen). Bone marrow and liver were homogenized with a Polytron homogenizer. RNA was then extracted with TRIzol Reagent (Life Technologies), purified with ethanol precipitation and diluted in an appropriate amount of TE buffer pH 8.0, following the manufacturer's protocol. RNA quantity and quality was determined with a Bioanalyzer 2000 (Agilent).

### **Protein isolation and Western blot analysis**

For protein isolation from cultured cells, these were washed in 1x PBS and homogenized in RIPA lysis buffer containing 100 mM Tris pH 7.4, 150 mM NaCl, 10 mM EDTA pH 8.0, 1% sodium deoxycholate, 1% Triton X-100 and 0.1% sodium dodecyl sulfate (SDS), supplemented with protease inhibitors cocktail (Complete, EDTA-free, Roche) and phosphatase inhibitors (PhosSTOP, Roche). In the case of tissues, these were snap-frozen after extraction and stored at -80 °C prior to being homogenized in the same RIPA lysis buffer with a Polytron homogenizer. Protein concentration was determined with the Pierce BCA Protein Assay Kit, and equal amounts of total proteins were loaded onto SDS-polyacrylamide gels. Then, gels were transferred to PVDF membranes, blocked with 5% bovine serum albumin (BSA) in TBS-T buffer (20 mM Tris pH 7.4, 150 mM NaCl and 0.05% Tween 20) and incubated overnight at 4 °C with primary antibodies diluted in TBST-3% BSA. After washing, membranes were incubated for 1 h with fluorescently labelled secondary antibodies and scanned on an Odyssey infrared scanner (LI-COR Biosciences). The primary antibodies used in this study were rabbit anti-BAF (PRS4017; Sigma-Aldrich), rabbit anti-LONP1 (HPA002192; Atlas Antibodies), mouse anti-TFAM (sc-166965; Santa Cruz), rabbit anti-POLRMT (PA5-28196; Invitrogen), mouse anti-OXPHOS cocktail (ab110413; Invitrogen), mouse Anti-NDUFA9 (459100; Invitrogen), mouse anti-SDHA (459200; Invitrogen), mouse anti-UQCRC1(459140; Invitrogen), mouse anti-COX4A (A21348; Invitrogen), mouse anti-ATP5A1 (ab14748; Abcam), mice anti- HSC70 (sc-

7298; Santa Cruz), mouse anti-GAPDH(ab9484; Abcam), goat anti-HSP60 (sc-1052; Santa Cruz) and mouse anti- $\beta$ -actin (A5441, Sigma-Aldrich).

### **Osteoblast and osteoclast activity**

To determine the bone formation and resorption rates, serum samples were collected from 4-6 months-old mice after 6 hours of fasting and immediately frozen in dry ice and stored at -80 °C. Osteoclast activity in bone resorption was assayed by measuring the level of type I collagen fragments (CTX-1) using RatLaps™ (CTX-I) EIA (IDS, AC-06F1). Osteoblast activity in bone formation was determined by quantifying the levels of N-terminal propeptide of type I procollagen (PINP) using Rat/Mouse PINP EIA assay (IDS, AC-33F1). In both cases, metabolite levels were determined by following the instructions from the manufacturer.

### **Aldosterone ELISA analysis**

Blood samples were collected from the mandibular sinus of mice using EDTA as anticoagulant. Blood was centrifuged at 2,000 g and 4 °C, and plasma in the supernatant was collected and stored at -80 °C until analysis. Aldosterone levels were quantified using the Aldosterone Competitive ELISA Kit (EIAALD; Invitrogen), following manufacturer's instructions.

## **Cell Biology methods**

### **Cell culture**

Fibroblasts were maintained in Dulbecco's modified Eagle's medium supplemented with 10% fetal bovine serum, 1% penicillin-streptomycin-l-glutamine and 1% antibiotic-antimycotic (Gibco), 1X non-essential amino acids, 10 mM HEPES buffer, 100  $\mu$ M 2-mercaptoethanol and 1X sodium pyruvate (Gibco) at 37 °C in 5% CO<sub>2</sub>. To perform the immortalization of wild-type and mutant fibroblast, HEK-293T cells were transfected using Lipofectamine and Plus Reagent (Invitrogen) with pLOX-Ttag-iresTK vector (#12246, Addgene) together with second-generation packaging plasmids following the manufacturer's protocol. Supernatants were filtered through

0.45 µm polyethersulfone filters to collect the viral particles and added at 1:3 dilution to previously seeded mouse fibroblasts supplemented with 0.8 µg polybrene (Millipore) per ml of media. Selection was performed by successive passages. For the proliferation assays, 2000 cells were seeded per well on day 0 and incubated either with control or 200µM H<sub>2</sub>O<sub>2</sub> serum at 37 °C in 5% CO<sub>2</sub> for 4-7 days as previously described<sup>166</sup>.

### Seahorse analysis

A12T and *Lonp1*<sup>TG</sup> fibroblasts were pre-plated on a Seahorse plate in the same enriched medium used for cell culture or in a fatty-acid-enriched medium. Oxygen consumption (OCR) and extracellular acidification rate (ECAR) were assessed using a Seahorse XFe96 Analyzer (Seahorse Biosciences, Agilent). Each measurement was performed over 3 min after 3 min mix period. Basal measurements were collected four times, followed by three measurements after addition of oligomycin (final concentration 1 µM), followed by three measurements after addition of carbonyl cyanide-4- (trifluoromethoxy) phenylhydrazone (FCCP) (final concentration 0.75 µM), followed by three measurements after addition of rotenone and antimycin A (final concentration 0.5 µM each). The experiments were performed in the laboratory of Prof. Aleksandra Trifunovic at the CECAD institute (University of Cologne).

### Immunofluorescence

For immunofluorescence analysis, cells were washed with PBS 1X and fixed in 4% formaldehyde solution for 10 min at room temperature. Then, cells were rinsed with PBS 1X, permeabilized using 0.5% Triton X-100 and blocked with 15% Goat Serum (Gibco) diluted in PBS for 1 h at room temperature. Incubation with primary antibodies diluted in 1% goat serum in PBS 1X was performed overnight at 4 °C in a humidity chamber. Secondary antibody incubation was carried out 1 h at room temperature in a humidity chamber. Then, cells were washed twice with PBS 1X for 5 min and nuclei were stained with 4',6-diamidino-2-phenylindole (DAPI, Invitrogen).

## Animal model procedures / methods

### Animal experiments

All mice required for the experiments were bred on a specific pathogen-free (SPF) area of the University of Oviedo's animal facility. All animal experiments were approved by the Committee for Animal Experimentation of the Universidad de Oviedo and the Consejería de Medio Rural y Cohesión Territorial, Principado de Asturias (Approvals reference: 17-INV-2013, PROAE 57-2019, 2016, PROAE 40-2016, 2017 PROAE 13-2017, 2018 PROAE 20-2018), and performed in accordance with the European and Spanish legislative and regulatory guidelines (European convention ETS-123, on the protection of vertebrate mammals used in experimentation and other scientific purposes, and Spanish Law 6/2013, and R.D. 53/2013 on the protection of animals used in scientific research), making every effort to minimize mouse discomfort. The experiments were carried out in a conventional area of our animal facility with exclusion barriers. All animals were housed with a photoperiod of 12 h light/12 h dark, at  $22 \pm 2$  °C,  $50 \pm 10\%$  of relative humidity, Mice were caged separately by sex and colonies and were checked daily for water and food supplies, as well as for good general condition. Mice were fed *ad libitum*, excepting those in western-like diets. Animals were sacrificed to obtain tissue samples at the age of either 3 or 18-24 months in the case of young and old individuals, respectively, in the A12T experiments; at the age of 4-5 months in the case of NAD<sup>+</sup> boost experiments in *Lmna*<sup>G609G/G609G</sup> and *Zmpste24*<sup>-/-</sup> mice; and either at 2-6 or 16 months in the different *Lonp1*<sup>TG</sup> mice experiments. Tissues were either frozen immediately with dry ice and stored at -80 °C or fixed in 4% paraformaldehyde for 24-48 h and conserved at 4 °C in 70% ethanol, 90% ethanol in the case of bones.

### Generation of new mouse models

*Banf1* knockout mouse model was generated via a recombineering-based method, as previously described<sup>167</sup>. To generate mutant A12T mice, the c.34G>A mutation was introduced in exon 2 of *Banf1* using direct mutagenesis. Integrity of the targeting vectors was verified by DNA sequencing and restriction mapping. After

linearization, both targeting vectors were electroporated into 129SV ES cells and positive clones were identified using Southern blot analysis. *Banf1*-targeted 129SV ES cells were microinjected into mouse C57BL/6N blastocysts to produce chimeric mice, that were then crossed with C57BL/6N mice to generate, first heterozygous and then homozygous, *Banf1*<sup>KO-first</sup> mice. Electroporation of the targeting vector and microinjection of ES cells were performed in the Transgenics Unit facilities of the Universidad de Oviedo. Neomycin resistance cassette was excised using the surrounding FRT sites, and a *Banf1*<sup>conditional-KO</sup> colony was generated after electroporating *Banf1*<sup>KO-first</sup> cells with a *Flippase* construct and microinjection into 129SV ES cells. Eventually, the *Banf1*<sup>KO</sup> line was established after *Banf1*<sup>conditional-KO</sup> and *Cre* transgenic mice were intercrossed, which triggered the excision of the second exon by Cre recombination using the loxP sites surrounding (Figure S1B). To generate the KI mice, the targeting vector that carried the mutation in exon 2 was treated with Flippase recombinase *in vitro* to excise the neomycin resistance cassette and let the mutated exon 2 flanked by loxP sites (Figure S1C). All the animals were in a mixed 129SV/BL6N background, excepting the ones used in the iron-overdose experiment and *Lmna*<sup>G609G</sup> colony mice which were in pure C57BL/6N background. For the generation of the LONP1 transgenic mouse, a large genomic DNA segment containing the murine *Lonp1* locus and cloned into the BAC (Bacterial Artificial Chromosome) vector pBAC3.6 was obtained from CHORI (identification no. RP23-421B5; RPCI-23 library, C57BL/6J) (<http://www.chori.org>). *Lonp1* gene was extracted from the BAC and cloned into the pBS (pBlueScript II SK) backbone. The plasmid containing the genomic sequence of *LonP1* was sent to Cyagen US Inc for linearization and microinjection into the pronuclei of fertilized oocytes, derived from intercrosses of C57BL/6J mice. Four founders capable of transmitting the transgene to the progeny and that overexpressed LONP1 were identified. From these, four transgenic colonies were generated, half of them carrying 2 extra copies and the last two carrying 6 extra copies. Finally, we decided to work with one of the transgenic colonies with 6 extra copies, abbreviated here as *Lonp1*<sup>TG</sup>. The transgenic mice used for the experiments were all heterozygous for the transgene. The *Lmna*<sup>G609G/G609G</sup> and *Zmpste24*<sup>-/-</sup> models were previously generated in our laboratory<sup>74,168</sup>.

### **Bone-stressing challenges by osteoporosis induction in ovariectomized mice (OVX) and iron-overdose treatment**

For the experiment of OVX females, animals were operated at the age of 2 months to either remove ovaries in the case OVX mice or to go under an open and sew surgery for control SHAM animals. After 2 months, mice were sacrificed to weight the uterus and to fixate both tibias as previously described. For the iron-overdose protocol, 2-month-old mice were treated intraperitoneally once a week for 2 months with iron dextran (D8517, Sigma-Aldrich) at a concentration of 1 g per kg of body weight as previously described <sup>169</sup>. At that time, animals were sacrificed and tissues were collected. Both protocols were carried at the Bioterio of Universidad de Oviedo with the assistance of the Transgenics Laboratory of the Bioterio.

### **Micro-CT analysis of tibias**

For the  $\mu$ CT analyses, all tibia samples were scanned by a high-resolution micro-computed tomography (SkyScan 1174, Bruker) by the Preclinical Imaging Unit of the University of Oviedo. The parameters were measured according to the American Society for Bone and Mineral Research (ASBMR) histomorphometry nomenclature <sup>170</sup>.

### **Glucose measurements and glucose/insulin tolerance test**

For routine glucose determinations, animals were starved for 6 hours prior to the tests. In the case glucose decay analysis in *Lonp1<sup>TG</sup>* mice, the measurements were performed at baseline and after 5-, 12- and 24-hour fast. For glucose and insulin tolerance test, mice were fasted 6-8 hours prior to studies. Then, blood glucose was measured at baseline and the animals received an intraperitoneal injection of either 2 mg of glucose per g of body weight (IPGTT) or 0.75-1 IU of insulin per kg of body weight (IPITT). Next, blood glucose was measured at 15, 30, 60 and 120 min after intraperitoneal injection of glucose or insulin. In case of severe hypoglycemia, mice under the insulin tolerance test were rescued by an intraperitoneal injection of glucose at the same concentration as in IPGTT. In all cases, glucose levels were then measured with an Accu-Check glucometer (Roche Diagnostics) using blood from the tail vein.

### **Serum metabolites and cell blood analysis**

For serum metabolites analysis, blood samples were collected from the mandibular sinus of 6h-fasted mice using heparin anticoagulant. Blood was centrifuged at 2,000 g and 4 °C, and plasma in the supernatant was collected and stored at -80 °C until analysis. Metabolites were determined by Indilab (León, Spain). For hematological analysis, blood was extracted as above from non-fasted mice using EDTA or heparin anticoagulants. Cell counting in blood was performed using an Abacus junior vet equipment (Diatron Labs).

### **Body temperature determination and thermogenesis induction by cold exposure**

Body temperature was measured in the rectum using a JKT Thermocouple Probe (WD-20250-91, Kent Scientific). For thermogenesis induction by acute cold exposure, mice were individually placed in sawdust-free cages, with water and food supplies *ad libitum*, at 4 °C during 8 h. Rectal temperature was monitored every hour and, in cases of a dramatic drop in body temperature, mice were euthanized.

### **Indirect calorimetry and locomotor activity measurements**

All measurements were performed using the Comprehensive Laboratory Animal Monitoring System (Oxymax CLAMS system by Columbus Instruments) and analyzed following manufacturer's instructions. Mice were housed individually and kept on control, NR, niacin or HFD diet on a 12:12-h light–dark cycle. Mice were monitored for 48 h and the first 24 h were discarded in the analysis, considering them as acclimation period. For fasting conditions analysis, mice were fed normally during the first 48 h and fasted during the next 24 h, discarding the first 24 h as acclimation period. Total ambulatory activity and food consumption were measured. Food intake was normalized to body weight. Rates of oxygen consumption ( $VO_2$ ),  $CO_2$  production ( $VCO_2$ ) and energy expenditure (EE) were determined and normalized to body weight.

## **Histological analysis**

Tissues were fixed in 4% PFA in PBS and embedded in paraffin by standard procedures. H&E staining was performed in transversal sections of quadriceps, stomach, colon, kidney, lung, heart, liver, gonads, intestine, aorta and white adipose tissue. The atrophy of kidney, lung and quadriceps were blindly assessed in three different sections per mouse, establishing a pathological score (0, normal; 1, mild; 2, moderate; 3, severe atrophy). For lipid detection, liver samples were embedded in Tissue-Tek OCT compound (Sakura Finetechnical) and stored at -80 °C. Samples were sectioned at 10 µm thickness and stained with Oil Red O. In all cases, tissue sections were evaluated by the pathologist of the Cancer Animal Models Histopathology Unit of the Universidad de Oviedo.

## **Diet-induced obesity by high-fat and high-sucrose diet administration**

For diet-induced obesity, 2-months-old mice were fed with a high-fat diet containing 60% fat (Harlan D12492) *ad libitum* for 4-5 months. For high-sucrose diet, at 2 months old mice were given 30% sucrose in their drinking water during 3 months.

## **Proteostatic and inflammatory stress protocols**

For proteostatic stress, paraquat was administrated intraperitoneally at a concentration of 60 mg per kg of mice in saline. Cisplatin was injected intraperitoneally at 10 mg per kg of body weight at day 0 and mice were sacrificed at day 3 to obtain urine, serum, kidney and liver samples. For acute inflammatory stress, LPS was administrated intraperitoneally at 20 mg per kg of body weight in saline and rectal temperature was measured after 24 h. In all cases, protocols were performed in mice of 2 months of age.

## **Colorectal carcinogenesis**

For colon tumor induction, females of 2 months of age were injected intraperitoneally with 12.5 mg/kg of azoxymethane (AOM; Sigma Aldrich, Ref. A5486). After 5 days, dextran sulfate sodium (DSS; MP Biomedicals, Ref. 160110) at 1.5%

was administered in the drinking water for 5 consecutive days. Next, normal water was given for 16 days, followed by two cycles of 5 days on DSS with another cycle of 16 days on standard water between them<sup>171,172</sup>. Ten days after the last DSS cycle, mice were euthanized and colons were extracted, flushed with PBS, measured and then fixed in 4% paraformaldehyde solution (PFA). Transversal sections of colons were stained by hematoxylin and eosin (H&E) and tumors were counted and evaluated by their histological features.

### **Treadmill endurance test in basal and trained conditions**

Mice endurance capacity was determined by using an incremental test in the treadmill (Panlab 8700, Barcelona, Spain) with an inclination of 10 grades. At 2 months of age, mice underwent a previous adaptation period of 8 days to avoid aversive stimuli and obtain reproducible results. Then, mice were tested in basal non-trained conditions with a 77-seconds step starting at 0.15 m/s with increments of 0.01 m/s, with 0.6 m/s as limit speed, until the mouse reached its maximum capacity. Next, mice were trained every day during 1 h at 0.2-0.24 m/s and repeated the test in trained conditions as described above. This method was adapted from other protocols previously described<sup>173,174</sup> and was performed with the assistance of Dr. Benjamín Fernández García from the Department of Morphology and Cellular Biology, Area of anatomy, Universidad de Oviedo.

### **Rotarod test**

Motor coordination in 2-year-old mice was evaluated with a Rotarod LE8500 (LSI, LETICA) system by measuring the running time in the rotating bar until fall. The bar started rotating at a speed of 4 rpm and progressively increased to 40 rpm after 5 min. Rotarod tests were performed for 5 days, considering the first 4 days as acclimation. Each day, the test was repeated 3 times in each mouse, leaving a minimum rest of 30 min between each run.

### **Hanging wire test**

The 2-year-old mice were placed on an 8 mm diameter wooden bar suspended about 30 cm from a box filled with sawdust, so that the mice would not be harmed in

case of a fall but could not voluntarily jump off. The number of falls during the first and the total three minutes of the experiment was measured, and if the mouse fell at least 10 times, the time spent was recorded. After each fall the mouse was gently placed in the center of the bar. The test was repeated three times on different days.

### **Aging score**

Frailty index was quantified based on the macroscopic evaluation of several clinical signs of deterioration <sup>175</sup> in 2-year-old mice including :

- Alopecia: Hair loss due to age-related balding and/or barbering (fur trimming).
- Loss of fur conditions: Change in fur colour from black to grey or brown.
- Dermatitis: Inflammation, overgrooming, barbering or scratching causing skin erosion. Can result in open sores anywhere on the body.
- Loss of whiskers: Loss of vibrissae (whiskers) due to aging and/or whisker trimming.
- Coat condition: Ruffled fur and/or matted fur. Ungroomed appearance. Coat does not look smooth, sleek, and shiny.
- Distended abdomen: Enlarged abdomen. May be due to tumor growth, organ enlargement, or intraperitoneal fluid accumulation.
- Kyphosis: Exaggerated outward curvature of the lower cervical/thoracic vertebral column. Hunched back or posture.
- Tail stiffening: Tail appears stiff, even when animal is moving in the cage. Tail does not wrap freely when stroked.
- Loss of coordination: Lack of coordination in movement including hopping, wobbling, or uncoordinated gait. Wide stance. Circling or weakness.
- Tremor: Involuntary shaking at rest or during movement.
- Forelimb grip strength: A decline in forelimb grip strength.
- General body condition: Visual signs of muscle wasting or obesity based on the amount of flesh covering bony protuberances.
- Vestibular disturbance: Disruption in the ability to perceive motion and gravity. Reflected in problems with balance, orientation and acceleration.
- Corneal opacity: Development of white spots on the cornea. Cloudy cornea.
- Eye discharge/swelling: Eyes are swollen or bulging (exophthalmia). They may exhibit abnormal secretions and/or crusting.
- Microphthalmia: Eyes are small and/or sunken. May involve one or both eyes.

- Loss of vision: Vision loss, indicated by failure to reach toward the ground when lowered by the tail.
- Menace reflex: Rapid eye blink and closure of the palpebral fissure in response to a nontactile visual threat to the eye. Measures the integrity of the entire visual pathway including cortical components.
- Nasal discharge: Signs of abnormal discharge from the nares.
- Digestive malocclusions: Incisor teeth are uneven or overgrown. Top teeth grow back into the roof of the mouth or bottom teeth are long and easily seen.
- Breathing rate: Difficulty breathing (dyspnea), pulmonary congestion (rales), and/or rapid breathing (tachypnea).

The intensity of these deterioration signs was blindly assessed in four different sections per mouse, establishing a pathological score (0, normal; 1, mild; 2, moderate; 3, severe; 4, complete)

## Bioinformatic and Statistical methods

### RNA-seq and bioinformatic analysis

Libraries were prepared using the TruSeq Stranded Total RNA with Ribo-Zero Gold (Illumina) and sequenced as 150 bp paired-end on a NovaSeq6000 Illumina platform with at least 20 million reads per sample by Macrogen. Paired-end reads were aligned to the GRCm39 genome (Ensembl release 106) using STAR (2.7.10a) with default parameters<sup>176</sup>. Raw counts were imported and summarized to gene-level count matrices using tximport (1.22.0) and differential expression analysis was performed using DESeq2 (1.34.0)<sup>177</sup>. An adjusted P-value  $\leq 0.05$  was used as the significance threshold for the identification of differentially expressed genes. Gene-set enrichment analysis (GSEA) were performed using the R package fgsea (1.20)<sup>178</sup>. Genes were pre-ranked by the logarithm (in base 2) of the fold change multiplied by the negative logarithm in base 10 of the p value ( $\log_2\text{FoldChange} * -\log_{10}(\text{pvalue})$ ). GSEA was tested for enriched gene-sets from the Hallmarks (H) and Canonical pathways (C2) categories extracted from the mouse Molecular Signatures Database through msigdf (7.4). Analysis were perform using R (4.1.3) within RStudio (<https://www.rstudio.com/>). Plots representing normalized enrichment scores (NESs)

from GSEA were generated using GraphPad Prism 9.0. The accession number for the RNA sequencing data reported in this paper is GSE207329.

### **Statistical Analysis**

Animals of the same age, sex and conditions were used for comparisons between mice groups. The number of mice included per group was based on previous experiments with randomized distribution. Unless otherwise specified in figure legends, all experimental data are reported as mean  $\pm$  95% of confidence interval (CI). Comparison between two groups with normal distribution was performed using a two-tailed Student's *t*-test assuming same deviation. Survival analysis was performed by using the Kaplan-Meier method, and statistical differences were analyzed with the log-rank (Mantel-Cox) test and Gehan-Breslow-Wilcoxon test. Body weight was analyzed using a multiple *t*-test method assuming same standard deviation (SD). All statistical tests, data analysis, and plots were generated using R and RStudio (R Core Team, Vienna, Austria, <https://www.r-project.org>; RStudio Team, Boston, MA, USA, <https://www.rstudio.com>) and GraphPad Prism 9.0. Plots and figures were modified using Adobe Illustrator CC.





# RESULTS



## 1. Development and characterization of genetically modified mouse models to investigate the involvement of nuclear envelope components in age-associated pathologies

Néstor-Guillermo Progeria Syndrome (NGPS) is an accelerated-aging disease first described in two unrelated Spanish patients<sup>179</sup>, and recently reported in a young patient of Mexican origin<sup>53</sup>. NGPS phenocopies multiple features of classical progeria such as growth retardation, lipodystrophy and alopecia; however, the bone phenotype is more severe compared to HGPS patients, reducing quality of life and becoming a major mortality risk in these patients. The scarcity of NGPS patients has hampered studies on their life expectancy, but they appear to show longer survival than HGPS patients<sup>179</sup>.

NGPS is caused by a homozygous c.34G>A (p.Ala12Thr) mutation in *BANF1*, which encodes an 89 amino acid protein called barrier-to-autointegration factor 1 (BAF)<sup>180</sup>. BAF interacts with DNA and nuclear lamina related proteins and is implicated in nuclear envelope assembly<sup>57,181,182</sup>. The p.Ala12Thr mutation generates profound nuclear abnormalities and emerin mislocalization away from the nuclear lamina<sup>56</sup>. Recently, BAF has been related to DNA damage responses in oxidative stress, through the binding and inhibition of PARP1<sup>183</sup>, and DNA double-strand breaks (DSB) repair pathways, by regulating non-homologous end joining<sup>63</sup>. However, the molecular basis of the progeroid phenotype seen in humans with alterations in BAF remains poorly understood.

To deepen in the roles of BAF in the nuclear envelope and to study the mechanism underlying p.Ala12Thr BAF mutation pathogenicity, in this section we have generated mouse models with different *Banf1* alterations. We show that mutant mice present bone alterations resembling those seen in NGPS patients, both under physiological and stress conditions. Together, our results validate *Banf1*<sup>A12T/A12T</sup> as an appropriate mouse model for studying NGPS and bone phenotypes of premature aging.

### 1.1. Generation and characterization of *Banf1*-deficient and *Banf1*<sup>A12T</sup> knock-in mice as potential Néstor-Guillermo Progeria Syndrome mouse models

To evaluate the roles of BAF protein *in vivo*, we first generated mutant mice with a knockout allele of *Banf1*. Heterozygous *Banf1*<sup>+/-</sup> mice were crossed to obtain null *Banf1* mice (Figure 3A-B); however, no homozygous mice were detected at weaning among over 250 pups, concluding that complete absence of BAF is lethal *in vivo* (Figure 3C). *Banf1*<sup>+/-</sup> mice developed normally, with both genders being fertile and indistinguishable from their wild-type littermates. No significant differences in lifespan or maximal survival were observed between *Banf1*<sup>+/-</sup> and control mice (Figure 3D).

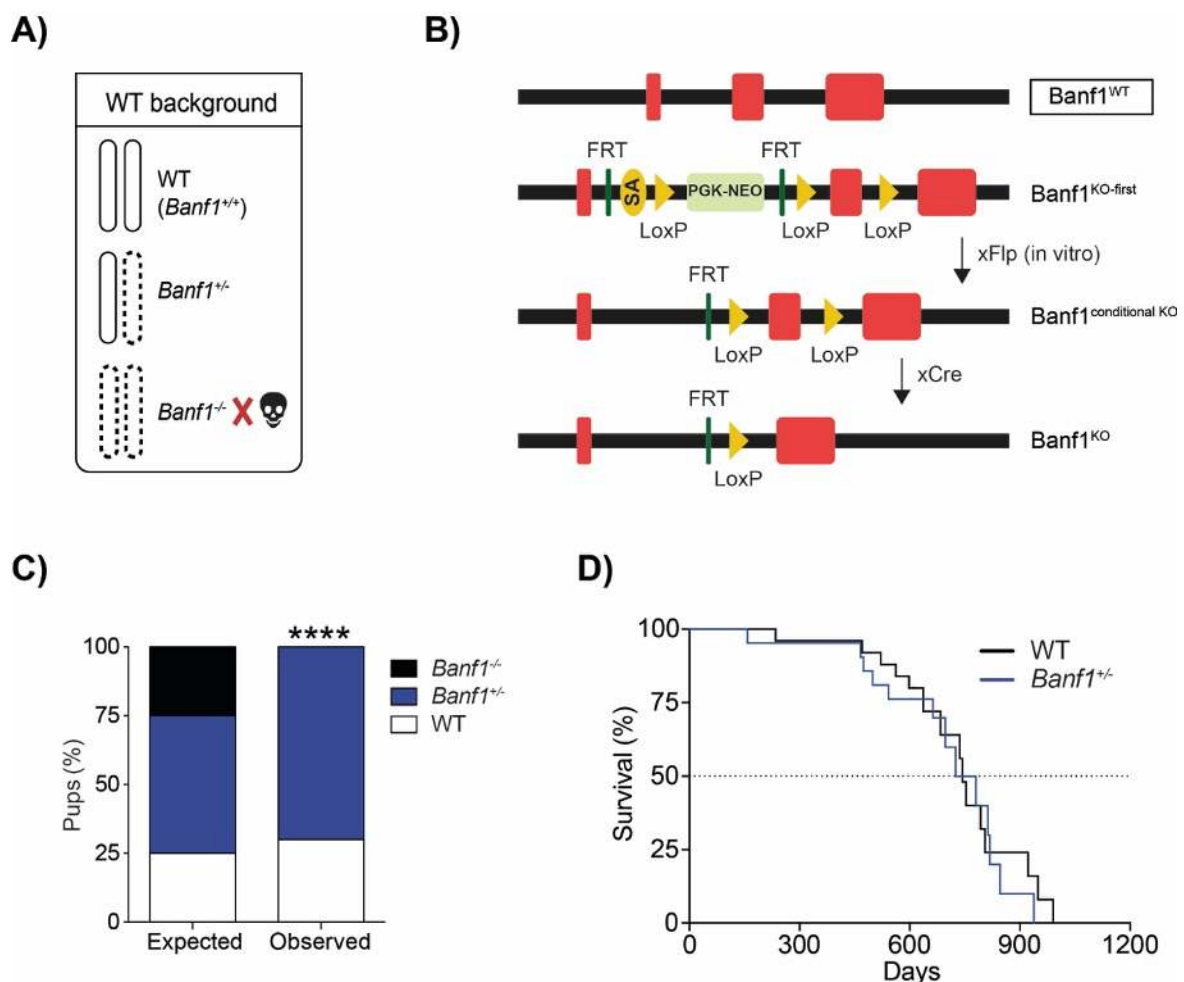


**Figure 3. Generation of heterozygous mice *Banf1*<sup>+/-</sup>.** **A)** Schematic diagram of the nomenclature used for the different *Banf1*-related mouse models developed in WT (white) background. Colored bars represent genotypes defined by WT (white) or knock-out (dotted line) alleles. **B)** Schematic representation of wild-type *Banf1* locus and targeted alleles after *Flippase* and *Cre* processing. A *Flippase* construction was electroporated in *Banf1*<sup>KO-first</sup> cells to excise the neomycin cassette using the FRT sites and generate *Banf1*<sup>conditional-KO</sup> cells. A *Banf1*<sup>KO</sup> line was finally established after *Banf1*<sup>conditional-KO</sup> and *Cre* transgenic mice intercross. **C)** Percentage of WT (white), *Banf1*<sup>+/-</sup> (blue) and *Banf1*<sup>-/-</sup> (black) pups born after crosses of heterozygous mice for *Banf1* (n=250). No *Banf1*-null pups were born. Chi-square test. **D)** Survival plot of WT and *Banf1*<sup>+/-</sup> mice (WT n=25; *Banf1*<sup>+/-</sup> n=21). Survival curves were analyzed with the log-rank (Mantel Cox) test and Gehan-Breslow-Wilcoxon test. \*\*\*\*p < 0.0001

Then, we decided to generate a mouse model for Néstor-Guillermo Progeria Syndrome (NGPS) by introducing the mutation c.34G>A, which corresponds to the protein change p.Ala12Thr, in the murine *Banf1* gene. We obtained heterozygous knock-in *Banf1*<sup>+/*A12T*</sup> mice which, after intercrosses, generated homozygous knock-in *Banf1*<sup>*A12T/A12T*</sup> mice (hereafter referred to as A12T) at the expected Mendelian ratio (Figure 4A-B). The c.34G>A change in the mutant allele was confirmed by Sanger sequencing (Figure 4C). Western-blot analyses of cells derived from A12T mice showed no changes in BAF levels compared to WT mice (Figure 4D), which is in line with recent *in vitro* studies in this regard<sup>183</sup>. A12T mice developed normally, being viable and fertile and with no evidence of accelerated aging, with median and maximum lifespan comparable to WT mice (Figure 4E). However, A12T mice showed a consistent decrease in body weight from 2 months of life, with a reduction of ~15% and 20% in the first and second year of life, respectively (Figure 4F). In an effort to make the mutant phenotype more evident, we generated a hemizygous mouse model, *Banf1*<sup>*A12T*/-</sup> (referred to as Hemi A12T), by crossing *Banf1*<sup>+/-</sup> and *Banf1*<sup>*A12T/A12T*</sup> mice (Figure 3A-B and 4A-B). Hemi A12T mice showed survival proportions comparable to their WT littermates and did not present signs of accelerated aging either (Figure 4G). Altogether, the p.Ala12Thr mutation in BAF does not entail significant changes in longevity in mice.

To deepen the study of the BAF p.Ala12Thr mutation, we evaluated aging and proliferation in A12T cells. Abnormal scaffold in the nuclear lamina, which also appears in physiological aging, is well-established as a classical characteristic of progeroid cells<sup>184,185</sup>. Accordingly, like NGPS cells, A12T cells showed an accumulation of nuclear abnormalities when compared to human and mouse control cells (Figure 5A). Fibroblasts derived from A12T mice showed decreased cell viability under normal and oxidative stress conditions compared to WT cells (Figure 5B-C). Further, A12T fibroblasts displayed a reduction in maximal mitochondrial respiration and an increment in glycolytic activity defined by higher extracellular acidification rate (Figure 5D-E). Collectively, we conclude that the p.Ala12Thr mutation in BAF enhances aging in cells, causing the accumulation of defects in the nuclear lamina, reducing proliferation and inducing mitochondrial dysfunction with increased glycolysis.

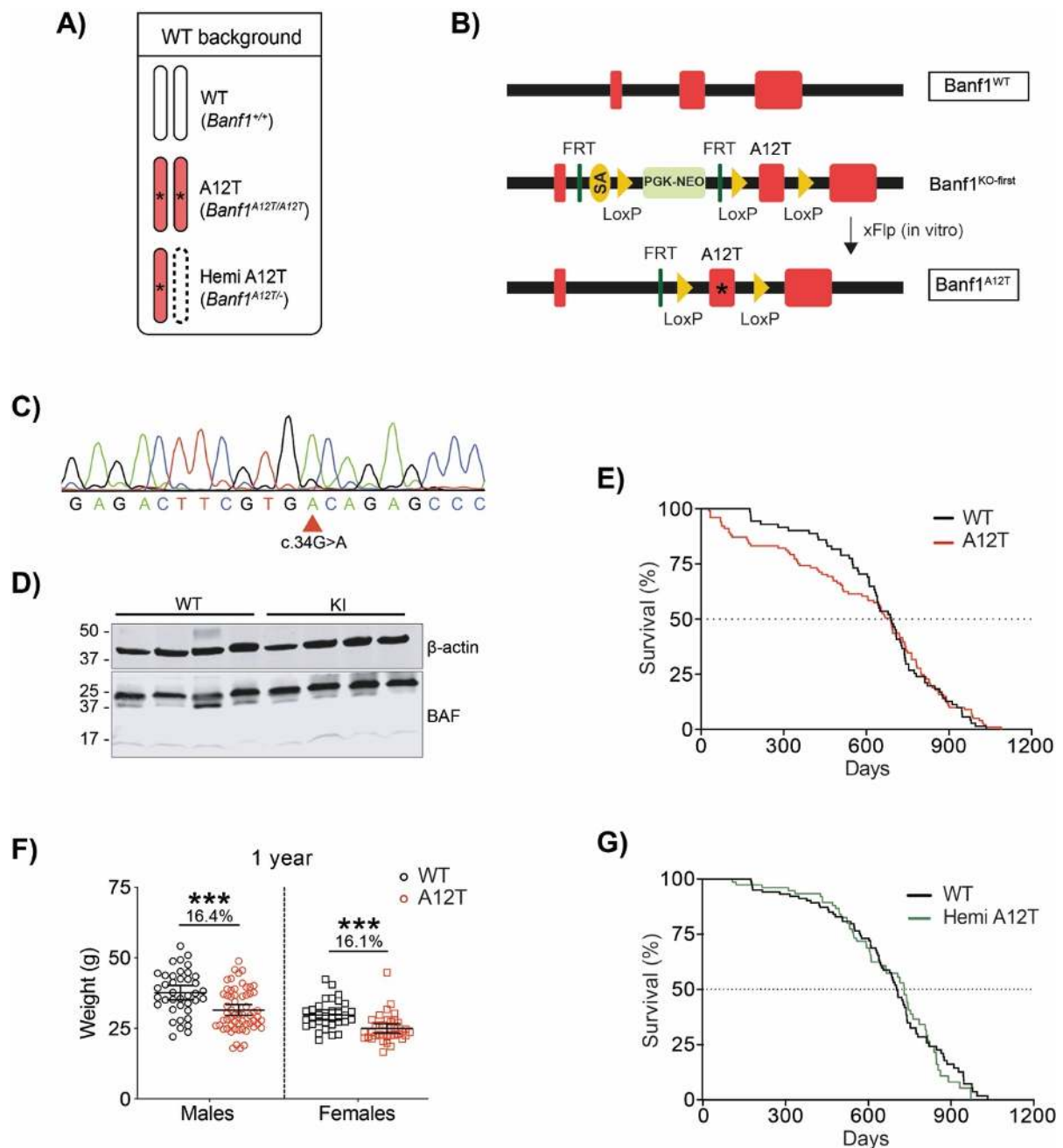


**Figure 4. Generation of the NGPS mouse model  $Banf1^{A12T/A12T}$  and hemizygous  $Banf1^{A12T/-}$  mice** **A)** Schematic diagram of the nomenclature used for the different  $Banf1^{A12T}$ -related mouse models developed in WT (white) background. Colored bars represent genotypes defined by WT (white), A12T (red) or knock-out (dotted line) alleles. **B)** Schematic representation of wild-type  $Banf1$  locus and p.Ala12Thr mutated alleles after the electroperation of *Flippase* construction, excising the neomycin cassette flanked by FRT sites, into  $Banf1^{KO-first}$  cells. **C)** Validation of c.34G>A mutation in  $Banf1^{A12T}$  alleles through Sanger sequencing. **D)** Western analysis shows BAF stability in liver samples from both p.Ala12Thr mutant and wild-type 7-month-old mice. Beta-actin was used as loading control (WT n=4, A12T n=4). **E)** Survival plot of WT and  $Banf1^{A12T/A12T}$  (A12T; red) mice (WT n=71; A12T n=101). Survival curves were analyzed with the log-rank (Mantel Cox) test ( $p=0.86$ ) and Gehan-Breslow-Wilcoxon test ( $p=0.65$ ). **F)** A12T mice show lower body weight at days 365 than WT littermates both in males and females (males, WT n=39, A12T n=60; females, WT n=32, A12T n=36). Circle dots represent male and square dots represent female individual measures with mean values and errors  $\pm$  95 % CI. Analyzed with Student's t test assuming same SD (males,  $p=0.0001$ ; females,  $p=0.0002$ ). **G)** Survival plot of WT and hemizygous  $Banf1^{A12T/-}$  (Hemi A12T; green) mice (WT n=88; Hemi A12T n=78). Survival curves were analyzed with the log-rank (Mantel Cox) test and Gehan-Breslow-Wilcoxon test. \*\* $p < 0.01$ , \*\*\*\* $p < 0.01$ .

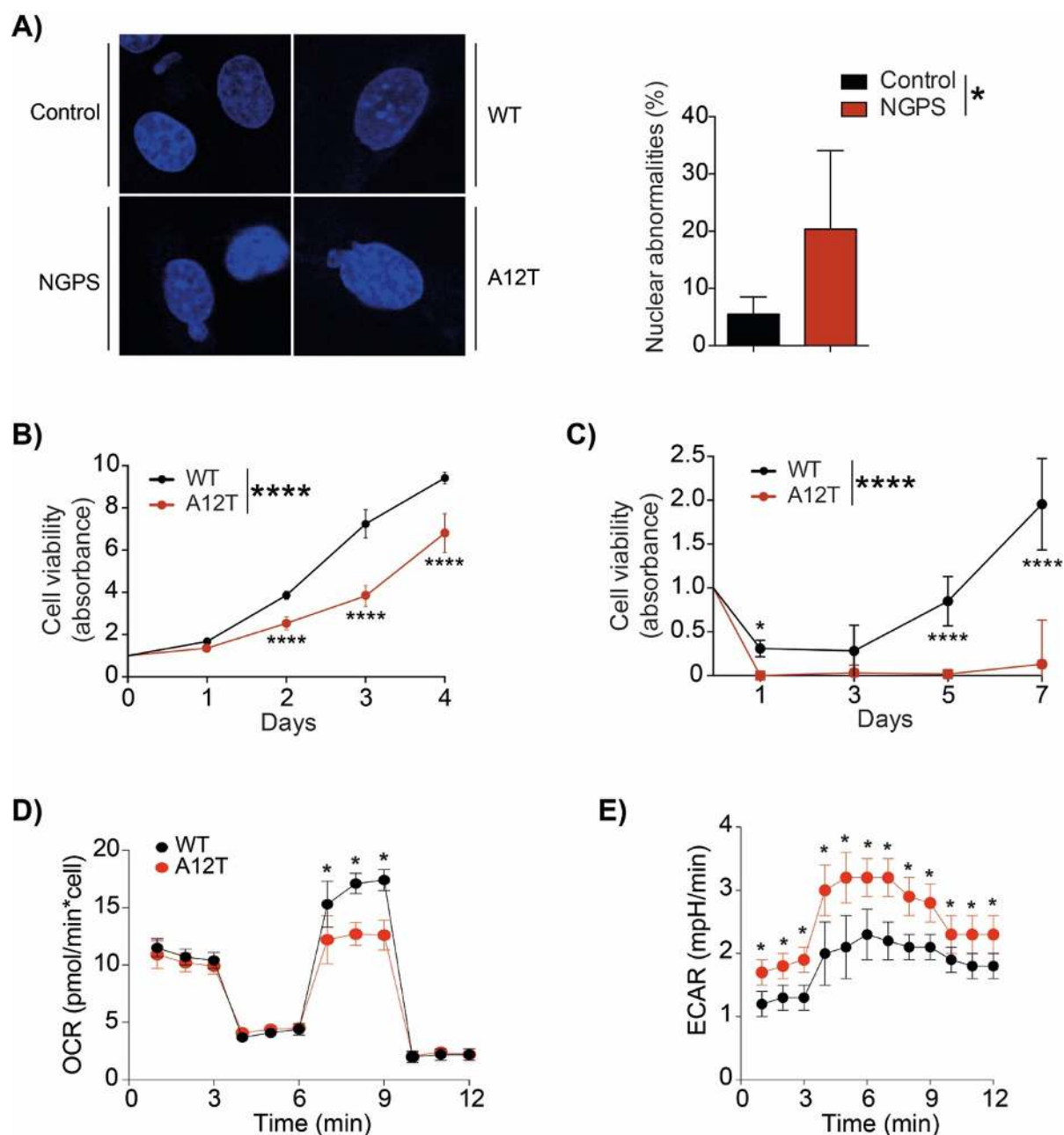


**Figure 5. Cellular characterization of model *Banf1*<sup>A12T/A12T</sup> fibroblasts.** **A)** Representative immunofluorescence images of fibroblast nuclei in human (control and NGPS) and mice (WT and A12T) cells. Increased percentage of nuclear abnormalities in NGPS fibroblast compared to human control cells (n=3 per group; p=0.038). Analysis made by Student's t test with Welch's correction. **B-C)** MTT analyses showed decreased cellular viability of A12T cells when compared to WT cells in B) basal conditions (n=12 per group) and C) after addition of 200  $\mu$ M H<sub>2</sub>O<sub>2</sub> (n=5 per group). Curves were analyzed with two-way ANOVA with Sidak's correction for multiple comparisons. **D-E)** Seahorse analysis of mouse fibroblasts shows D) a decrease in the maximal respiration capacity, measured as the oxygen consumption rate (OCR, pmol/ min/ $\mu$ g protein) after FCCP injection, and E) increased extracellular acidification rate in A12T cells (red) compared to WT (black) fibroblasts. Curves were analyzed with multiple t-test assuming same standard deviation (SD). Bar and dots represent mean  $\pm$  95% CI. \*p < 0.05, \*\*\*\*p < 0.0001.

## 1.2. Study of BANF1 and LMNA interaction in double mutant *Banf1*<sup>A12T/A12T</sup> *Lmna*<sup>G609G/G609G</sup> mice

Several mouse models of segmental progeroid disorders show mild aging phenotypes that are exacerbated under specific conditions, such as TP53 or TERC deficiency<sup>186–189</sup>. *Lmna*<sup>G609G/G609G</sup> mice, a well-established model of HGPS<sup>168</sup>, have been recently used as a tool for the study of other aging-related mouse models because of their close relation with physiological aging and their reduced lifespan<sup>190–194</sup>. Due to the role of BAF in the nuclear lamina scaffold<sup>181,182,195</sup>, we decided to explore the effects of p.Ala12Thr BAF mutation in a progeroid background by crossing *Banf1*<sup>A12T/A12T</sup> with *Lmna*<sup>G609G/+</sup> mice. In this background, double *knock-in* *Banf1*<sup>A12T/A12T</sup> *Lmna*<sup>G609G/G609G</sup> (hereafter referred to as DKI) exhibited a drastic reduction in median and maximum lifespan compared to *Banf1*<sup>+/+</sup> *Lmna*<sup>G609G/G609G</sup> mice (referred to as G609G) (Figure 6A). Indeed, DKI mice showed consistently reduced weight compared to their G609G littermates (Figure 6B).

Bone evaluation by high-resolution micro-computed tomography confirmed the basal loss of bone tissue and the defects in trabecular organization previously observed in G609G mice<sup>196,197</sup> and evidenced an exacerbated bone phenotype in DKI mice (Figure 6C). Thus, compared to their G609G littermates, DKI mice showed a smaller bone size in both relative and absolute parameters, together with a greater bone tissue damage defined by a reduction in trabecular number and thickness, and increased inter-trabecular distance (Figure 6D-G). Trabecular and cortical regions also evidenced a loss of bone and tissue mineral density in DKI mice compared to G609G mice (Figure 6H-I).

In summary, *Lmna*<sup>G609G</sup>-derived nuclear lamina alterations expose the deleterious effects of p.Ala12Thr BAF mutation, reducing mouse lifespan and healthspan.

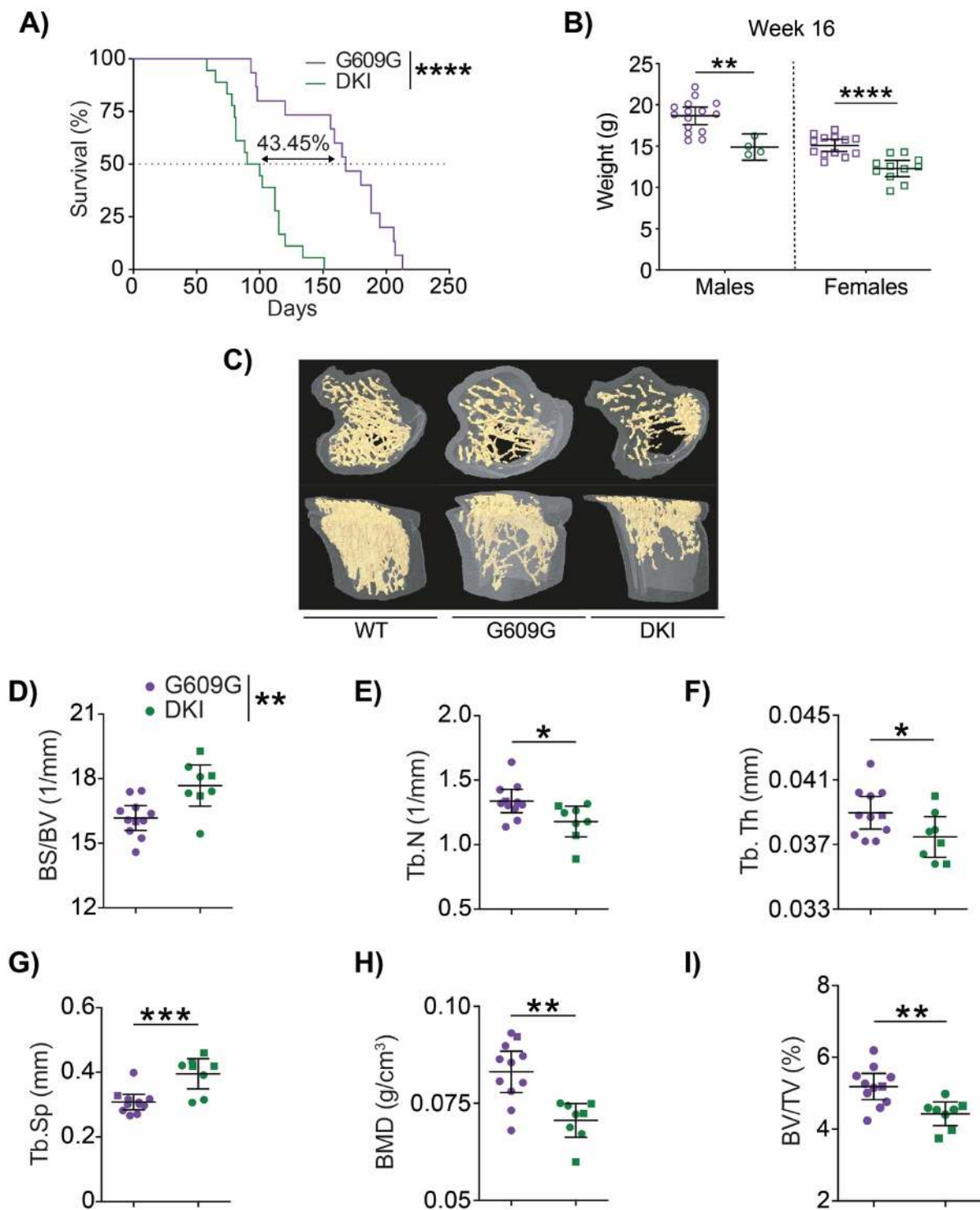


**Figure 6. Progeroid background accelerates progeria onset and reduces lifespan in *Banf1*<sup>A12T/A12T</sup> mice.** **A)** Survival plot of *Banf1*<sup>+/+</sup> *Lmna*<sup>G609G/G609G</sup> (G609G) and *Banf1*<sup>A12T/A12T</sup> *Lmna*<sup>G609G/G609G</sup> (DKI) mice (G609G n=15; DKI n=18). Survival curves were analyzed with the log-rank (Mantel Cox) test ( $p < 0.0001$ ) and Gehan-Breslow-Wilcoxon test ( $p < 0.0001$ ). **B)** Body weight of G609G and DKI mice at week 6 (males, G609G n=15, DKI n=4; females, G609G n=13, DKI n=11). Analyzed by Student's t test assuming same SD (males,  $p=0.0017$ ; females,  $p<0.0001$ ). **C)** Representative three-dimensional longitudinal and transversal images of WT, G609G and DKI tibiae generated with  $\mu$ CT analysis. **D-I)** Quantitative analysis of cortical and trabecular bone parameters measured by high-resolution micro-computed tomography in tibiae. **D)** Bone size (BS/BV; 1/mm). **E)** Trabeculae number (Tb.N; 1/mm). **F)** Trabecular thickness (Tb.Th; mm). **G)** Trabecular distance (Tb.Sp; mm). **H)** Bone mineral density (BMD; g/cm<sup>3</sup>). **I)** Bone volume (BV/TV; %) (G609G n=11; DKI n=8). Analyzed by Student's t test assuming same SD. Circle dots represent male and square dots represent female individual values. Scatter dot blots and box-plots represent mean  $\pm$  95% CI. \* $p < 0.05$ , \*\* $p < 0.01$ , \*\*\* $p < 0.01$ , \*\*\*\* $p < 0.0001$

### 1.3. Physiological and transcriptional characterization of bone phenotype in the *Banf1*<sup>A12T/A12T</sup> NGPS mouse model

Considering the important implication of bone alterations in NGPS pathology compared to other progeroid syndromes, we studied the mouse bone architecture after different bone-stressing challenges (Figure 7A). During physiological aging, bones suffer a progressive decline in homeostasis that triggers osteoporosis and other aging-related bone alterations. At 21 months, A12T males tended to show a reduction in bone mineral density at the trabecular region (Figure 7B-C) and smaller absolute bone size (Figure 7D-G). Also, old A12T mice exhibited alterations in trabecular structure, displaying reduced number of trabeculae with greater distance between them (Figure 7H-J). These results, together with the NGPS phenotype, suggest an impact of the p.Ala12Thr mutation in BAF on bone remodeling and bone tissue damage.

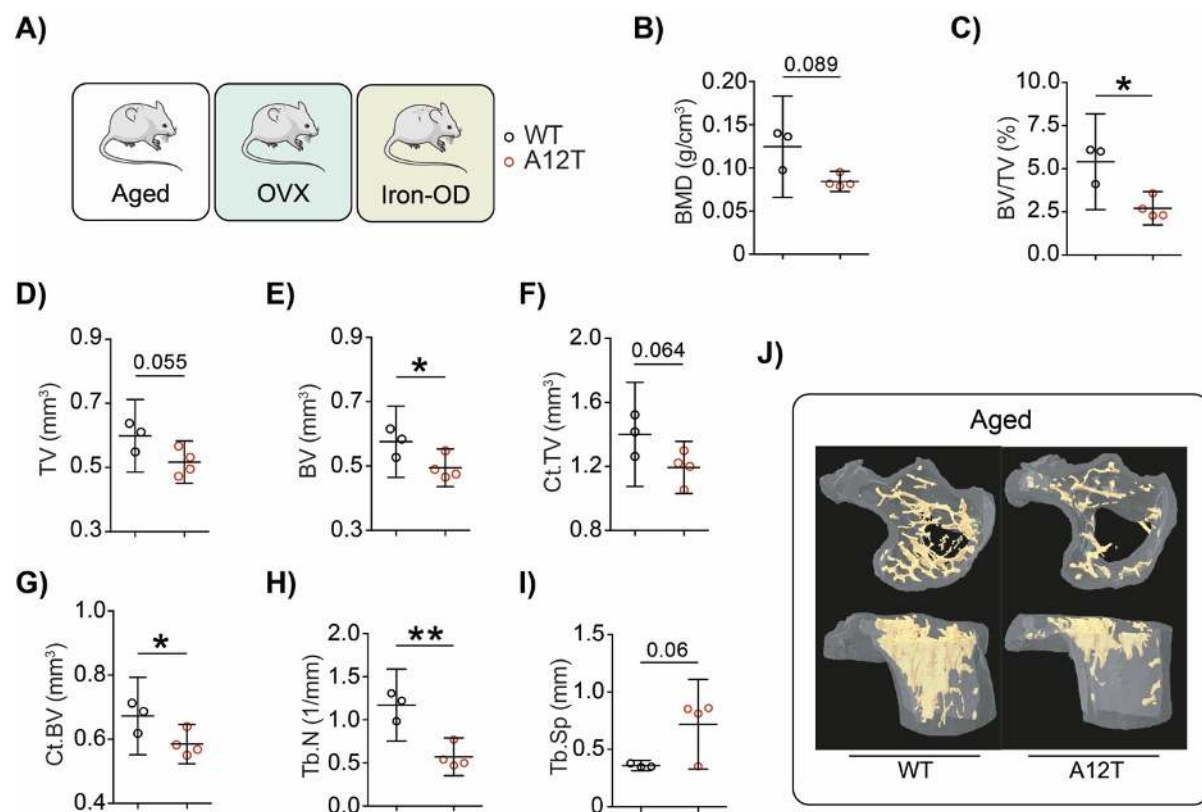


**Figure 7. BAF p.Ala12Thr enhances bone damage under physiological aging.** **A)** Scheme of the experimental design describing the three conditions examined in A12T mice, which include physiological aging (Aged), osteoporosis induced by ovariectomy (OVX) and oxidative stress induced by iron-overdose (Iron-OD). **B-I)** Quantitative analysis of cortical and trabecular bone parameters measured by high-resolution micro-computed tomography in tibiae in 21-month-old A12T males. **B)** Bone mineral density (BMD; g/cm<sup>3</sup>). **C)** Trabecular bone volume (BV/TV; %). **D-E)** Porous cortical bone volume (TV, mm<sup>3</sup>; BV, mm<sup>3</sup>). **F-G)** Cortical bone volume (Ct.TV, mm<sup>3</sup>; Ct.BV, mm<sup>3</sup>). **H)** Trabeculae number (Tb.N; 1/mm). **I)** Trabecular distance (Tb.Sp; mm). **J)** Representative three-dimensional longitudinal and transversal images of tibiae from 21-month-old WT and A12T males, generated with  $\mu$ CT analysis. Dots represent mean values  $\pm$  95% CI (WT n=3, A12T n=4). Analyzed by two-tailed Student's t test assuming same SD. \*p < 0.05, \*\*p < 0.01

To further evaluate these findings, we decided to expose A12T mice to two different bone stress conditions (Figure 8A). First, we induced an osteoporosis-like state by ovariectomizing 2-month-old wild-type and mutant female mice, which triggered the loss of crucial hormones in bone development<sup>198</sup>. Osteoporosis induction was confirmed by the decrease in uterus weight in ovariectomized mice (OVX) compared to control SHAM mice (Figure 8A). Two months after ovariectomy, A12T females showed a smaller relative and absolute bone size, and reduced trabecular thickness and connectivity compared to their WT littermates (Figure 8B-I). Further, ovariectomy was also performed in Hemi A12T females to evaluate if bone alterations could be also observed even with the presence of just one mutated allele of *Banf1* (Figure 4A). Interestingly, Hemi A12T mice showed a reduction in trabecular thickness, even under SHAM conditions (Figure 8J-K). Also, ovariectomized Hemi A12T females displayed a reduction in bone volume and size (Figure 8L-O) compared to ovariectomized WT animals.

Second, we exposed 2-month-old mice to an iron-overdose treatment that induced bone damage through oxidative stress<sup>169</sup>. Despite the different severity of the treatment between sexes, both treated male and female A12T mice showed lower bone mineral density than treated WT mice (Figure 9A-C). A12T female mice showed increased porosity with greater pore diameter, and fewer trabeculae and less connected (Figure 9D-H). In contrast, A12T male mice displayed a decrease in trabecular thickness and bone volume compared to WT littermates (Figure 9I-L).

Collectively, these findings under different bone-stressing challenges robustly link the development of bone defective structure with p.Ala12Thr mutation in mouse BAF, recapitulating the bone phenotype seen in NGPS patients.

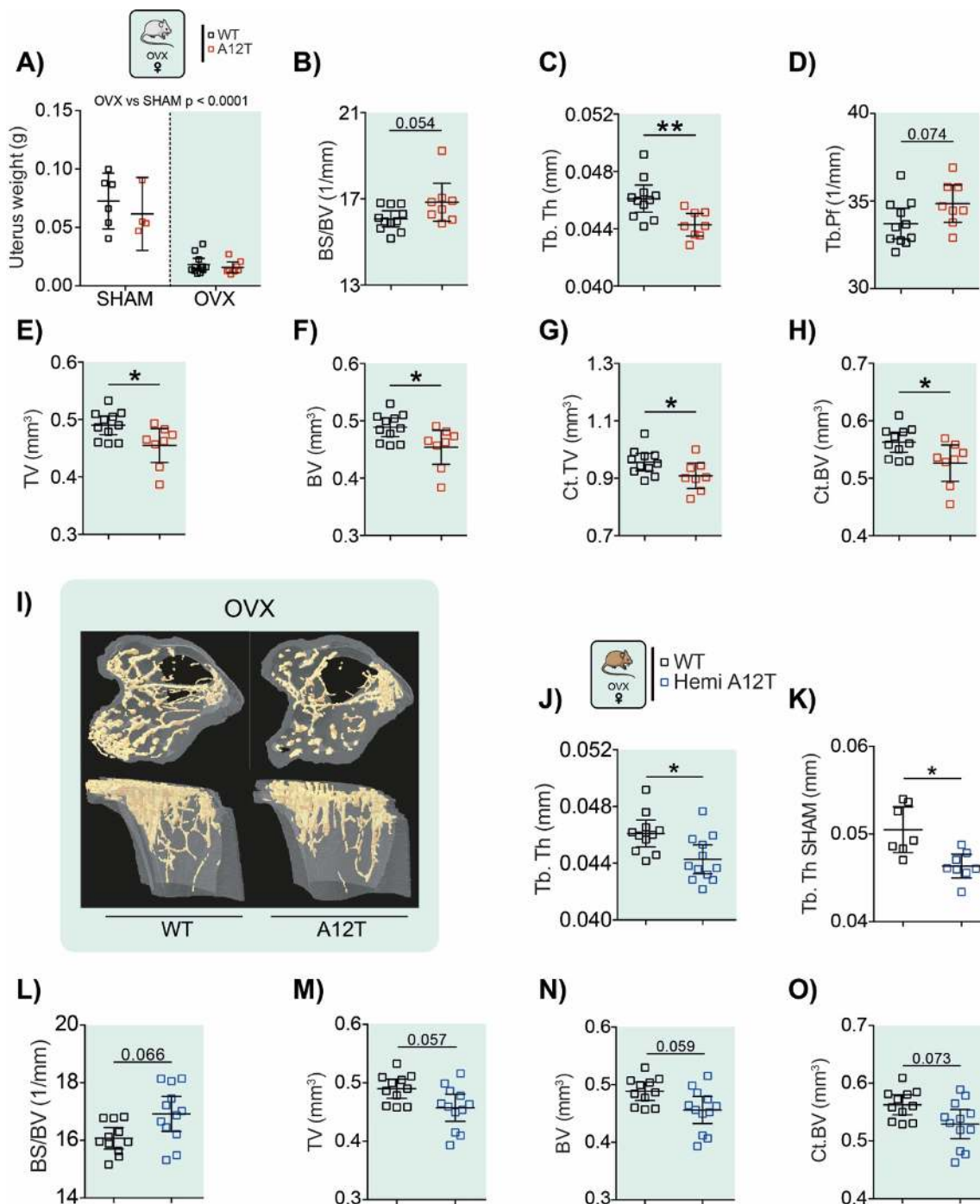


**Figure 8. Ala12Thr enhances bone damage under osteoporosis induction in ovariectomized mice (OVX).** **A)** Uterus weight in WT and A12T mice in SHAM or ovariectomy (OVX) conditions. Reduced uterus weight validates ovary depletion in OVX experimental groups (SHAM WT n=6, A12T n=4; OVX WT n=12, A12T n=8). Analyzed by two-way ANOVA ( $p < 0.0001$  for OVX-vs-SHAM analyses) with Sidak's correction for multiple comparisons. **B-H)** Quantitative analysis of cortical and trabecular bone parameters measured by high-resolution micro-computed tomography in tibiae in ovariectomized (OVX) mice. **B)** Bone size (BS/BV; 1/mm). **C)** Trabecular thickness (Tb.Th; mm). **D)** Trabecular connectivity (trabecular bone pattern factor, Tb.Pf, 1/mm). **E-F)** Porous cortical bone volume (TV, mm<sup>3</sup>; BV, mm<sup>3</sup>). **G-H)** Cortical bone volume (Ct.TV, mm<sup>3</sup>; Ct.BV, mm<sup>3</sup>) (OVX, WT n=11, A12T n=8; SHAM, WT n=6, A12T n=8). Analyzed by two-tailed Student's t test. **I)** Representative three-dimensional longitudinal and transversal images of WT and A12T tibiae in OVX conditions generated with  $\mu$ CT analysis. **J-O)** Quantitative analysis of cortical and trabecular bone parameters measured by high-resolution micro-computed tomography in tibiae in Hemi A12T ovariectomized (OVX) females. **J)** Trabecular thickness in OVX conditions (Tb.Th; mm). **K)** Trabecular thickness in SHAM conditions (Tb.Th SHAM; mm). **L)** Bone size (BS/BV; 1/mm). **M-N)** Porous cortical bone volume (TV, mm<sup>3</sup>; BV, mm<sup>3</sup>). **O)** Cortical bone volume (Ct.BV; mm<sup>3</sup>) (SHAM WT n=7, Hemi A12T n=8; OVX WT n=11, Hemi A12T n=12). Analyzed by Student's t test assuming same SD. \* $p < 0.05$ . Scatter dot blots represent mean  $\pm$  95% CI. \* $p < 0.05$ , \*\* $p < 0.01$ .

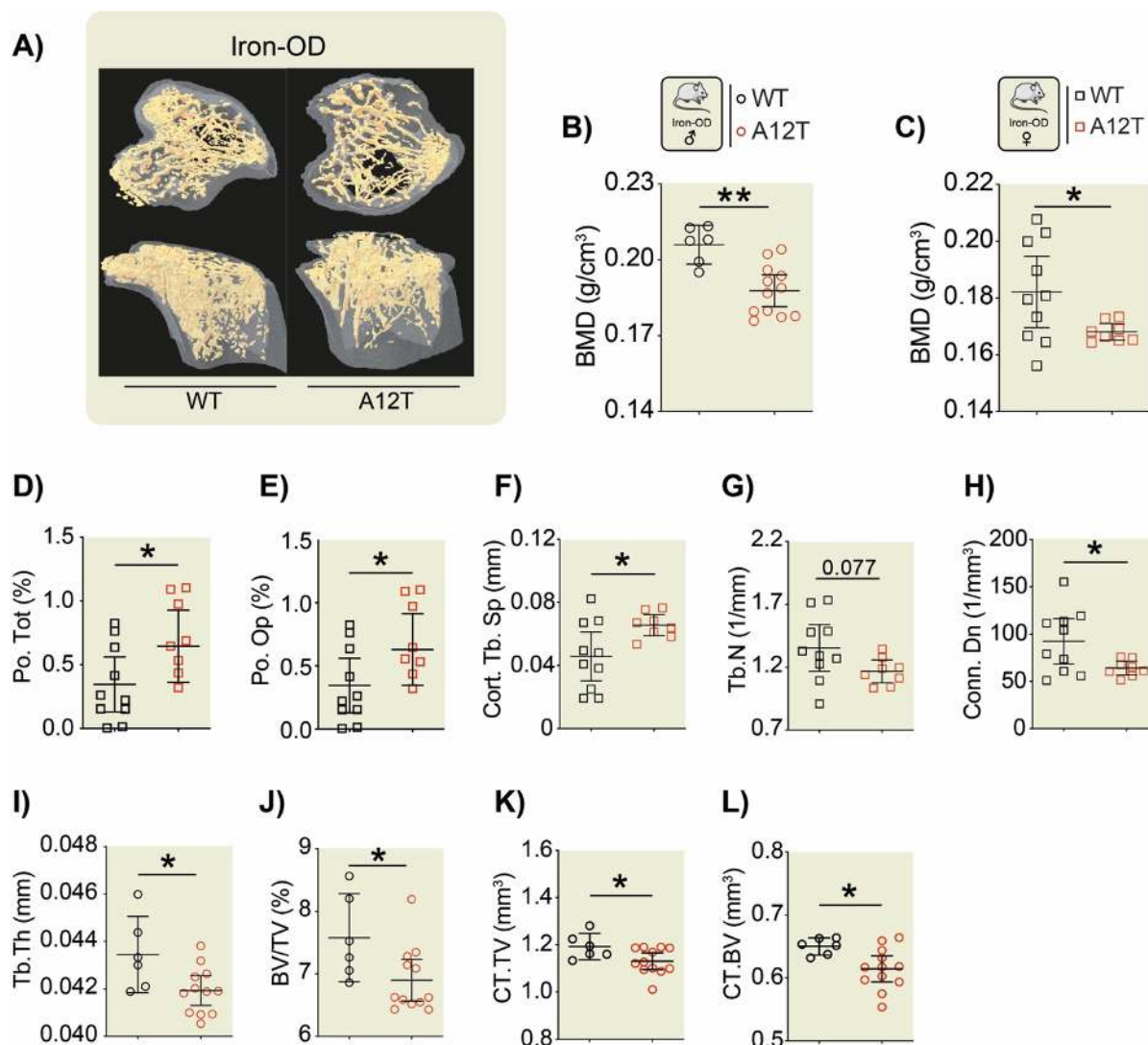


**Figure 9. Ala12Thr enhances bone damage under iron-overdose treatment in oxidative stress conditions.** **A)** Representative three-dimensional longitudinal and transversal images of WT and A12T tibiae in iron-overdose conditions generated with  $\mu$ CT analysis. **B-L)** Quantitative analysis of trabecular bone parameters measured by high-resolution micro-computed tomography in tibiae in iron-overdosed mice. **B-C)** Bone mineral density in B) males and C) females (BMD;  $\text{g}/\text{cm}^3$ ). In females: **D-E)** Porosity (Po. Tot, %; Po. Op, %). **F)** Pore thickness (Cort. Tb. Sp; mm). **G)** Trabecular number (Tb. N;  $1/\text{mm}$ ). **H)** Trabecular connectivity (Conn. Dn;  $1/\text{mm}^2$ ). In males: **I)** Trabecular thickness (Tb.Th; mm). **J)** Bone volume (BV/TV; %). **K-L)** Cortical bone volume (Ct.TV,  $\text{mm}^3$ ; Ct.BV,  $\text{mm}^3$ ). Scatter dot blots represent mean  $\pm$  95% CI (WT n=6, A12T n=12). Analyzed by two-tailed Student's t test. Empty circle dots represent males and empty square dots represent females. \* $p < 0.05$ , \*\* $p < 0.01$ .

To gain insight into the molecular mechanisms by which the BAF p.Ala12Thr mutation causes bone alterations, we explored bone turnover in A12T mice. Osteoclast and osteoblast activity was determined by measuring fragments of type I collagen (CTX-I) and procollagen I N-terminal propeptide (PINP) released in serum during renewal of the skeleton matrix or bone formation, respectively. In both cases, A12T mice displayed similar levels of CTX-I and PINP compared to WT mice, suggesting that the bone alterations observed in mice were not likely caused by changes in bone formation or resorption rates (Figure 10A-B). We then performed

RNAseq of bone marrow and bone tissue extracted from tibia from 2-year-old A12T and WT mice. Differential expression analysis in bone marrow showed no differences in A12T compared to WT mice (Figure 10C), which, together with CTX-I and PINP values, suggests that bone alterations would not come from a dysregulation in osteoclast/osteoblast differentiation. Differential expression analysis in bone tissue, however, showed increased levels of 28 transcripts in A12T mice compared to WT littermates (Figure 10D). Among those, there were several genes associated with collagen biosynthesis and bone physiology, some of them related to a rare syndrome known as Osteogenesis Imperfecta (OI). OI is a heterogeneous group of disorders characterized by low bone mass, reduced bone material strength and bone fragility<sup>199,200</sup>. 85-90% of the cases are defined by autosomal dominant mutations in the collagen genes *Col1a1* and *Col1a2* and their clinical phenotypes vary from mild to lethal<sup>201</sup>. When we compared our transcriptome from bone tissue of A12T animals with data from *Col1a1<sup>irt/+</sup>* and *Col1a2<sup>oim/oim</sup>* mice, two well-established mouse models of OI, we observed that some genes representative of both models, such as *Cyp2e1*, *Col11a2*, *Fkbp10*, *Cpz* or *Ano1*, were also upregulated in A12T mice (Table S1)<sup>202</sup>. In addition, gene set enrichment analysis (GSEA) of A12T data showed a strong correlation with the transcriptome of *Col1a1<sup>irt/+</sup>* and *Col1a2<sup>oim/oim</sup>*, triggering the idea that A12T mice phenocopies some of the bone alterations seen in OI (Figure 10E-F). GSEA of bone tissue using hallmarks gene sets also showed an upregulation of epithelial dedifferentiation, interferon, and UV-damage response pathways, while G2M checkpoints and E2F targets appeared downregulated (Figure 10G). Further, this aging phenotype was confirmed analyzing gene ontology (GO) and Reactome pathways, which showed an upregulation of bone and inflammation related pathways and a downregulation of mitotic and mitochondrial pathways (Figure 10H-I).

Altogether, bone alterations in A12T mice recapitulate an OI-like phenotype rather than osteoblast or osteoclast activity unbalance. Bone transcriptomics revealed an inflammatory state through an increase in the interferon response and a boost of skeletal development pathways, probably due to a compensation of bone damage. Also, the transcriptomic profile indicated that DNA damage checkpoints and mitosis-related pathways were downregulated, probably implying increased senescence and accumulation of mutations. Finally, consistent with a cell aging phenotype, bone transcriptomics exhibited a downregulation of mitochondrial activity and cellular respiration.

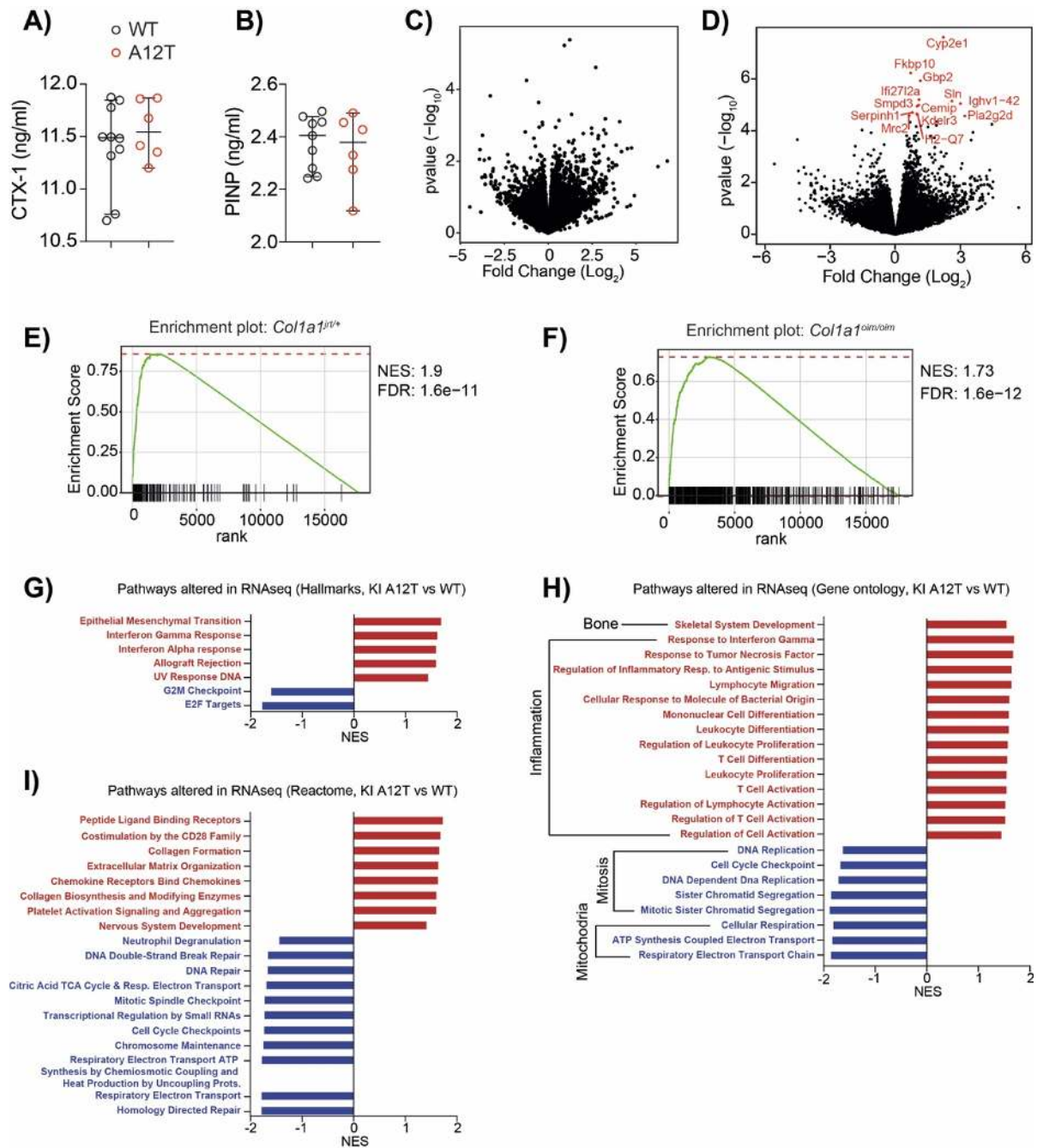


**Figure 10. Gene expression in tibia and bone marrow of 24-month-old A12T mice. A-B)** Levels of **A)** CTX-1 and **B)** PINP as markers of osteoclast and osteoblast activity respectively, in 4-6 month-old males. (WT, black, n=9-10; A12T, red, n=6). Analyzed by two-tailed Student's t test. Scatter dot blots represent mean  $\pm$  95% CI. **C-D)** Volcano plots of the **C)** tibia and **D)** bone transcriptomics. X-axis represent the logarithm (base 2) of fold change (log<sub>2</sub>) and Y-axis shows the antilogarithm (base 10) of the p-value (p value, -log<sub>10</sub>). Transcripts significantly up-regulated (FDR < 0.05) are depicted in red. **E-F)** Enrichment score plots from GSEA in A12T bone samples using gene-sets derived from the upregulated genes in **E)** *Col1a1<sup>fl/fl</sup>* and **F)** *Col1a1<sup>oim/oim</sup>* transcriptomes. ES: enrichment score; FDR: false discovery rate. **G-I)** Gene-set enrichment analysis of **G)** hallmarks, **H)** gene ontology (GO) (biological process) and **I)** reactome gene sets in A12T compared to WT mice. Bars represent the normalized enrichment score (NES). Red color indicates upregulated pathways and blue indicates downregulated pathways. GO pathways are grouped according to their role in bone remodeling, inflammation, mitosis or mitochondrial activity.

## 2. Evaluation of dietary interventions to counteract nutrient sensing deregulation associated to pathological aging.

Nicotinamide adenine dinucleotide (NAD<sup>+</sup>) is an essential metabolite with several roles in cellular biology. High-energy states, which are defined by a low NAD<sup>+</sup>/NADH ratio, have been correlated with aging and the appearance of aging-related diseases<sup>203</sup>. In fact, premature aging syndromes usually present an aging-like metabolic shift with low NAD<sup>+</sup> levels and marked catabolism due to the overactivation of DNA-damage responses. Meanwhile, low-energy states with high levels of NAD<sup>+</sup> trigger the activation of pro-survival pathways that enhance lifespan and health<sup>204</sup>. Hence, NAD<sup>+</sup> metabolism has arisen as a promising therapeutic approach to delay aging onset.

Amon others, NAD<sup>+</sup> levels can be increased directly through diet supplementation with NAD<sup>+</sup> precursors such as nicotinamide riboside (NR), nicotinamide (NAM), nicotinamide mononucleotide (NMN) and nicotinic acid or niacin (NA)<sup>205,206</sup>. In this regard, recent studies have proven the beneficial effects of NAD<sup>+</sup> supplementation *in vivo* to treat several aging-related diseases in mice, while diet supplementation with NAD<sup>+</sup> precursors appear to be safe and efficient both in mice and humans<sup>207-210</sup>.

Taking this in consideration, in this section we explored the potential benefits of NR and niacin supplementation in premature aging, using *Zmpste24*<sup>-/-</sup> mice as a well-established model of premature aging. *Zmpste24* is a key enzyme of lamin A maturation and its absence produces an aberrant farnesylated lamin A form that disturbs nuclear envelope scaffold and causes a premature aging syndrome known as Restrictive Dermopathy<sup>211,212</sup>. *Zmpste24*<sup>-/-</sup> mice are characterized by an extreme aged phenotype with bone, cardiovascular and metabolic alterations that shorten their lifespan<sup>213</sup>. NR and niacin supplementation improves many of these aging features, enhancing healthspan and extending lifespan. Altogether, this study opens the possibility to introduce NAD<sup>+</sup> boosting with NR and niacin supplementation in diet as a reliable therapy of premature aging disorders.

## 2.1. Physiological characterization of NAD<sup>+</sup> boost through NR and niacin supplementation in *Zmpste24*<sup>-/-</sup> and *Lmna*<sup>G609G/G609G</sup> mice

To evaluate the potential benefits of a direct NAD<sup>+</sup> supplementation in diet, *Zmpste24*<sup>-/-</sup> and wild-type mice were fed either with NR-supplemented or control diets. The NR-supplemented diet extended median lifespan in *Zmpste24*<sup>-/-</sup> mice by 17%, especially in females (Figure 11A-C), while body weight remained unchanged compared to the progeroid mice fed a control diet (Figure 11D-E). Notably, *Zmpste24*<sup>-/-</sup> males with NR diet showed decreased glucose levels and body temperature compared to *Zmpste24*<sup>-/-</sup> males under control diet, an effect that was not observed in females (Figure 11F-G). The metabolic shift observed in *Zmpste24*<sup>-/-</sup> mice was partially reverted by NR-diet, including energy expenditure and oxygen consumption during the day, together with a greater carbohydrate-based metabolism during the inactive phase (Figure 11H-J).

At the histological level, *Zmpste24*<sup>-/-</sup> mice supplemented with NR displayed a macroscopic recovery of spleen size compared to untreated *Zmpste24*<sup>-/-</sup> mice (Figure 12A). Also, NR induced an amelioration in several histological alterations previously described in progeroid mice<sup>214</sup>, with an improvement of the lesion score in quadriceps, a thicker stomach wall and a reduction of the pathological thickness of adventitia in the aorta (Figure 12B-D). At the blood level, NR-supplemented diet induced a reduction of MID cells (monocytes, eosinophils, basophils, blasts and other precursor white cells) and both total and oxygen-carrying hemoglobin (Figure 12E-H). Bones in *Zmpste24*<sup>-/-</sup> mice exhibit large alterations compared to wild-type mice that were partially recovered with NR-diet. Tibiae of *Zmpste24*<sup>-/-</sup> mice showed increased density with higher and better-connected trabeculae (Figure 12I-M). Surprisingly, wild-type mice fed with NR diet displayed a bone structure closer to the progeria-phenotype (Figure 12I-M), losing bone density and trabeculae connection even in the cortical bone, which was not so affected in *Zmpste24*<sup>-/-</sup> mice under the NR diet (Figure 12N-R).

To validate our results with NR supplementation, we decided to boost the NAD<sup>+</sup> pool in *Zmpste24*<sup>-/-</sup> mice by feeding either with niacin-supplemented or control diet. *Zmpste24*<sup>-/-</sup> mice supplemented with niacin showed a medium and maximal lifespan extension compared to untreated progeroid littermates, especially in males (Figure 13A-C). *Zmpste24*<sup>-/-</sup> mice under niacin diet did not display changes in body weight,

while a body weight decrease was described in wild-type animals fed with niacin (Figure 13D-F). Despite the lack of changes in weight, *Zmpste24*<sup>-/-</sup> mice fed with niacin diet showed a healthier aspect (Figure 13G) that was accompanied by a marked increase in glucose levels and body temperature compared to *Zmpste24*<sup>-/-</sup> mice kept under control diet, exhibiting a restoration of the progeroid phenotype in both parameters (Figure 13H-I).

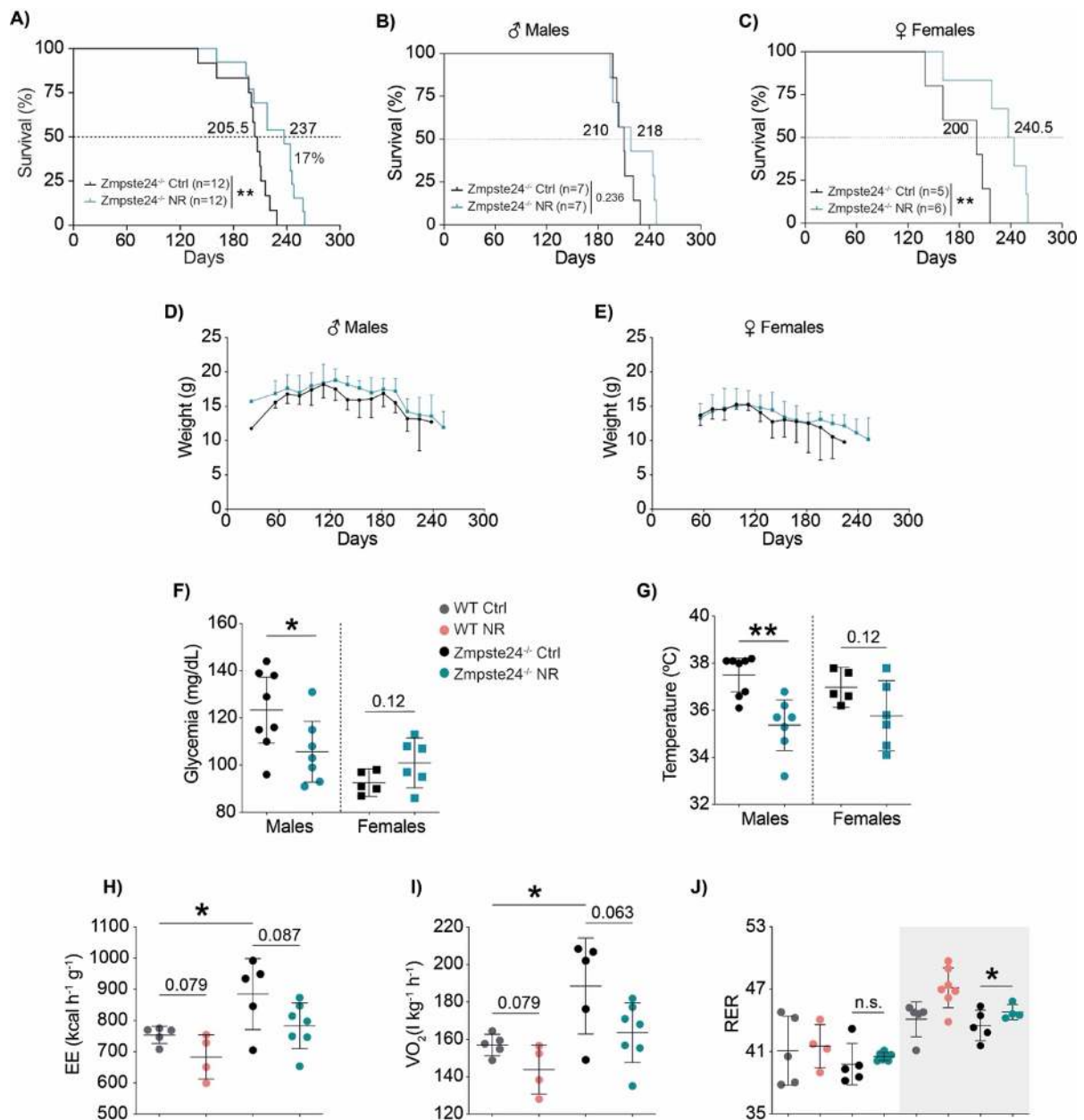
Taking into account the lifespan extension observed in *Zmpste24*<sup>-/-</sup> mice under both NR and niacin supplementation, we decided to explore these interventions in the well-established mouse model of progeria *Lmna*<sup>G609G/G609G</sup>. *Lmna*<sup>G609G/G609G</sup> males fed with NR-supplemented diet did not display any changes in longevity compared to their *Lmna*<sup>G609G/G609G</sup> littermates under control diet (Figure 14A). However, *Lmna*<sup>G609G/G609G</sup> NR showed lower body weight at the age of 4 months, when the phenotype-related body weight decline begins (Figure 14B). Further, hypoglycemia was accentuated under NR diet in *Lmna*<sup>G609G/G609G</sup> mice (Figure 14C).

Hemogram analysis showed great alterations in *Lmna*<sup>G609G/G609G</sup> compared to wild-type mice (Figure 14D-H). When supplemented with NR, *Lmna*<sup>G609G/G609G</sup> mice displayed an enhanced blood cell phenotype specially in the red line, exhibiting alterations in red blood size and shape (Figure 14D-E) and changes in hemoglobin distribution, with increased total concentration but lower levels of oxygen-carrying hemoglobin in the red blood cells (Figure 14F-G). Additionally, platelet size was also further reduced under NR supplementation (Figure 14H).

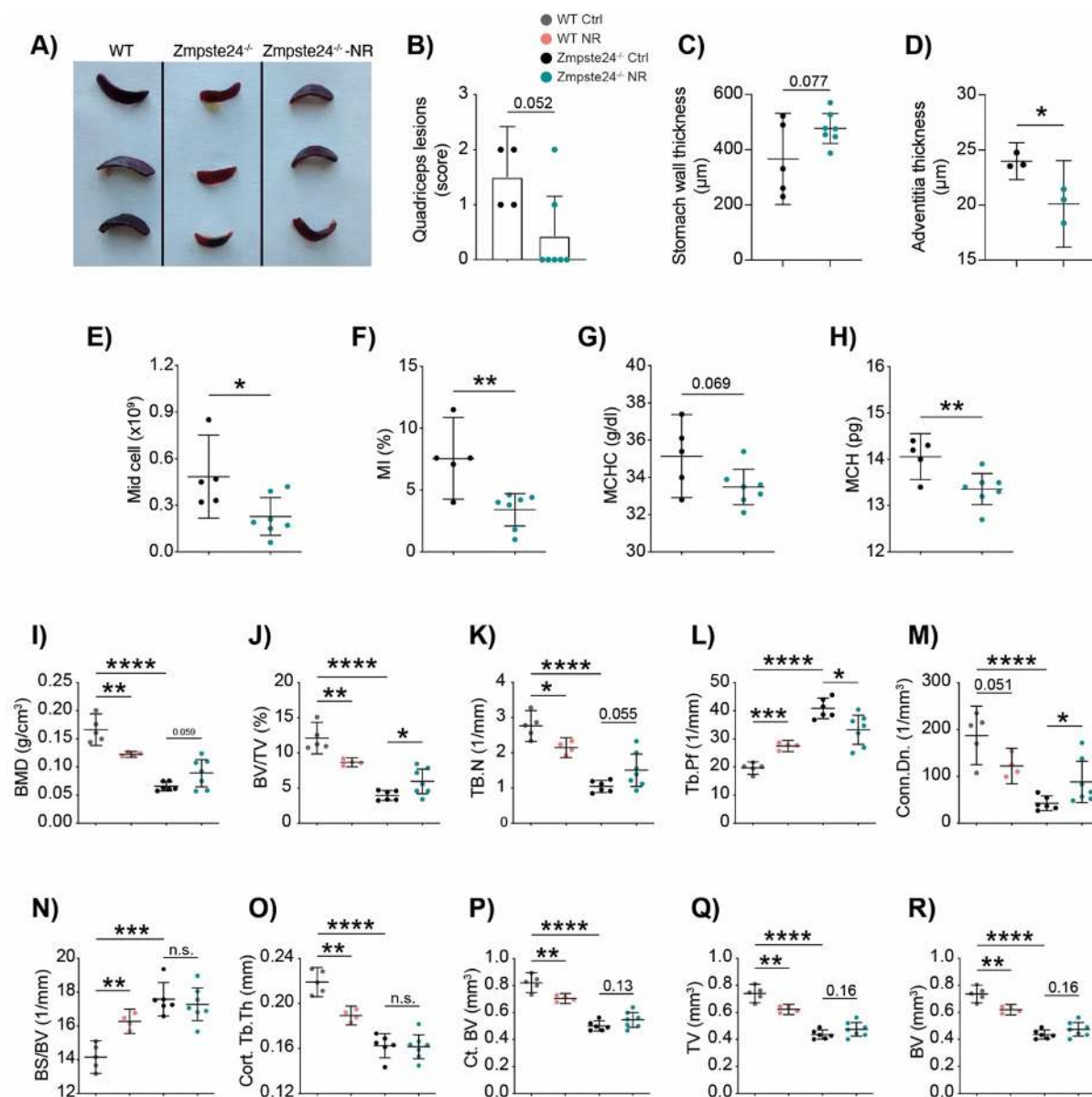
As described in previous studies<sup>214</sup>, *Lmna*<sup>G609G/G609G</sup> mice suffer severe metabolic adaptations and lipodystrophy. When fed with NR diet, *Lmna*<sup>G609G/G609G</sup> mice intensified those metabolic adaptations with increased CO<sub>2</sub>-VO<sub>2</sub> interchange and increased energy expenditure, observations that were absent in the WT mice with and without supplementation (Figure 14I-K). However, wild-type mice fed with NR diet switched their metabolism to an enhanced carbohydrate-metabolism, similar to what is seen in progeroid mice (Figure 14L).

Finally, we tested the effect of niacin in *Lmna*<sup>G609G/G609G</sup> males by feeding the mice with either niacin-supplemented or control diet. Niacin supplementation did not affect lifespan nor body weight in *Lmna*<sup>G609G/G609G</sup> males (Figure 15A-B). Also, contrary to NR supplementation, WT mice fed a niacin-enriched diet did not show a reduced body weight (Figure 15B). As seen in NR diet, *Lmna*<sup>G609G/G609G</sup> males fed niacin did not evidence any change neither in the progeroid metabolic switch nor movement

compared to progeroid mice under control diet (Figure 15C-D). However, *Lmna*<sup>G609G/G609G</sup> males fed the niacin diet evidenced an increase in body temperature compared to *Lmna*<sup>G609G/G609G</sup> males fed control diet (Figure 15E). Altogether, these results show that feeding *Lmna*<sup>G609G/G609G</sup> mice either NR or niacin-enriched diets does not ameliorate the accelerated-aging phenotype and it could be even detrimental for several of the classically affected parameters in progeria, such as body weight, glycemia, blood cells composition and energetic metabolism.



**Figure 11. NR supplementation in *Zmpste24*<sup>-/-</sup> mice increases lifespan and alters metabolism *in vivo*.** **A-C)** Survival plot of *Zmpste24*<sup>-/-</sup> **A)** mice, **B)** males and **C)** females fed with control and NR diets. Survival curves were analyzed with the log-rank (Mantel Cox) test (p=0.0059; males p=0.236; females p=0.0091) and Gehan-Breslow-Wilcoxon test (p=0.0384; males p=0.61; females p=0.0232). **D-E)** Body weight curve in *Zmpste24*<sup>-/-</sup> **D)** males and **E)** females. Multiple t-test assuming same standard deviation (SD). **F)** Glucose levels of *Zmpste24*<sup>-/-</sup> males and females fed with control or NR diet after 6h of fasting at the age of 3 months. Analysis made by Student's t test assuming same SD (males, p=0.0465; females, p=0.12). **G)** Body temperatures of *Zmpste24*<sup>-/-</sup> males and females fed with control and NR diet at the age of 3 months. Analysis made by Student's t test assuming same SD (males, p=0.0013; females, p=0.12). (*Zmpste24*<sup>-/-</sup> Ctrl, black, all n=12-13, males n=7-8, females n=5; *Zmpste24*<sup>-/-</sup> NR, green, all n=13, males n=7, females n=6). **H-J)** Indirect calorimetry measured with the Oxymax-CLAMS system, representing the mean measurements during day and night in 4-month-old males. **H)** Energy expenditure (EE; kilocalories per kilogram per hour). **I)** Oxygen consumption (VO<sub>2</sub>; milliliters per kilogram per hour). **J)** Respiratory exchange ratio (RER; VCO<sub>2</sub>/VO<sub>2</sub>) (WT Ctrl, grey, n=5; WT NR, red, n=4; *Zmpste24*<sup>-/-</sup> Ctrl, black, n=5; *Zmpste24*<sup>-/-</sup> NR, green, n=7). White background means day analysis while grey background indicates night measurements. Analyzed by Student's t test assuming same SD. Dots and scatter dot blots represent mean ± 95% CI. \*p < 0.5, \*\*p < 0.01.



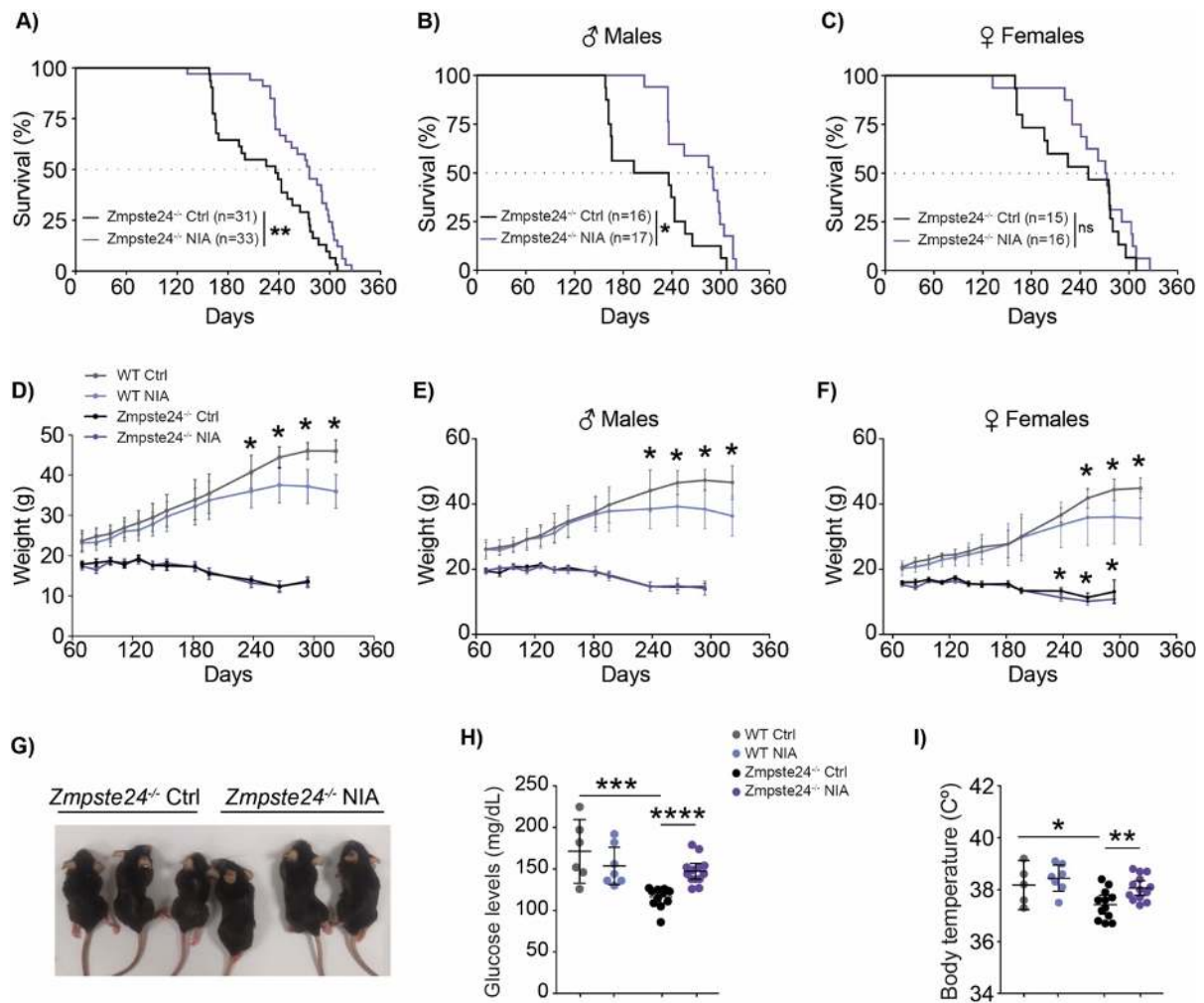


**Figure 13. NAD<sup>+</sup> boost with niacin supplementation extends lifespan and improves health in *Zmpste24*<sup>-/-</sup> mice.** **A-C)** Survival plot of *Zmpste24*<sup>-/-</sup> **A)** mice, **B)** males and **C)** females fed with control and niacin diet (*Zmpste24*<sup>-/-</sup> Ctrl, black, n=31; *Zmpste24*<sup>-/-</sup> NIA, purple, n=33). Survival curves were analyzed with the log-rank (Mantel Cox) test (p=0.0037) and Gehan-Breslow-Wilcoxon test (p=0.0022). **D-F)** Body weight curve in wild-type and *Zmpste24*<sup>-/-</sup> **D)** mice, **E)** males and **F)** females (WT Ctrl, grey, all n=9, males n=5, females n=4; WT NIA, blue, all n=12, males n=6, females n=6; *Zmpste24*<sup>-/-</sup> Ctrl, black, all n=32, males n=17, females n=15; *Zmpste24*<sup>-/-</sup> NIA, purple, all n=33, males n=17, females n=16). Multiple t-test assuming same standard deviation (SD). **G)** Representative photograph 7-month-old mice of the indicated genotypes representing the phenotype improvement in *Zmpste24*<sup>-/-</sup> mice with niacin diet compared to *Zmpste24*<sup>-/-</sup> control after 5.5 months of niacin treatment. **H)** Glucose levels and body temperatures of wild-type and *Zmpste24*<sup>-/-</sup> mice fed with control or niacin diet (after 6h of fasting in the glucose test) at the age of 4 months (WT Ctrl, n=5-6; WT NIA, n=7; *Zmpste24*<sup>-/-</sup> Ctrl, n=12; *Zmpste24*<sup>-/-</sup> NIA, n=13). Analysis made by Student's t test assuming same SD. Glucose, *Zmpste24*<sup>-/-</sup> vs WT, p=0.0002; *Zmpste24*<sup>-/-</sup> NIA vs Ctrl, p < 0.0001. Body temperature, *Zmpste24*<sup>-/-</sup> vs WT, p=0.039; *Zmpste24*<sup>-/-</sup> NIA vs Ctrl, p=0.0058. Dots and scatter dot blots represent mean values and errors ± 95 % of confidence interval (CI). \*p < 0.05, \*\*p < 0.01, \*\*\*p < 0.001, \*\*\*\*p < 0.0001.

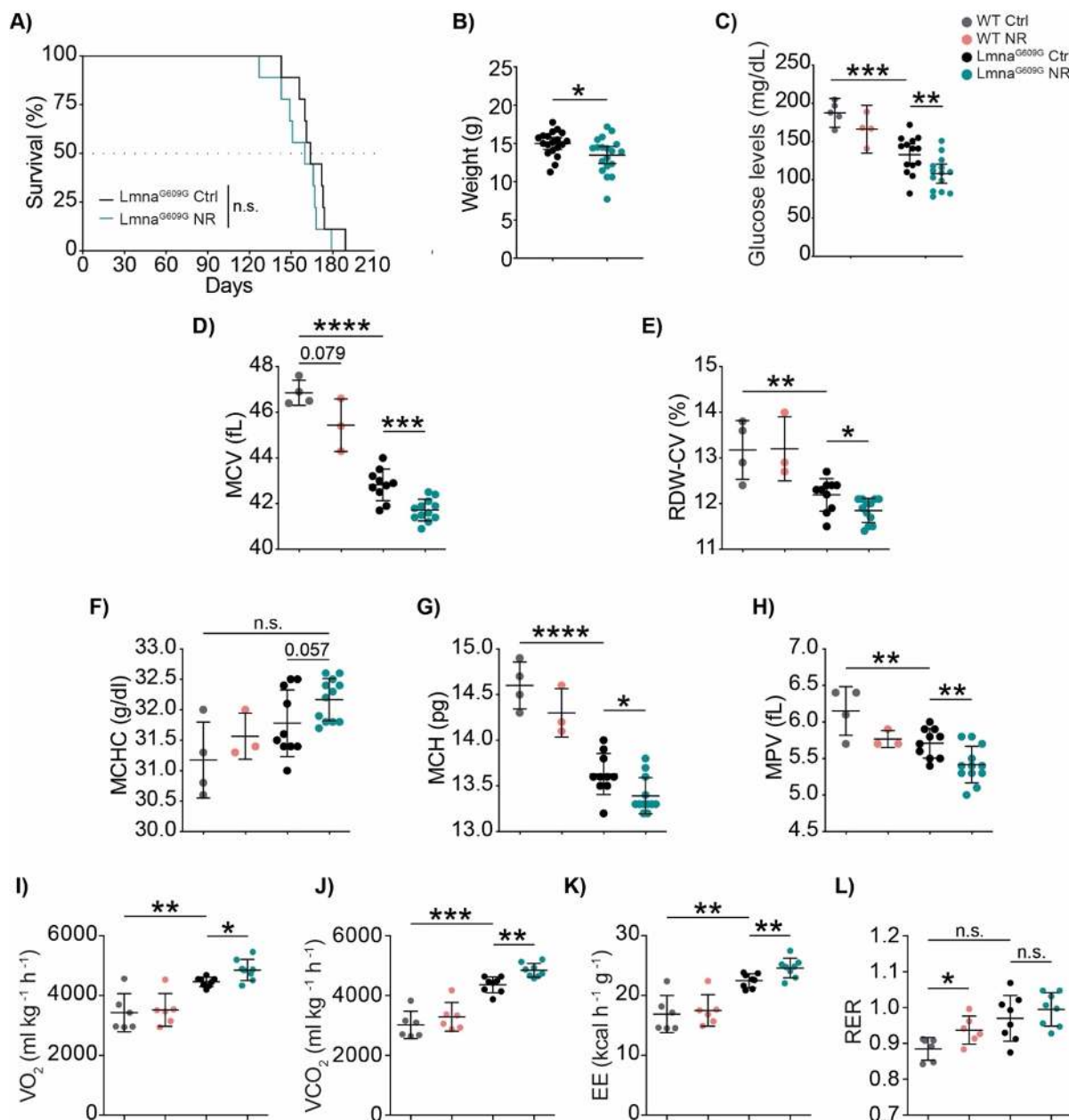


**Figure 14. The main features of accelerated aging are not ameliorated in the *Lmna*<sup>G609G/G609G</sup> progeria mouse model under NR diet.** **A)** Survival plot of *Lmna*<sup>G609G/G609G</sup> males fed with control and NR diet (*Lmna*<sup>G609G</sup> Ctrl, black, n=9; *Lmna*<sup>G609G</sup> NR, green, n=9). Survival curves were analyzed with the log-rank (Mantel Cox) test (p = 0.3) and Gehan-Breslow-Wilcoxon test (p = 0.27). **B)** Body weight analysis of *Lmna*<sup>G609G/G609G</sup> mice at the age of 4 months fed with control and NR diet (*Lmna*<sup>G609G</sup> Ctrl, n=19; *Lmna*<sup>G609G</sup> NR, n=19). Analysis made by Student's t test assuming same SD (p = 0.026). **C)** Glucose levels of wild-type and *Lmna*<sup>G609G/G609G</sup> males fed with control or NR diet at the age of 4 months after 5h of fasting (WT Ctrl, grey, n=5; WT NR, red, n=4; *Lmna*<sup>G609G</sup> Ctrl, black, n=14; *Lmna*<sup>G609G</sup> NR, green, n=14). Analysis made by Student's t test assuming same SD (*Lmna*<sup>G609G</sup> vs WT, p=0.0002; WT NR vs Ctrl, p=0.108; *Lmna*<sup>G609G</sup> NR vs Ctrl p=0.0078). **D-H)** Blood counts of peripheral blood from 4-months-old males. **D)** Mean corpuscular volume (MCV; fL). **E)** Red cell distribution width (RDW-CV; %). **F)** Mean corpuscular hemoglobin concentration (MCHC; g/dl). **G)** Mean corpuscular hemoglobin (MCH; pg). **H)** Mean platelet volume (MPV; fL) (WT Ctrl, n=4; WT NR, n=3; *Lmna*<sup>G609G</sup> Ctrl, n=10; *Lmna*<sup>G609G</sup> NR, n=12). Analysis made by Student's t test assuming same SD. **I-L)** Indirect calorimetry measured by Oxymax-CLAMS system, representing the mean measurements during night in 4-month-old males. **I)** Oxygen consumption (VO<sub>2</sub>; milliliters per kilogram per hour). **J)** Carbon dioxide production (VCO<sub>2</sub>; milliliters per kilogram per hour). **K)** Energy expenditure (kilocalories per kilogram per hour). **L)** Respiratory exchange ratio (RER; VCO<sub>2</sub>/VO<sub>2</sub>) (WT Ctrl, n=6; WT NR, n=6; *Lmna*<sup>G609G</sup> Ctrl, n=8; *Lmna*<sup>G609G</sup> NR, n=8). Analyzed by Student's t test assuming same SD. Dots represent mean values and errors ± 95 % of confidence interval (CI). \*p < 0.05, \*\*p < 0.01, \*\*\*p < 0.001, \*\*\*\*p < 0.0001.

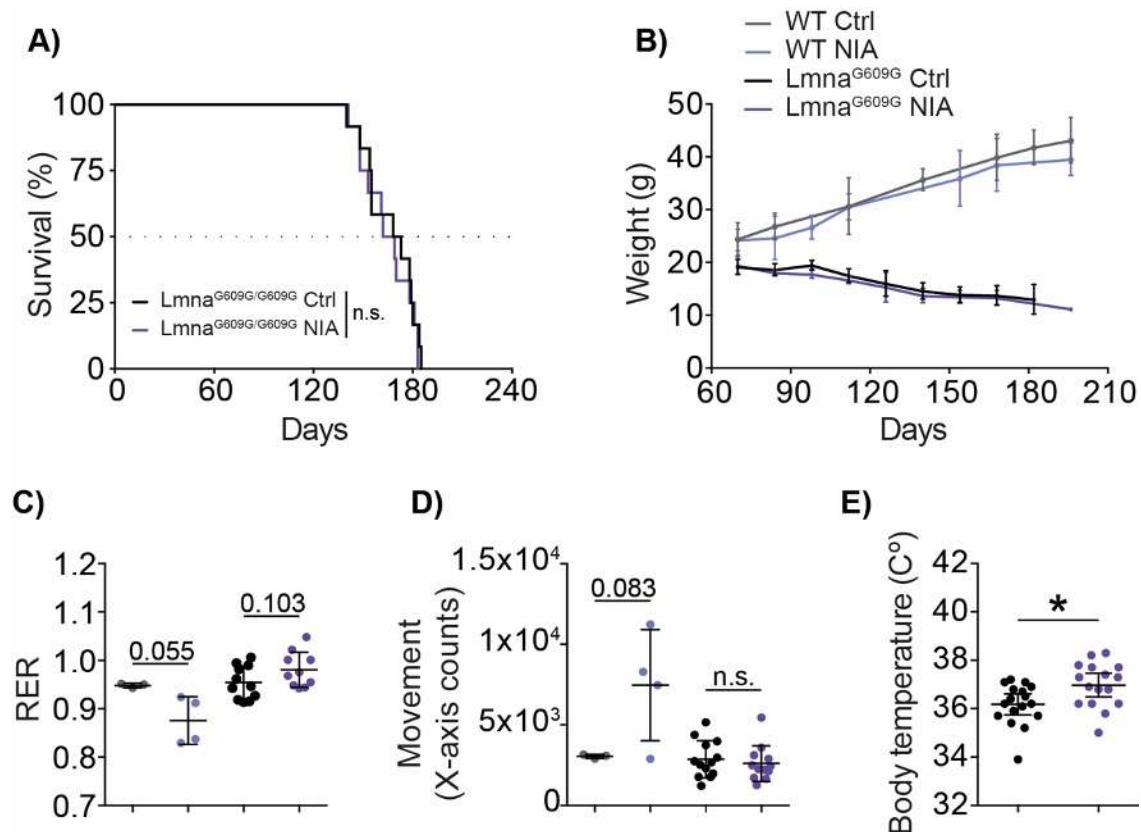


**Figure 15. The main features of accelerated aging are not ameliorated in the *Lmna*<sup>G609G/G609G</sup> progeria mouse model under niacin diet.** **A)** Survival plot of *Lmna*<sup>G609G/G609G</sup> males fed control and niacin diet (*Lmna*<sup>G609G</sup> Ctrl, black, n=12; *Lmna*<sup>G609G</sup> NIA, purple, n=12). Survival curves were analyzed with the log-rank (Mantel Cox) test and Gehan-Breslow-Wilcoxon test. **B)** Body weight curve in wild-type and *Lmna*<sup>G609G/G609G</sup> males (WT Ctrl, grey, n=3; WT NIA, blue, n=4; *Lmna*<sup>G609G</sup> Ctrl, black, n=12; *Lmna*<sup>G609G</sup> NIA, purple, n=12). Multiple t-test assuming same standard deviation (SD). **C-D)** Indirect calorimetry measured by Oxymax-CLAMS system, representing the mean measurements during night in 4-month-old males. **C)** Respiratory exchange ratio (RER;  $VCO_2/VO_2$ ). **D)** Movement (movement X-axis; counts) (WT Ctrl, n=3; WT NIA, n=4; *Lmna*<sup>G609G</sup> Ctrl, n=11; *Lmna*<sup>G609G</sup> NIA, n=10). Analyzed by Student's t test assuming same SD. **E)** Body temperatures of *Lmna*<sup>G609G/G609G</sup> males fed control and niacin diet at the age of 4 months (*Lmna*<sup>G609G</sup> Ctrl, n=17; *Lmna*<sup>G609G</sup> NIA, n=16). Analysis made by Student's t test assuming same SD (p=0.014). Dots and scatter dot blots represent mean  $\pm$  95% CI. \*p < 0.05.

## 2.2. Description of the transcriptomic profile in liver of *Zmpste24*<sup>-/-</sup> mice after NAD<sup>+</sup> supplementation

To deepen the molecular basis of this global amelioration of *Zmpste24*<sup>-/-</sup> mice fed NR diet, we performed RNA-seq analysis in liver tissues of 4-months-old mice. PCA analysis exposed profound differences in the transcriptome of *Zmpste24*<sup>-/-</sup> mice compared to wild type littermates. Supplementation with NR induced a partial recovery of the *Zmpste24*<sup>-/-</sup> transcriptome while it did not evidence major changes in wild-type mice (Figure 16A). Based on the GSEA results, we observed large basal differences between *Zmpste24*<sup>-/-</sup> and WT mice in many central and metabolic pathways from cellular to systemic level, similar to previous studies<sup>214</sup>. At the cellular level, growth signaling via mTORC1 and KRAS signaling is markedly upregulated in *Zmpste24*<sup>-/-</sup> mice, together with a shift in cellular energetics with a decrease in peroxisome and oxidative phosphorylation, and an upregulation of hypoxic genes expression. At the systemic level, adipogenesis, fatty acid and bile acid metabolism are notably decreased, while cholesterol homeostasis genes increase their expression (Figure 16B). Further, inflammation, including interferon and inflammatory responses and IL6-JAK-STAT3 signaling, was highly increased in *Zmpste24*<sup>-/-</sup>. NR diet reverts many of these changes in cellular pathways in *Zmpste24*<sup>-/-</sup> mice, inducing a recovery in pathways such as growth signaling, peroxisome genes and ROS defense. The amelioration is also observed in the main metabolic pathways, with an increase in adipogenesis, fatty acid and bile acid metabolism, which is especially relevant taking into account the last interventions described in *Zmpste24*<sup>-/-</sup> mice (Figure 16B-D)<sup>214,215</sup>. Although inflammation does not seem to be altered after NAD<sup>+</sup> boost, NR-supplementation in *Zmpste24*<sup>-/-</sup> mice increases heme metabolism and reduces hypoxia responses (Figure 16D), which could be related with the changes in hemoglobin described in blood cells (Figure 12G-H). Finally, we also observed in the *Zmpste24*<sup>-/-</sup> mice kept under the NR diet a complete recovery in the levels of major urinary proteins (MUPs), which are dramatically downregulated as part of the progeroid phenotype of these mice<sup>216,217</sup>. Thus, while *Zmpste24*<sup>-/-</sup> had a reduction in the transcript levels of MUPs, NR diet restored the expression of almost all proteins to levels comparable to wild-type (Figure 16E).

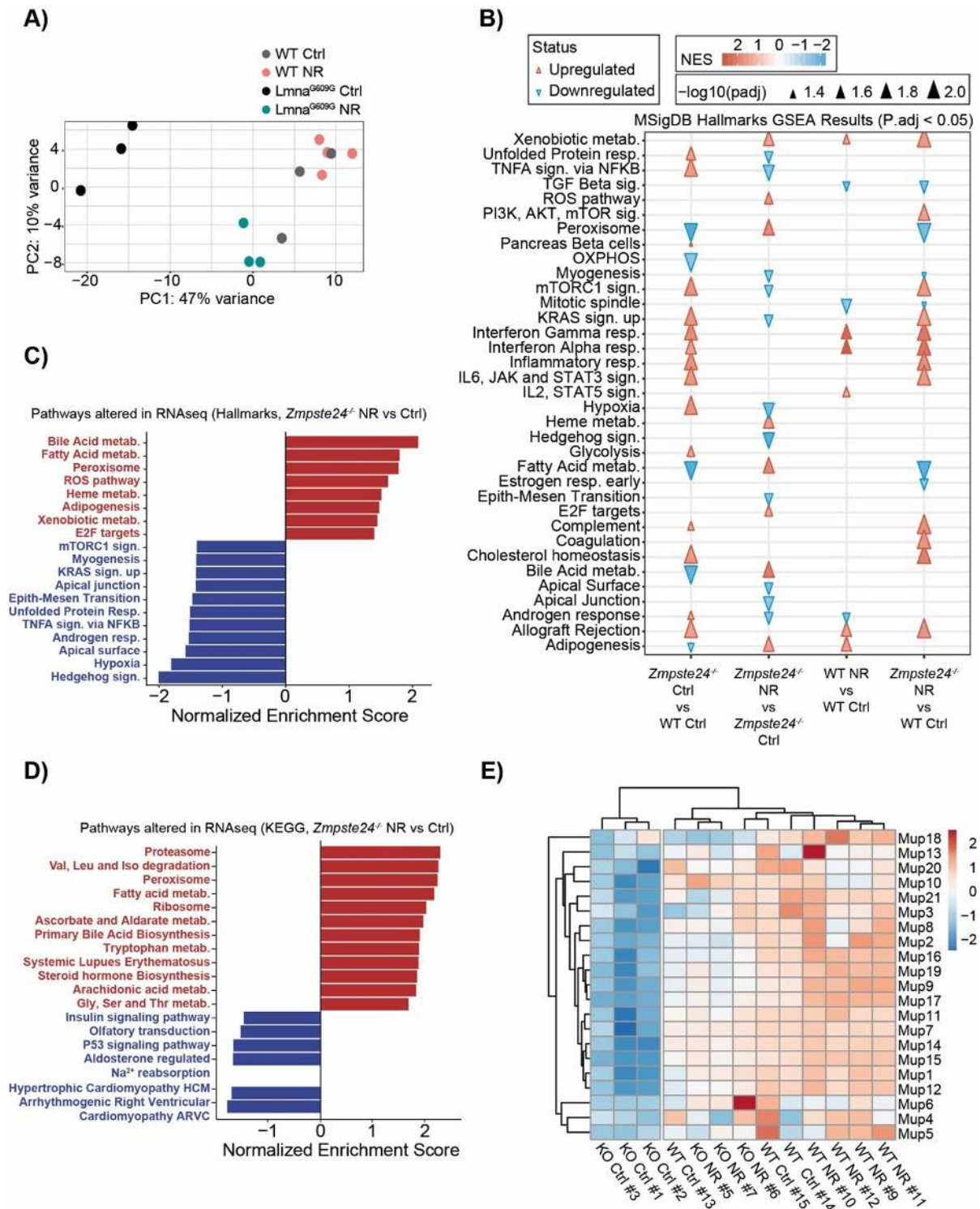


**Figure 16. NR diet reverses the premature aging metabolic shift of *Zmpste24*<sup>-/-</sup> mice.** **A)** Principal-component analysis (PCA) of the proteomic profiles of *Zmpste24*<sup>-/-</sup> and WT fed with NR or control diet. **B)** Summary table of Hallmarks GSEA results between groups representing the change status, NES value and adjusted p-value. **C-D)** Gene set enrichment analysis of **C)** Hallmarks and **D)** KEGG gene sets in *Zmpste24*<sup>-/-</sup> NR compared to *Zmpste24*<sup>-/-</sup> control mice. Bars represent the normalized enrichment score (NES). Red color indicates upregulated pathways and blue indicates downregulated pathways. **E)** Heatmap of MUP family proteins abundance in all the experimental groups.

### **3. Analysis of the anti-aging potential of genetic approaches designed to counteract mitochondrial dysfunction based on overexpression of the LONP1 protease**

LONP1 is an ATP-dependent protease located in the mitochondrial matrix<sup>148,155</sup>, although it has also been described in the nucleus under heat shock conditions<sup>147</sup>. The main function of LONP1 is to degrade damaged or misfolded proteins, maintaining mitochondrial function and proteostasis under stress conditions such as hypoxia and oxidative or endoplasmic reticulum stress<sup>149–152</sup>. However, the essential role of LONP1 in mitochondria goes beyond proteostasis, regulating gene expression by binding to DNA, and replication and transcription by degrading TFAM and controlling the TFAM/mtDNA ratio<sup>160–162</sup>.

LONP1 deficiency causes embryonic lethality in mice, while the partial absence of LONP1 alters the expression and stability of OXPHOS subunits and complexes, as well as the organization between them in the so-called supercomplexes. These changes can alter the mitochondrial energy balance by reducing oxygen consumption, increasing glucose metabolism and reducing lactate production. Physiologically, it is manifested in mice with a resistance to the incidence and severity of papillomas and colon tumors<sup>165</sup>. Consequently, we speculate that increased LONP1 expression would have antagonistic results in mitochondria with respect to its partial absence. In this sense, increased LONP1 expression is associated with increased incidence and mortality in certain human cancers of the colon and melanoma. Further, although up- and down-regulation of *Lonp1* appear to lead to some similar effects on the remodeling of OXPHOS complexes, the underlying causes are opposite in both cases. Down-regulation of *Lonp1* results in the reduction of functional OXPHOS complexes by degradation, loss, and destabilization, whereas overexpression of LONP1 also results in the decrease of OXPHOS complexes by direct regulation instead<sup>165</sup>.

To understand the implications of LONP1 in mitochondrial energy metabolism and cancer, in this section we have generated a transgenic mouse model overexpressing LONP1. After describing the mouse phenotypically, we have explored the consequences of LONP1 transgenesis on mitochondria and metabolism at the cellular and systemic level. Finally, hypothesizing that LONP1 overexpression could affect energetic fitness, we evaluated the longevity and health of these mice to analyze the consequences of LONP1 overexpression in cancer and aging.

### 3.1. Generation and description of the new transgenic *Lonp1* mouse model

The LONP1 transgenic mouse was generated by injecting the linearized genomic sequence of mouse *Lonp1* into the pronuclei of fertilized oocytes. A large genomic DNA segment containing the murine *Lonp1* locus, cloned into the BAC (Bacterial Artificial Chromosome) vector pBAC3.6, was obtained from CHORI (identification no. RP23-421B5; RPCI-23 library, C57BL/6J) (<http://www.chori.org>). *Lonp1* gene was extracted from the BAC and cloned into the pBS (pBlueScript II SK) backbone. The plasmid containing the genomic sequence of *LonP1* was sent to Cyagen US Inc for linearization and microinjection into the pronuclei of fertilized oocytes, derived from intercrosses of C57BL/6J mice. Four transgenic mice lines were generated with 2 and 6 extra copies of *Lonp1* validated by mRNA expression and protein levels in different tissues (Figure 17A-D). All of them were indistinguishable from their wild type littermates and showed no changes in body weight (Figure 17E).

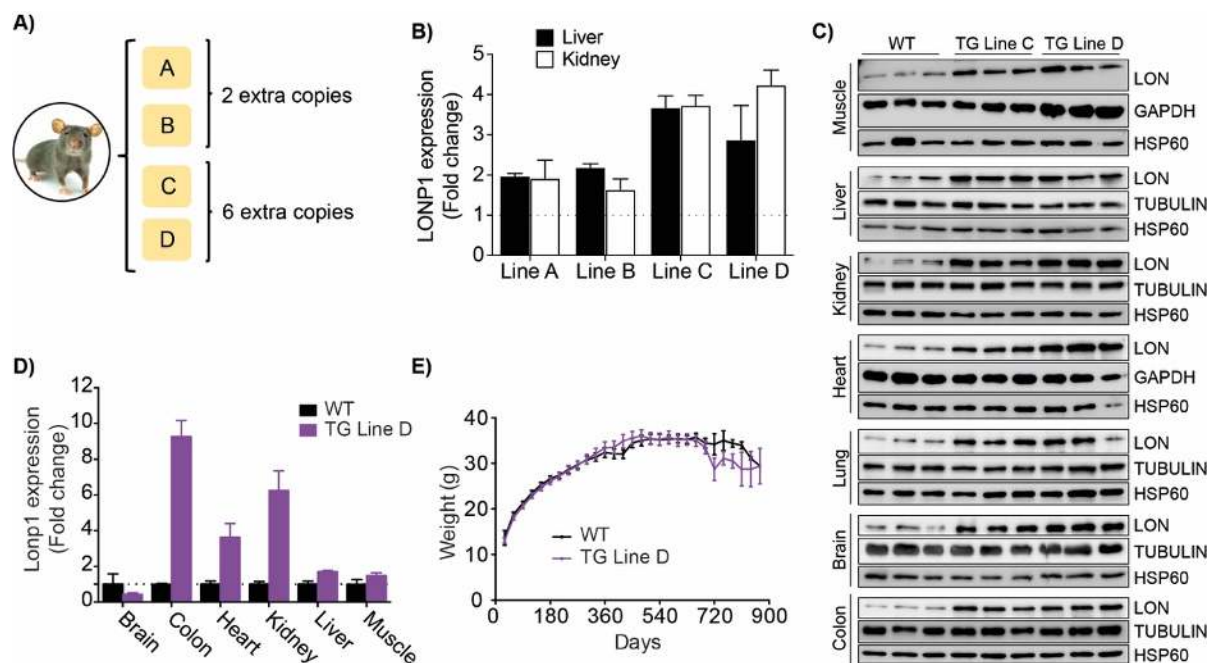


**Figure 17. Generation of the transgenic *Lonp1* mouse model.** **A)** Scheme of the four transgenic lines established, including two lines with 2 extra copies of *Lonp1* and two lines with 6 extra copies. **B)** LONP1 protein levels in the four transgenic lines in liver and kidney tissue compared to WT mice, using GAPDH as loading control (Line A n=2, Line B n=4, Line C n=3, Line D n=2). **C)** Western analysis showing LONP1 protein levels in the two initially selected lines with 6 extra copies in diverse tissues compared to WT mice, using GAPDH and HSP60 as loading controls. (n=3 per group). **D)** *Lonp1* mRNA expression in WT and TG (line D) samples of diverse tissues (WT, black, n=3-4; TG, purple, n=4). **E)** Body weight curve in wild-type and TG (line D) mice (WT, black, n=35; TG, purple, n=34). Multiple t-test assuming same standard deviation (SD). Bars and dots represent mean  $\pm$  95% CI.

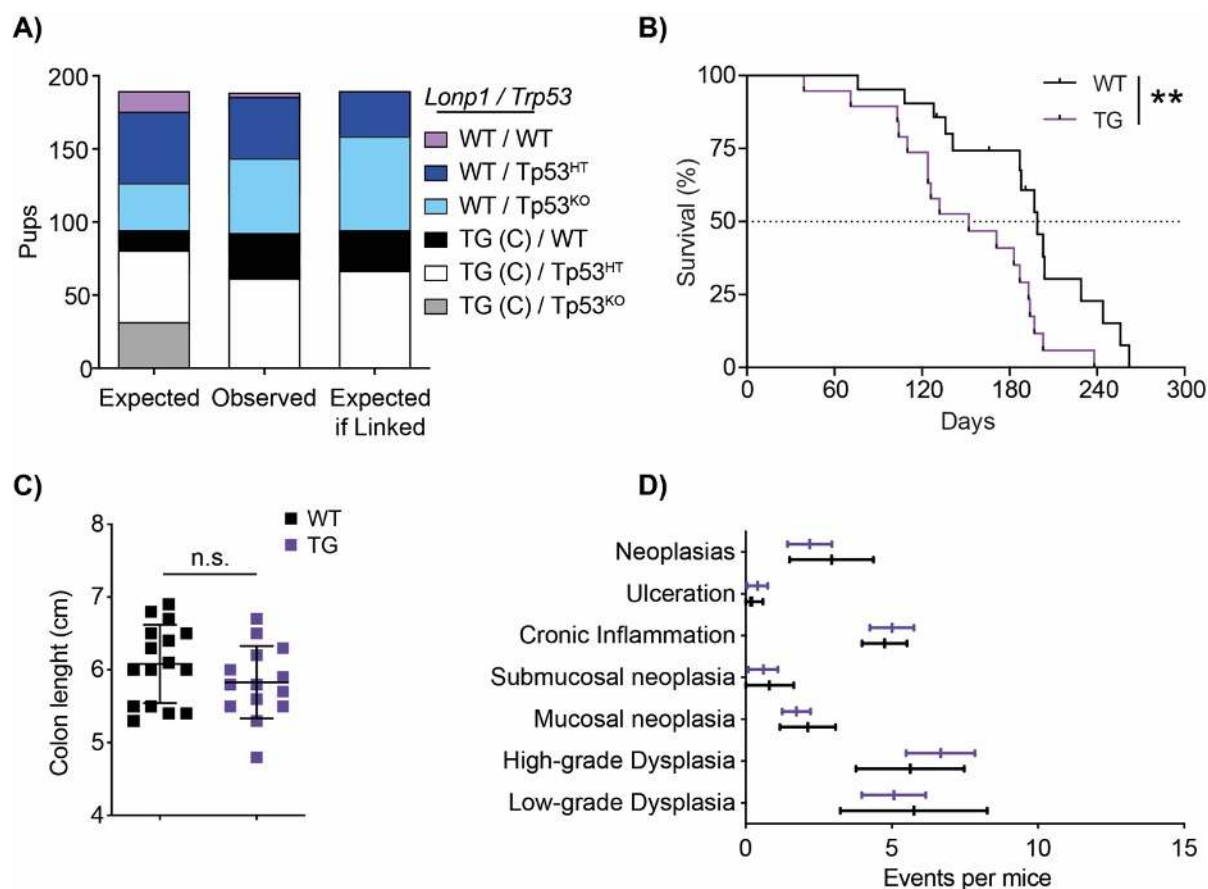


**Figure 18. Effects of LONP1 overexpression in cancer development in mice.** **A)** Graphical representation of pups born after TG (Line C) and TP53-deficient mice intercross, reflecting the imbalance between the percentage of mice born of each genotype and the percentages expected if the genes were independent or linked. **B)** Survival plot of TG and WT mice in the context of TP53-deficiency (*Lonp1<sup>+/+</sup> Trp53<sup>-/-</sup>*, black, n=21; *Lonp1<sup>TG</sup> Trp53<sup>-/-</sup>*, purple, n=19). Survival curves were analyzed with the log-rank (Mantel Cox) test (p=0.005) and Gehan-Breslow-Wilcoxon test (p=0.0097). **C)** Colon length of wild-type and TG females after chemical induction of colon carcinogenesis. (*Lonp1<sup>+/+</sup>*, n=16; *Lonp1<sup>TG</sup>*, n=14). Analysis made by Student's t test assuming same SD (p=0.194). **D)** Incidence of tumor lesions in wild-type and TG females after chemical induction of colon carcinogenesis. (*Lonp1<sup>+/+</sup>*, n=16; *Lonp1<sup>TG</sup>*, n=14). Analyzed by two-way ANOVA with Sidak's correction for multiple comparisons (p=0.694) Scatter dot blots represent mean ± 95% CI. \*\*p < 0.01

Given the relationship of this protease with the development of certain cancers such as colon and papilloma, we first decided to analyze whether the increase in LONP1 affects cancer incidence in an appropriate genetic context. For this, we crossed both transgenic lines with a TP53-deficient murine model that develops spontaneous tumors. Surprisingly, one of the LONP1 transgenic colonies was unable to generate TP53-deficient animals after crossover (Figure 18A). This deviation from the expected Mendelian frequencies could be explained if the transgenic vector had been inserted into a sequence close to the *Trp53* locus, keeping both gene and

transgene linked. Therefore, in order to properly evaluate the effects of LONP1 independently of the consequences of its insertion at the *Trp53* locus, we decided to abandon that transgenic line and focus on the other one presenting the 6 extra copies that we will refer to in hereafter as *Lonp1*<sup>TG</sup> or simply TG. Thus, *Lonp1*<sup>TG</sup> *Trp53*<sup>-/-</sup> animals had higher mortality than their *Lonp1*<sup>WT/WT</sup> *Trp53*<sup>-/-</sup> littermates, indicating that increased levels of LONP1 promote tumor development at least in the absence of TP53 (Figure 18B). Additionally, we carried out a chemical carcinogenesis induction protocol in colon that did not show any differences between TG and WT females (Figure 18C-D), indicating that the relationship between LONP1 and cancer seems to depend on a particular environment.

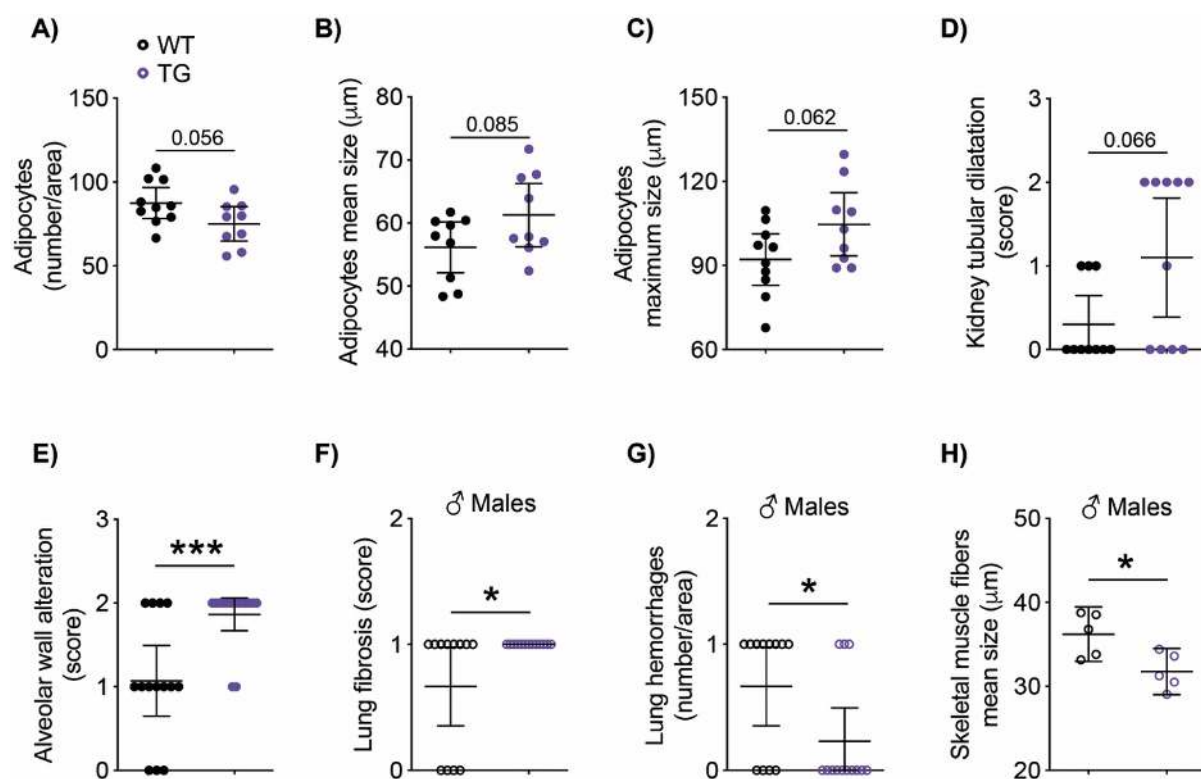


**Figure 19. Histological characterization of 16-month-old *Lonp1*<sup>TG</sup> mice. A-H)** Measurement of some histological parameters in kidney, lung, skeletal muscle and white adipose tissue. In 16-months-old mice: **A)** Density (events/area), **B)** mean and **C)** maximum size (µm) of adipocytes. **D)** Tubular dilatation score in kidney (WT, black, n=9-10; TG, purple, n=9). **E)** Alveolar wall alteration score in lung (p=0.0008) (WT n=14, TG n=15). In 16-months-old males. **F)** Fibrosis score (p=0.023) and **G)** hemorrhages density (events/area) (p=0.028) in lung (WT n=12, TG n=13). **H)** Mean size of skeletal muscle fibers (µm) (p=0.02) (WT n=5, TG n=5). Analysis made by Mann-Whitney test and Student's t-test assuming same SD. Scatter dot blots represent mean ± 95% CI. \*p < 0.05, \*\*p < 0.01, \*\*\*p < 0.001, \*\*\*\*p < 0.0001

At the histological level, white adipose tissue (WAT) of 16-months-old TG mice reflected a tendency to a lower number of adipocytes, with greater mean and maximal size relative to control animals (Figure 19A-C). Kidneys showed a trend towards greater tubular dilatation, while lungs exhibited a greater alteration of the alveolar wall, which was accompanied in males by a higher percentage of fibrosis and less hemorrhages (Figure 19D-G). Also, TG male mice showed a smaller diameter of skeletal muscle fibers (Figure 19H). We did not observe significant alterations in other tissues such as liver, gonads, heart or intestinal system and, overall, it seems that the changes at the histological level are very limited, without major alterations affecting tissue physiology.

Due to the relevance of LONP1 in the degradation of damaged or misfolded proteins, we decided to carry out some chemical proteostasis and inflammatory stress protocols with cisplatin, paraquat and lipopolysaccharide (LPS) to evaluate whether the transgenic animals showed increased resistance to stress. Paraquat is a herbicide that reacts with the electron transport chain producing superoxides and an oxidative stress response<sup>218,219</sup>, while LPS induces mitochondrial fragmentation<sup>220,221</sup>. Cisplatin is used alone or in combination with other drugs for the treatment of various cancers. In mitochondria, cisplatin promotes mtDNA damage, induces ROS, and disrupts mitochondrial communication and energy balance<sup>222</sup>. Although overexpression of other mitochondrial proteases, such as OPA1 or CLPP, has been reported to protect against some of those stress conditions<sup>223–225</sup>, *Lonp1*<sup>TG</sup> mice showed no differences compared to WT littermates in any of the 3 stress conditions (Figure 20A-C).

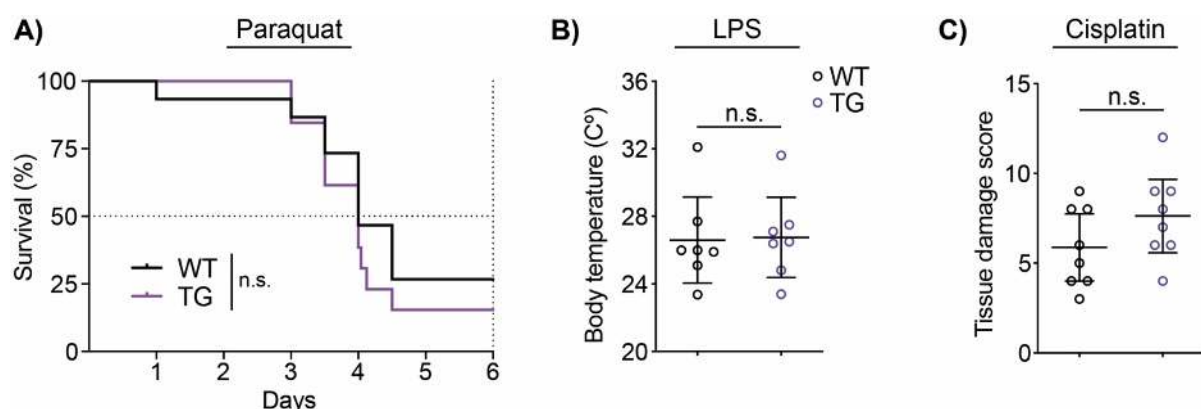


**Figure 20. Induction of proteostasis and inflammatory stress in *Lonp1*<sup>TG</sup> mice. A)** Survival plot of wild-type and transgenic mice upon paraquat administration (WT, black, n=15; TG, purple, n=13). Survival curves were analyzed with the log-rank (Mantel Cox) test (p=0.357) and Gehan-Breslow-Wilcoxon test (p=0.563). **B)** Body temperature of wild-type and transgenic males at 24-hours after LPS injection (WT, n=7; TG, n=7). Analysis done by Student's t-test assuming same SD. **C)** Kidney tissue damage score of wild-type and transgenic males after cisplatin administration (WT, n=8; TG, n=8). Analysis done by Mann-Whitney test and Student's t test assuming same SD (p=0.157). Scatter dot blots represent mean  $\pm$  95% CI.

### 3.2. Characterization of mitochondrial and systemic metabolism in *Lonp1<sup>TG</sup>* mice

Considering the bioenergetic alterations observed in the *Lonp1<sup>+/-</sup>* model, we hypothesized that the TG mouse might present changes in energetic metabolism. We sampled peripheral blood serum and performed a general metabolic profile. The changes observed were modest and sex-dependent, with a tendency to higher gamma-glutamyl transferase (GGT) and total bilirubin in females, while males showed increased levels of alkaline phosphatase and decreased levels of phosphorus (Figure 21A-D). No changes in circulating cholesterol or aldosterone levels were observed (Figure 21E-F), despite the relationship between LONP1, StAR and aldosterone synthesis<sup>158,226</sup>. Similarly, no differences in blood glucose either at baseline or after a 4-, 12- or 24-hour fast were found (Figure 21G). To obtain a complete picture of systemic energy use, we performed a metabolic study with the Oxymax CLAMS system. However, no clear differences were found between TG and WT mice at any age under either basal or fasting conditions (Figure 21H-K).

To explore LONP1 overexpression in a context of metabolic stress, we exposed mice to high-fat (HFD) and high-sucrose diets (HSD). During HFD, both experimental groups gained weight similarly and no significant differences in blood glucose or intraperitoneal glucose and insulin tolerance tests (IPGTT and IPITT, respectively) were observed (Figure 22A-C). No changes in fat deposits were observed at histological level, nor were systemic metabolic alterations observed in the Oxymax system or by inducing thermogenesis after exposure to cold (Figure 22D-H). Identical results were observed in mice supplemented with up to 30% sucrose in the beverage, with TG mice showing no changes in body weight or basal glycemia compared to their WT littermates (Figure 22I-J). Overall, *Lonp1<sup>TG</sup>* mice did not show remarkable metabolic differences compared to control animals neither under basal conditions nor under metabolic stresses.

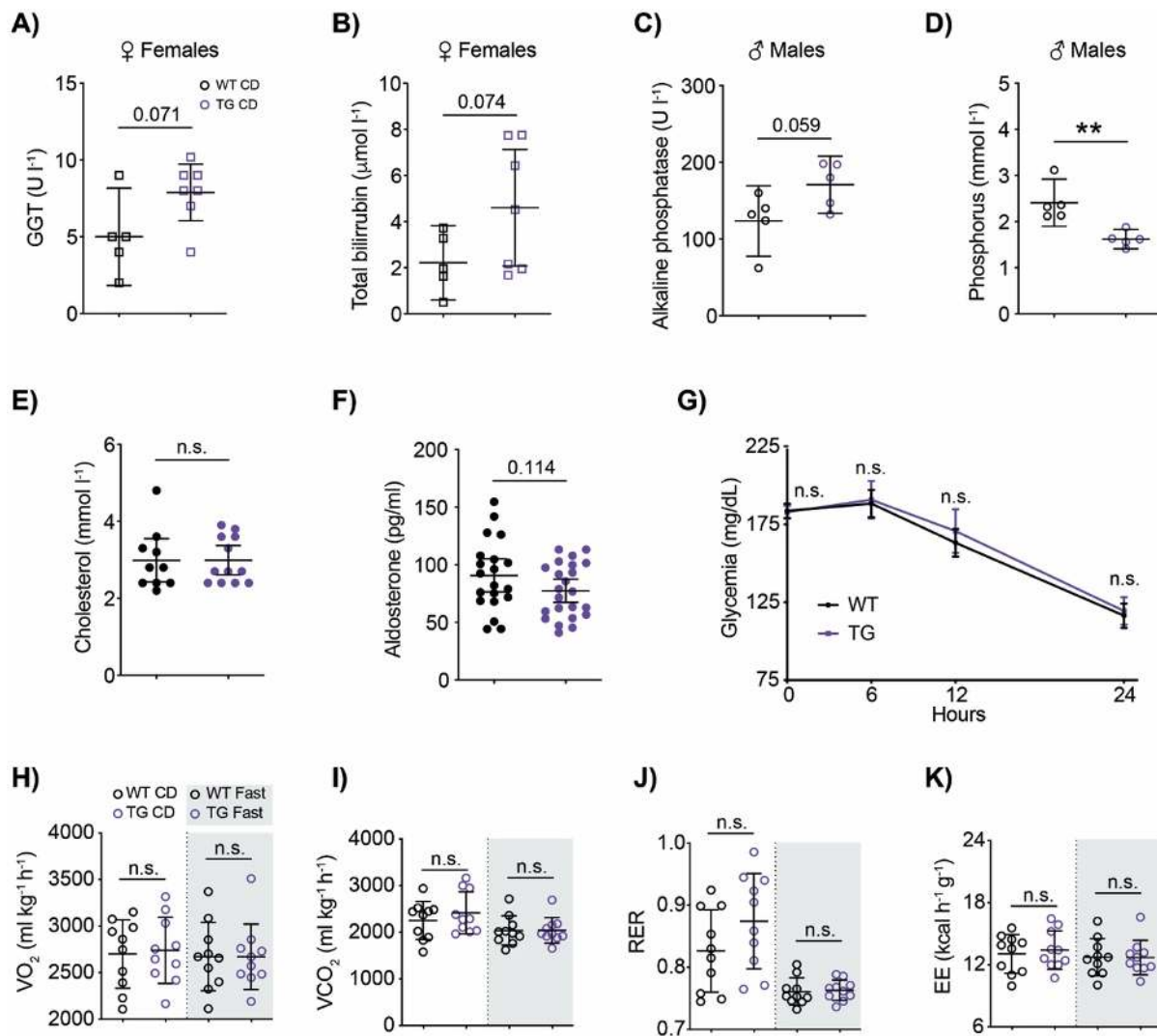


**Figure 21. Serum metabolites evaluation and Oxymax analysis of *Lonp1<sup>TG</sup>* mice. A-F** Serum metabolites in 6-months-old wild-type and transgenic mice. In females: **A)** Gamma-glutamyl transferase (GGT, U/l). **B)** Total bilirubin ( $\mu\text{mol/l}$ ) (WT, black, n=5; TG, purple, n=7). In males: **C)** Alkaline phosphatase (U/l). **D)** Phosphorus (mmol/l) (p=0.0094) (WT, n=5; TG, n=5). In all mice: **E)** Cholesterol (mmol/l) (WT, n=10; TG, n=12). **F)** Aldosterone (pg/ml) (WT, n=20; TG, n=23). Analysis made by Student's t-test assuming same SD. **G)** Glycemic analysis in wild-type and transgenic mice at baseline and after a 4-, 12- or 24-hour fast (mg/dl) (WT, n=25; TG, n=26). Multiple t-test assuming same standard deviation (SD) and Student's t-test assuming same SD. **H-K)** Indirect calorimetry measured by Oxymax-CLAMS system, representing the mean measurements during day and night in 1-year-old mice. **H)** Oxygen consumption ( $\text{VO}_2$ ; milliliters per kilogram per hour). **I)** Carbon dioxide production ( $\text{VCO}_2$ ; milliliters per kilogram per hour). **J)** Respiratory exchange ratio (RER;  $\text{VCO}_2/\text{VO}_2$ ) (CD, p=0.152). **K)** Energy expenditure (EE; kilocalories per kilogram per hour) (WT, n=10; TG, n=10; WT Fast, n=10; TG Fast, n=10). Analyzed by Student's t-test assuming same SD. White background means feeding conditions analysis while grey background indicates fasting conditions measurements. Circle dots represent males, square dots represent females and filled dots represent both genders. Dots and scatter dot blots represent mean  $\pm$  95% CI. \*\*p < 0.01.

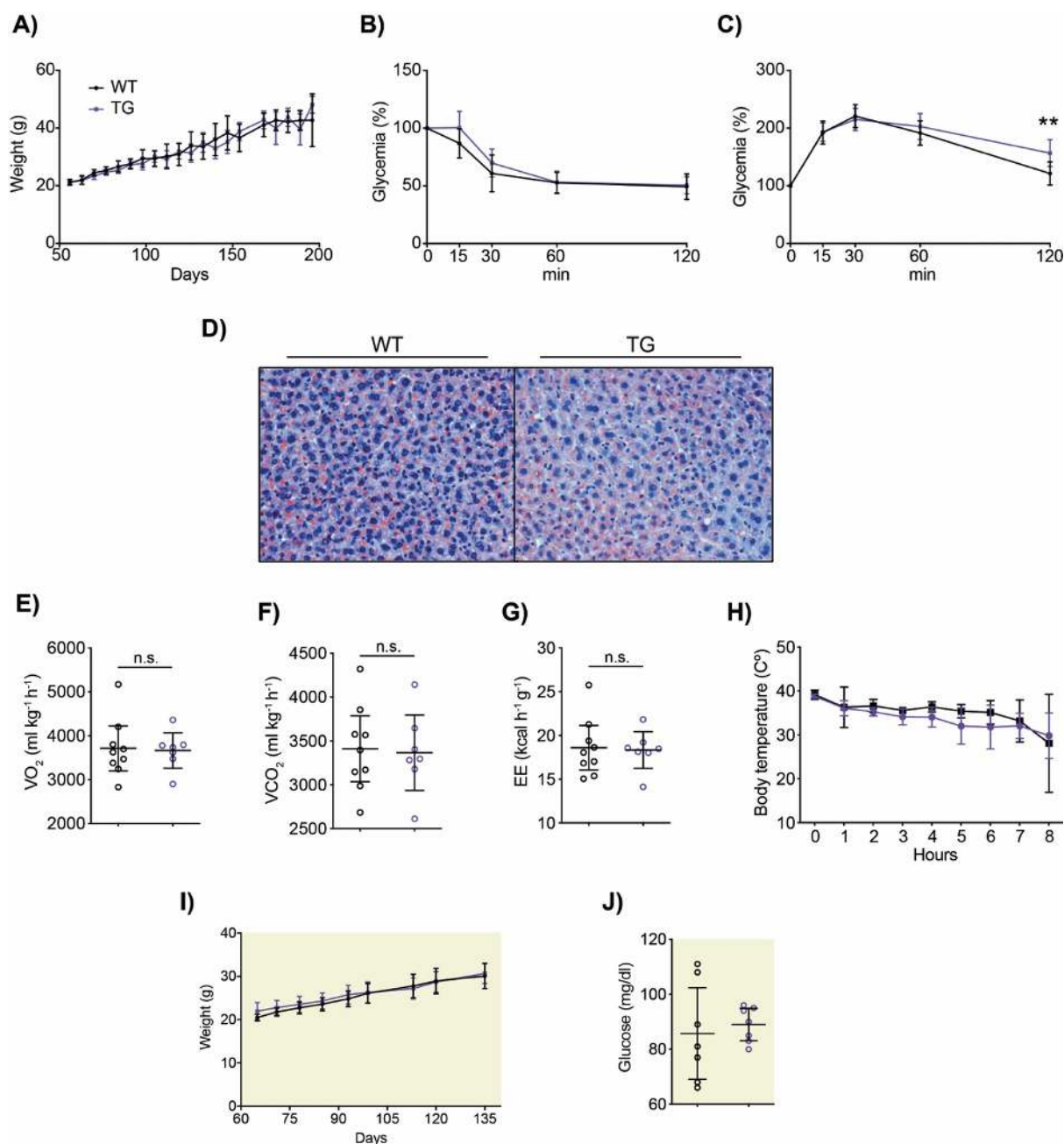


**Figure 22. Metabolic characterization of *Lonp1<sup>TG</sup>* males in a context of metabolic stress after feeding with HFD and HSD.** **A)** Body weight curve in wild-type and TG males fed with HFD (WT, black, n=12; TG, purple, n=14). Multiple t-test assuming same standard deviation (SD). **B-C)** Blood glucose analysis in wild-type and transgenic mice at 0, 15, 30, 60 and 120 minutes after **B)** insulin (IPITT) or **C)** glucose (IPGTT) administration (WT, n=9-10; TG, n=13-14). Multiple t-test assuming same standard deviation (SD). **D)** Representative histological image of oil-red staining in liver tissues of 6.5-months-old males under HFD. **E-G)** Indirect calorimetry measured by Oxymax-CLAMS system, representing the mean measurements during day and night in 6-months-old males under HFD. **E)** Oxygen consumption ( $VO_2$ ; milliliters per kilogram per hour). **F)** Carbon dioxide production ( $VCO_2$ ; milliliters per kilogram per hour). **G)** Energy expenditure (EE; kilocalories per kilogram per hour) (WT, n=9; TG, n=7). **H)** Body temperature of wild-type and transgenic males fed with HFD during 8 hours of cold exposure to induce thermogenesis (WT, n=4; TG, n=8). Multiple t-test assuming same standard deviation (SD). **I)** Body weight curve in wild-type and TG males fed with HSD (WT, n=8; TG, n=8). Multiple t-test assuming same standard deviation (SD). **J)** Glucose levels of wild-type and TG males fed with HSD after 6h of fasting at the age of 5 months (WT, n=7; TG, n=7). Analysis made by Student's t test assuming same SD. White background means HFD conditions while yellow background indicates HSD conditions. Dots and scatter dot blots represent mean  $\pm$  95% CI. \*\*p < 0.01.

Despite the absence of systemic metabolic changes, we performed a comprehensive mitochondrial profiling to explore the effects of *Lonp1* transgenesis on mitochondrial biology. Since LONP1 regulates mtDNA and TFAM levels, we assessed mtDNA copy number by estimating the levels of mitochondrial NADH dehydrogenase subunit 1 (ND1) and nuclear hexokinase 2 (HK2) genes by qPCR. In addition, we assessed mtDNA stability and deletions by comparing the copy number of the NADH dehydrogenase subunit 4 (ND4) gene with ND1, since the mtDNA locus containing ND4 is usually deleted with age whereas ND1 is stable<sup>227</sup>. Both mtDNA copy number and sequence stability of ND4 were comparable in TG and WT mice in liver, kidney, heart and colon samples, which are mitochondria-enriched tissues (Figure 23A-B). Next, to evaluate mitochondrial transcription we measured the levels of TFAM and the mitochondrial polymerase POLRMT in liver and heart samples by western blotting. Again, TG mice did not show changes in the levels of these proteins relative to mitochondrial controls HSP60 and HSC70 compared to WT mice (Figure 23C-D). Therefore, *Lonp1*<sup>TG</sup> mice appear to show no changes in mtDNA copies, maintenance or transcription.

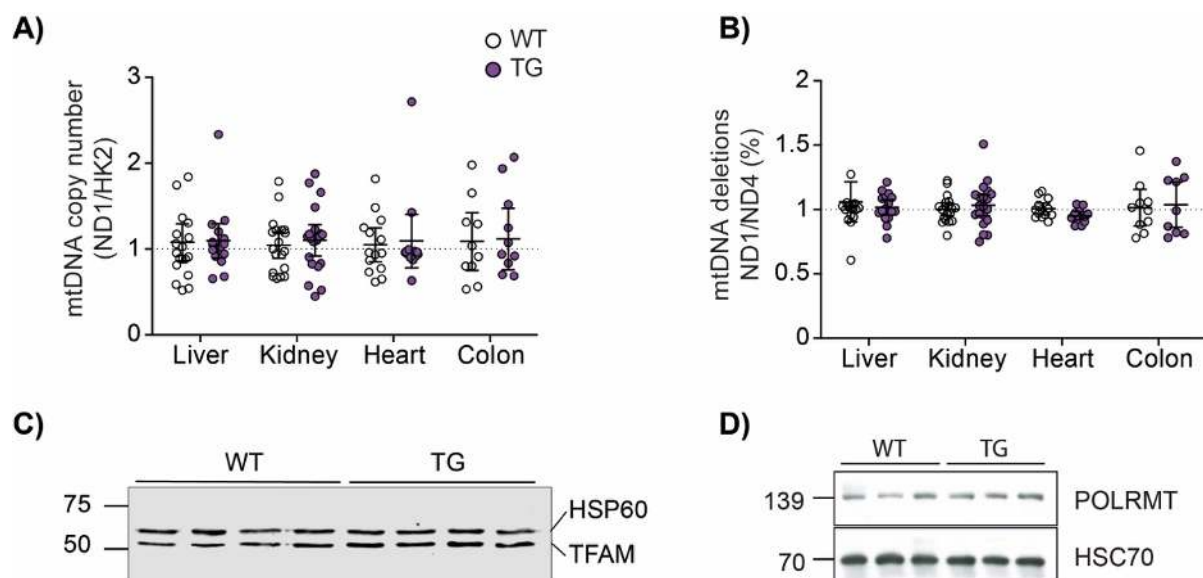


**Figure 23. Evaluation of mtDNA copy number, maintenance and transcription in *Lonp1*<sup>TG</sup> mice.** **A)** Determination of mtDNA **A)** copy number (ND1/HK2, %) and **B)** mtDNA deletions (ND1/ND4, %) by qPCR (Liver, WT, black, n=18, TG, purple, n=16; Kidney, WT n=19, TG n=20; Heart, WT n=14, TG n=13; Colon, WT n=10, TG n=9-10). Analyzed with two-way ANOVA with Sidak's correction for multiple comparisons. Scatter dot blots represent mean  $\pm$  95% CI. **C-D)** Western analysis of wild-type and transgenic samples showing the proteins levels of **C)** TFAM in 16-months-old liver tissues (n=4 per group) and **D)** POLRMT in 14-months-old heart tissues (n=3 per group). HSP60 and HSC70 were used as loading controls, respectively.

Next, we evaluated the OXPHOS complex organization level, first by assessing the protein expression of individual subunits by western blotting and then by examining the complexes and supercomplexes by blue native electrophoresis (BN-PAGE). *Lonp1<sup>TG</sup>* mice did not exhibit differences in the levels of NDUFB8 (CI), SDHB (CII), UQCRC2 (CIII), MTCO1 (CIV) or ATP5A (CV) in liver nor heart samples relative to the mitochondrial marker HSP60 (Figure 24A-B). Then, we measured the levels of complexes and supercomplexes under native conditions and again, we observed no differences between transgenic and wild-type animals (Figure 24C-D). Interestingly, Seahorse analysis of TG fibroblasts did show a decrease in respiration measured as oxygen consumption in the basal and proton leak phases, accompanied by a significant reduction in the extracellular acidification ratio, with respect to control animals (Figure 24E-F). However, these differences disappeared when the Seahorse analysis was performed under fatty acid enrichment conditions (Figure 24G-H). In summary, *Lonp1<sup>TG</sup>* mice do not appear to undergo changes in the stability or abundance of the mitochondrial genome. They also do not evidence alterations in protein expression or in the organization of OXPHOS complexes, although surprisingly they appear to have less respiration and more glycolysis-based respiration than control animals.

### 3.3. Longevity and healthspan evaluation in *Lonp1<sup>TG</sup>* mice

Partial absence of LONP1 reduced mitochondrial respiration, increased glucose consumption, and decreased the incidence of certain cancers in mice and humans. In contrast, high expression of this protease is associated with increased cancer mortality, although its role in metabolic remodeling appears to be limited<sup>165</sup>. With these considerations, we hypothesized that *Lonp1<sup>TG</sup>* mice might undergo a mitochondrial optimization resulting in improved health with the trade-off of increased tumor incidence. To elucidate this, we sought to quantify longevity and healthspan in old mice. *Lonp1<sup>TG</sup>* animals showed no changes in survival relative to their WT littermates (Figure 25A), which could be explained by the higher incidence of cancer in the appropriate context (Figure 18B)<sup>165</sup>.

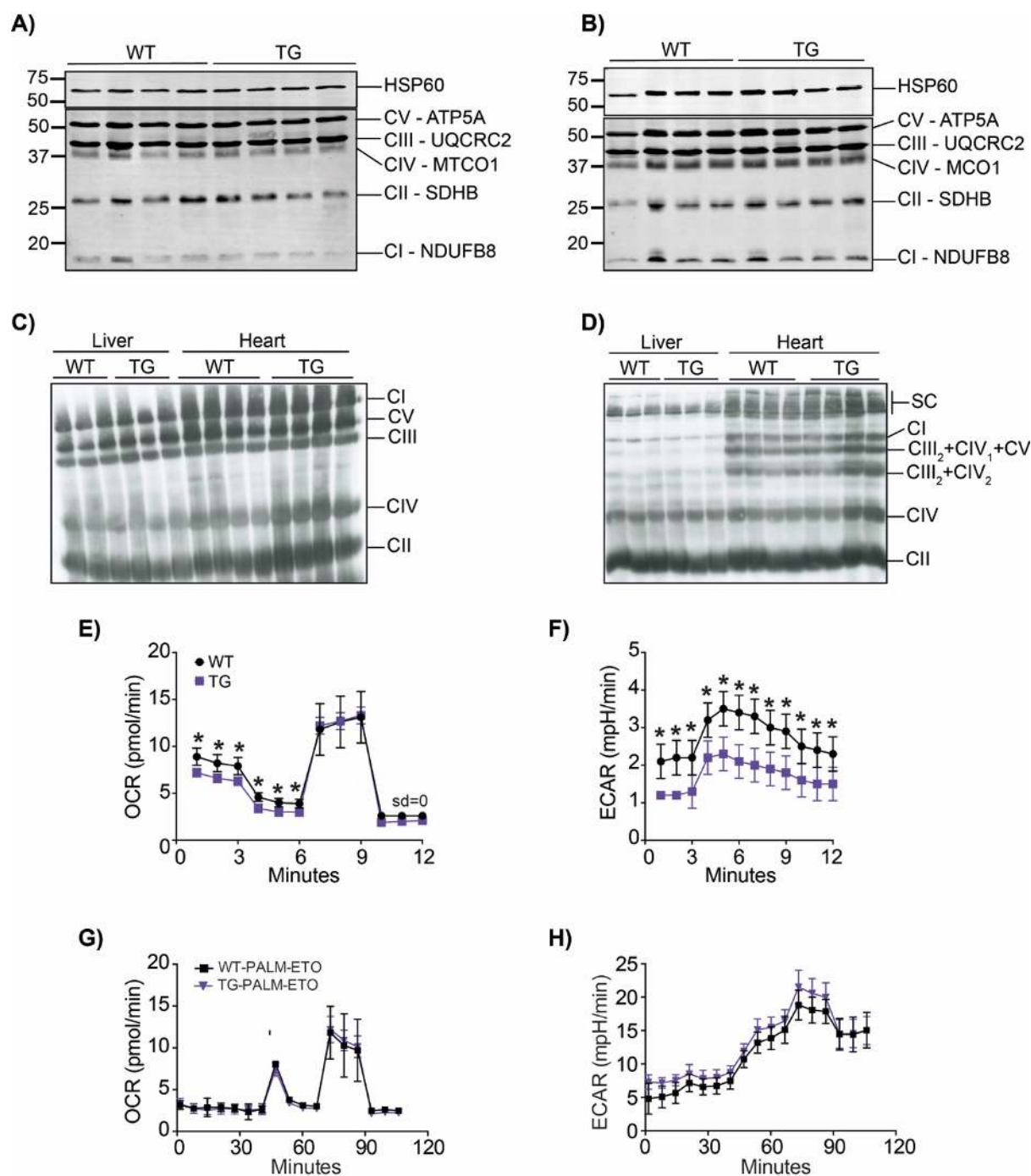


**Figure 24. Mitochondrial characterization in *Lonp1<sup>TG</sup>* mice.** **A)** Western analysis of wild-type and transgenic 16-months-old samples of **A)** liver and **B)** heart tissues showing protein levels of NDUFB8 (CI), SDHB (CII), UQCRC2 (CIII), MTCO1 (CIV) and ATP5A (CV) (n=4 per group). HSP60 was used as loading control. **C-D)** Blue Native PAGE (BN-PAGE) analysis of the respiratory chain **C)** complexes with DDM and **D)** supercomplexes with digitonin followed by Western blot analysis using antibodies against OXPHOS subunits in liver and heart tissues of 2-months-old mice (Liver, n=3 per group; heart, n=4 per group). **E-F)** Seahorse analysis of wild-type and transgenic mice fibroblasts showing **E)** oxygen consumption rate (OCR, pmol/min/ $\mu$ g protein) and **F)** extracellular acidification rate (ECAR, mpH/min) under basal conditions and after oligomycin, FCCP and antimycin/rotenone injection (WT, black, n=3; TG, purple, n=3). Curves were analyzed with multiple t-test assuming same standard deviation (SD). **G-H)** Seahorse analysis of wild-type and transgenic mice fibroblasts in fatty-acids enrichment conditions showing **G)** oxygen consumption rate (OCR, pmol/min/ $\mu$ g protein) and **H)** extracellular acidification rate (ECAR, mpH/min) under basal conditions and after oligomycin, FCCP and antimycin/rotenone injection (WT, n=3; TG, n=3). Curves were analyzed with multiple t-test assuming same standard deviation (SD). Dots represent mean  $\pm$  95% CI. \*p < 0.05, \*\*\*\*p < 0.0001.

Next, we examined health status from several perspectives. First, we assessed the muscular system in a treadmill endurance test under basal and post-training conditions to explore whether *Lonp1* transgenesis would provide an increased ability for fatigue adaptation. Under basal conditions, only TG females showed greater endurance than their WT littermates, whereas, after training, all experimental groups improved their performance and there were no differences between them (Figure 25B-C). At the level of motor coordination, at 2 years of age, no differences were observed between experimental groups in a Rotarod test, although females seemed to perform worse (Figure 25D). However, the same mice at 2 years of age exhibited a lower propensity to fall in a hanging wire test (Figure 25E). Finally, we performed an aging score evaluation in which we assessed aspects such as alopecia, whisker loss, coat condition, kyphosis, body tremor, corneal opacity, respiration rate and general condition<sup>175</sup>. *Lonp1*<sup>TG</sup> mice did not show significant differences in the overall score but did show some improvement in some key aspects such as whisker loss, kyphosis, vision loss or corneal opacity (Figure 25F-H). Finally, as a way of estimating aging molecularly, we measured telomere length in liver, heart and kidney samples from 16-month-old mice, without observing any significant difference between the experimental groups (Figure 25I). Overall, the longevity of *Lonp1*<sup>TG</sup> mice does not appear to be affected by hypothetical mitochondrial optimization. In old animals, the health of TG mice appears to be improved in some tests of endurance and motor coordination, as well as in aspects of general appearance. However, these possible health benefits are very limited and do not represent effective improvements for *Lonp1*<sup>TG</sup> mice.

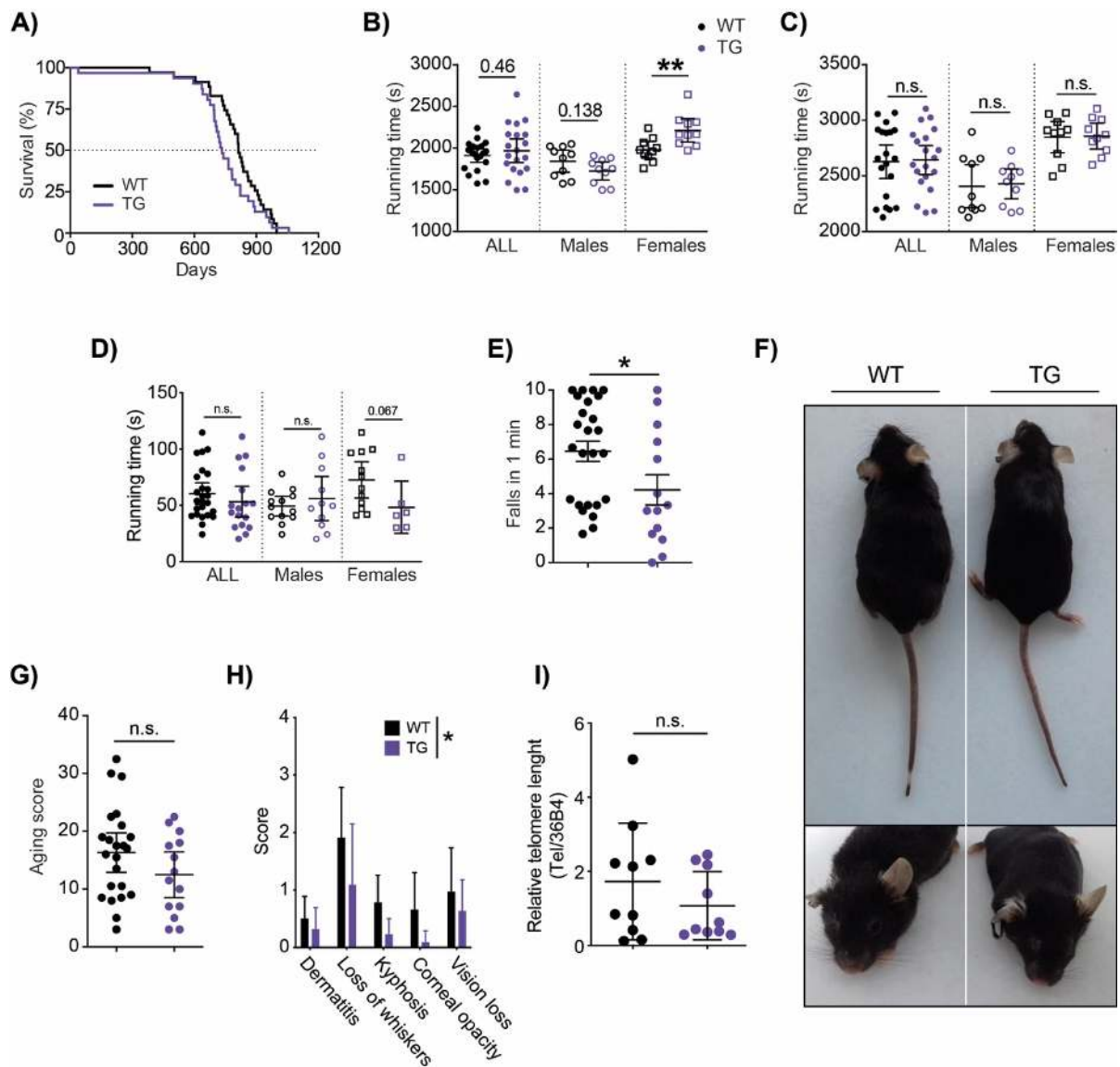


**Figure 25. Longevity and healthspan evaluation in *Lonp1*<sup>TG</sup> mice.** **A)** Survival plot of wild-type and transgenic mice (WT, black, n=35; TG, purple, n=31). Survival curves were analyzed with the log-rank (Mantel Cox) test ( $p=0.131$ ) and Gehan-Breslow-Wilcoxon test ( $p=0.029$ ). **B-C)** Running time during the treadmill endurance test of wild-type and transgenic mice under **B)** baseline and **C)** trained conditions (n=20 per genotype, n=10 per sex/genotype). Analysis made by Student's t-test assuming same SD (females in basal conditions  $p=0.0065$ ). **D)** Latency to fall during an increasing speed rotarod experiment of wild-type and transgenic mice at 2-years-old (all, WT n=25, TG n=17; males, WT n=13, TG n=11; females, WT n=12, TG n=6). Analysis made by Student's t-test assuming same SD (all  $p=0.363$ ; males  $p=0.467$ ; females  $p=0.0665$ ). **E)** Falls during the first minute in a hanging wire test of wild-type and transgenic mice at 2-years-old (WT, n=25; TG, n=14). Analysis made by Mann-Whitney test ( $p=0.0352$ ). **F)** Representative photograph of 2-years-old mice of the indicated genotypes showing the improvement in some aging-score features in *Lonp1*<sup>TG</sup> mice compared to control mice. **G-H)** Health evaluation in 2-years-old wild-type and transgenic mice by **G)** scoring some aging-related features, showing a delay in the appearance of **H)** dermatitis, whiskers loss, kyphosis, corneal opacity and vision loss (WT, n=23; TG, n=14). Analysis made by Mann-Whitney test ( $p=0.141$ ) and two-way ANOVA with Sidak's correction for multiple comparisons ( $p < 0.012$  for TG-vs-WT analyses). **I)** Analysis of relative telomere length by qPCR using the relation between telomere sequence and 36B4 monogen (n=10 per group). Analysis made by Student's t-test assuming same SD ( $p=0.271$ ). Circle dots represent males, square dots represent females and filled dots represent both genders. Bars and scatter dot blots represent mean  $\pm$  95% CI. \* $p < 0.05$ , \*\* $p < 0.01$ .







# **DISCUSSION**



Aging is a complex multivariate process whose molecular foundations are extensively interconnected. Part of the determinants of our health and longevity are acquired at birth in our genome. From small variables that make us more susceptible or resistant to disease, to severe mutations that alter the machinery that maintains homeostasis, our genetic code predisposes us as individuals to a determined longevity<sup>9,10</sup>. This is the case of progeroid syndromes, and in particular laminopathies, which are pathologies caused by mutations in nuclear envelope genes that cause premature aging and a dramatic reduction in lifespan. Nevertheless, our life expectancy and healthspan are not governed solely by deterministic factors. Our interaction with the environment has a decisive influence on aging through aspects such as diet, physical exercise and lifestyle, regulating metabolism on our cells<sup>11,15,18,19</sup>. Some dietary interventions, such as caloric restriction or restriction of certain nutrients, have been validated in animals as robust interventions to delay aging<sup>76,81</sup>. Other interventions based on caloric-restriction mimetic drugs are being explored as simpler options for application with similar benefits<sup>228</sup>. All of them act on the hallmarks of aging and intervene in our cellular energy balance. Likewise, the study of the mitochondria, an organelle involved in several of these hallmarks of aging and an essential regulator of cellular energy, could allow the development of new specific therapies that delay physiological and pathological aging<sup>124</sup>.

Therefore, in the present Doctoral Thesis we have deepened in the study of new mutations that cause premature aging through the development and characterization of the NGPS mouse model. We have also explored supplementation of NAD<sup>+</sup>, an essential regulator of metabolism, as a mechanism to delay accelerated aging in mouse models of progeria. Finally, based on the fundamental role of mitochondria in metabolism and aging, we have evaluated the effects of overexpression of the LONP1 mitochondrial protease in cancer development, health and longevity.

Over the last decades, there have been great advances in the study of aging. Some of these new discoveries have been achieved through the study of accelerated aging syndromes and the use of animal models of these conditions, among which the *Zmpste24*<sup>-/-</sup> and *Lmna*<sup>G609G/G609G</sup> mouse models stand out as robust research tools<sup>229</sup>. At the same time, the widespread use of Next-Generation Sequencing technologies has allowed the identification of new progeroid syndromes, and to deepen into their transcriptional characterization<sup>230</sup>. Our laboratory has recently described a new

progeroid syndrome, called NGPS in honor of the first two patients reported, caused by the p.Ala12Thr mutation in the nuclear envelope protein BAF<sup>180</sup>. The phenotype was similar to that observed in HGPS patients, characterized by growth retardation, lipodystrophy, alopecia, and skeletal affectation, among other symptoms. However, these two NGPS patients did not present the classic cardiovascular alterations of HGPS, while their bone damage was more severe, becoming the main life-threatening alteration for them. Surprisingly, their lifespan was considerably longer than that of HGPS patients and led to classify their condition as a type of chronic progeria<sup>179</sup>. Therefore, the **first objective of this Doctoral Thesis** was the development of a murine model carrying the p.Ala12Thr mutation in BAF, in order to physiologically and molecularly characterize this pathology.

Since the role of BAF in cells continues to be a matter of study, we have generated different animal models that included both homozygous and heterozygous deficiency of BAF in its wild-type or mutated forms. The results obtained in this work show that the complete absence of BAF is lethal in mice while its haploinsufficiency does not affect their viability. As in other murine models of accelerated aging, the extreme phenotype observed in patients is recapitulated in mice in a milder form, probably due to their long telomeres, among other reasons<sup>231</sup>. In many cases, it is necessary to study these animal models in appropriate genetic contexts or to expose them to different stresses to uncover their progeroid phenotypes<sup>232,233</sup>. In this regard, homozygous A12T mice were apparently indistinguishable from their WT littermates and not even the particular genotype of the A12T Hemi mice, which have a single and mutated copy of *Banf1*, reflected the dramatic features observed in humans. In the absence of a more severe phenotype in the Hemi A12T animals we decided to focus mostly on the study of the homozygous A12T model. However, it would be interesting in the future to study the relevance of potentially toxic properties of the mutant protein itself in the pathogenesis of the disease, rather than the mere loss of functionality due to the absence of BAF<sup>62</sup>.

Besides an increase in nuclear aberrations, a mild mitochondrial dysfunctionality and slower cell proliferation, A12T animals did not show major changes compared to control animals. Considering that the most important threat to the health span and life expectancy of NGPS patients lies on their major bone alterations and given the tendency of murine models to show milder aging phenotypes than humans, we decided to perform further bone-stressing experiments to unveil the

potential underlying bone alterations elicited by the A12T mutation. First, we studied the bone architecture in older individuals because, as happens in physiological aging, bone structure suffers a non-gradual degradation with marked loss of functionality at old ages. We decided to work with males because, due to the impact of estrogens in bone biology, mature females display a marked osteoporosis<sup>234,235</sup>, among others, that covers any possible differences between A12T and WT. In this context of aged individuals, the major alterations observed were a lower mineral density and loss of bone tissue, with some structure alterations in trabecular bone as lesser and more spaced trabeculae. Considering that ageing induces a bone stress in all individuals and the reduced number of samples available, the marked differences found are very relevant. Second, we exposed 2-months-old A12T mice to bone stress protocols such as induction of osteoporosis by ovariectomy and bone damage by iron overdose. OVX is a well-established protocol to induce osteoporosis in females<sup>198</sup>. To ensure that ovaries were correctly extracted, we checked the uterus weight – as this protocol reduces its weight due to the loss of estrogens. SHAM mice were used to validate the OVX-derived alterations, but no changes in bone architecture were seen in these mice. The major changes in KI A12T mice were a loss of bone tissue and the presence of thicker and less connected trabeculae, but no changes in mineral density were observed. Further, Hemi A12T mice also display these bone alterations in tissue volume and thicker trabeculae, which is very interesting in relation to the p.Ala12Thr BAF toxic hypothesis<sup>183</sup>. Finally, the iron-overdose is another well-established bone damage protocol where the harm is mediated by oxidative stress<sup>169</sup>. Both KI A12T males and females exhibited lower mineral density, but the effects on bone structure were sex-dependent. In males, the iron-OD led to a loss in bone tissue volume with restricted effects in trabecular bone, mostly defined by thicker trabeculae. However, females displayed greater alterations in trabecular architecture with lesser, more spaced and less connected trabeculae and increased porosity, in line with what has been observed in physiological aging in females<sup>234,235</sup>. Altogether, although with variable severities, we were able to observe in all cases a greater affectation in the tibiae of A12T animals, resembling the premature aging of patients under an appropriate context and validating our model as a useful tool for NGPS research (Figure 26).

				A12T				Hemi A12T
				Aged	OVX	Iron-OD	<i>Lmna</i> <sup>G609G</sup>	OVX
Trabecular Bone	BMD	g/cm <sup>3</sup>	Bone Mineral Density	⚠♂	=	↓♂♀	↓♂♀	=
	BV/TV	%	Bone and tissue volume relation	↓♂	=	↓♂	↓♂♀	=
	Conn. Dn	1/mm <sup>3</sup>	Trabecular connectivity	=	=	↓♀	=	=
	Tb. Pf	1/mm	Trabecular connectivity (inverse)	=	⚠♀	=	=	=
	Tb. Th	mm	Trabecular thickness	=	↓♀	↓♂	↓♂♀	↓♀
	Tb. Sp	mm	Trabecular distance or separation	⚠♂	=	=	↑♂♀	=
	Tb. N	1/mm	Trabeculae number	↓♂	=	⚠♀	↓♂♀	=
Cortical Bone	TMD	g/cm <sup>3</sup>	Tissue Mineral Density	=	=	=	⚠♂♀	=
	TV	mm <sup>3</sup>	Cortical bone volume with pores	⚠♂	↓♀	=	↓♂♀	⚠♀
	BV	mm <sup>3</sup>	Cortical bone volume without pores	↓♂	↓♀	=	↓♂♀	⚠♀
	BS/BV	1/mm	Bone surface and volume relation (size)	=	⚠♀	=	↑♂♀	⚠♀
	Cort. Tb. Th	mm	Cortical bone thickness without pores	=	=	=	↓♂♀	↓♀
	Cort. Tb. Sp	mm	Pore diameter of cortical bone	=	=	↑♀	=	=
	Po(tot)	%	Total porosity	=	=	↑♀	=	=
	Po(op)	%	Percentage of open porosity	=	=	↑♀	=	=
	Ct. TV	mm <sup>3</sup>	Total volume of cortical bone and bone marrow	⚠♂	↓♀	↓♂	↓♂♀	=
	Ct. BV	mm <sup>3</sup>	Cortical bone volume	↓♂	↓♀	↓♂	↓♂♀	⚠♀

**Figure 26. Review of bone alterations of KI and Hemi A12T mice under different challenges.** The first column indicates the bone area where the parameters included in the second column belong to. Third and fourth columns include the parameter magnitude and a brief description of each parameter. The next 4 columns, ordered from “Aged” to “*Lmna*<sup>G609G</sup>” show the changes observed in A12T mice in each condition compared to WT littermates. The last column shows the changes displayed in Hemi A12T females under osteoporosis-induction by ovariectomy. The direction and color of arrows represent the sense of the change, including down-sided red arrows to indicate a reduction compared to WT mice and up-sided green arrows for the opposite change. A striped pattern in the arrows indicate that the p-value in that parameter is between 0.05 and 0.1 and solid color is used when the parameter reaches statistical significance.

BAF is a nuclear envelope protein that binds to the nuclear lamina and nuclear envelope proteins such as emerin or LAP2<sup>55</sup> and whose functions in the cell remain still poorly understood. Considering that the NGPS phenotype is quite similar to HGPS, caused by mutations in *LMNA*, we decided to cross the A12T mice with the *Lmna*<sup>G609G/G609G</sup> colony to study the consequences of the interaction of both alterations. Compared to the already pronounced premature aging of *Lmna*<sup>G609G/G609G</sup> mice, the double-mutant *Banf1*<sup>A12T/A12T</sup> *Lmna*<sup>G609G/G609G</sup> (DKI) mice showed a remarkably aggravated progeroid phenotype. DKI mice exhibited lower body weights than their littermates and their average life expectancy was reduced from 168 days in

*Lmna*<sup>G609G/G609G</sup> mice to barely 90 days in DKI animals. At the skeletal level, despite being already severely altered in the HGPS model, DKI mice presented a worsening in most of the evaluated features (Figure 26). In summary, the presence of the two mutations seems to have a synergistic effect on aging and aggravates the progeroid phenotype *in vivo*.

To understand how the p.Ala12Thr mutation of BAF affects bone biology, we performed an RNAseq study in bone marrow and tibia. Although no changes were observed in bone marrow with respect to controls, in bone we observed a gene expression pattern reminiscent of a pathology called Osteogenesis Imperfecta<sup>236</sup>. In addition to the alteration in bone development genes, an increase in the expression of inflammatory pathways and a reduction in those related to mitosis and mitochondria were observed. Thus, we have described the transcriptional and physiological modifications that validate the A12T mouse as a suitable model for NGPS research and for the study of bone aging. However, the implications of these experiments are challenging to interpret without an in-depth study of BAF activity and functionality in the nuclear envelope. BAF has been shown to be essential for cell replication by protecting the genome and enabling cell division. Among other functions, BAF has been implicated in chromosome rearrangement after mitosis, repair of nuclear envelope breaks, innate immunity, and DNA damage response<sup>59–61,67,237,238</sup>. However, beyond a possible connection with nuclear aberrations or with the response to cellular damage via PARP1 and repair through the NHEJ pathway, we do not know exactly the association of BAF and the p.Ala12Thr mutation to aging<sup>62,63</sup>. More studies will be needed to understand precisely its mechanism of action.

The development and characterization of the murine model of NGPS aims to deepen into the study of new mutations causing premature aging. In turn, it facilitates the search of new drugs specifically targeted to wild-type or mutated BAF isoforms that would delay physiological and pathological aging. In addition to therapies targeting specific mutations, many of the anti-aging interventions being currently studied are related to the regulation of metabolism, either through diet, as in caloric restriction or restriction of specific nutrients, or through mimetic drugs, such as resveratrol or metformin<sup>11,228</sup>. In all cases, the aim would be the inhibition of anabolic trophic pathways, slowing of the metabolic rate and activation of pro-longevity pathways<sup>77</sup>. NAD<sup>+</sup> is a central metabolite of cellular energy balance and a key mediator of many of the benefits of these interventions to delay aging<sup>97,239</sup>. NAD<sup>+</sup> levels in the body are

decreased in aged individuals, whereas they increase, for example, with physical exercise<sup>87,240,241</sup>. The increase in the NAD<sup>+</sup>/NADH ratio determines a state of low cellular energy that triggers survival and pro-longevity pathways. NAD<sup>+</sup> supplementation in the diet with NAD<sup>+</sup> precursors has been a strategy evaluated in recent years for the treatment of various progeroid syndromes<sup>119,242–244</sup> and aging-associated diseases due to its systemic effect and easy application<sup>105,109,111–115,245</sup>. With this background, in the **second objective of this Doctoral Thesis** we approach a potential intervention with the NAD<sup>+</sup> precursors niacin and NR in the *Zmpste24<sup>-/-</sup>* and *Lmna<sup>G609G/G609G</sup>* progeria mouse models. While the increase in cellular NAD<sup>+</sup> in dietary supplementation with NR occurs through the salvage pathway, supplementation with niacin involves the Preiss-Handler pathway. Although in both cases the result would be the increase of cellular NAD<sup>+</sup>, niacin supplementation would have the added advantage of its lower cost compared to the NR precursor.

We decided to start with the *Zmpste24<sup>-/-</sup>* model due to its more pronounced metabolic phenotype and longer survival compared to the *Lmna<sup>G609G/G609G</sup>* model, which would allow a better detection of any potential benefits over a longer time window. NR treatment significantly improved the health of *Zmpste24<sup>-/-</sup>* mice by counteracting many of the most characteristic features of progeria. Thus, NR treatment reduced the levels of medium-sized cells (monocytes and eosinophils among others) and the amount of total and oxygen-loaded hemoglobin in blood. At the tissue level, specific improvements were observed in various tissues such as skeletal muscle, stomach, spleen or aorta, while there was a general improvement in bone structure compared to control progeroid animals. Interestingly, WT animals supplemented with NR also exhibited an apparent worsening of bone values. In other metabolic interventions against aging, such as methionine restriction, there were also similar results of an apparent metabolic decay in WT mice that was hypothesized to optimize physiological fitness<sup>76</sup>. In the particular case of bone structure, it is difficult to imagine that this shift in the NR-supplemented control animals would result in an optimization of bone structure, and a detailed study of bone metabolism would be necessary to analyze the effect of NR in healthy individuals. Finally, the results at the metabolic level are difficult to interpret despite the clear improvement in lifespan. Although they seem to counteract the metabolic shift observed in the Oxymax studies of progeroid animals, neither body weight nor glycemia recovery was observed, in addition to the increased hypothermia of these progeroid mice.

With niacin supplementation, *Zmpste24<sup>-/-</sup>* mice also showed a delay in their accelerated aging phenotype and a marked survival extension. Despite the absence of changes in their body weight, the mice seemed macroscopically bigger in size and apparently healthier than their control progeroid littermates. This could be explained by a reduction in their kyphosis, although further experiments will be necessary to demonstrate this. At the metabolic level, in this case we did observe a recovery from the hypoglycemia and hypothermia characteristic of *Zmpste24<sup>-/-</sup>* mice, although without changes in Oxymax analysis. Altogether, supplementation with both precursors appears to be beneficial for longevity in a progeroid context, although their consequences on metabolism probably differ depending on the cellular pathway by which NAD<sup>+</sup> is increased. In addition to the fact that it would be interesting to evaluate its benefits in healthy individuals, further studies that allow us to accurately measure NAD<sup>+</sup> levels in various tissues before and after supplementation are indispensable.

Subsequently, we decided to perform an RNA sequencing analysis on liver samples from NR-supplemented *Zmpste24<sup>-/-</sup>* mice to investigate the transcriptional changes involved in the observed health improvement. PCA analysis classified samples from progeroid and WT animals into two clearly distinct groups, while NR-treated *Zmpste24<sup>-/-</sup>* mice partially reversed their transcriptomic alteration and clustered into an intermediate state, in excellent agreement with the beneficial effects of this treatment. Moreover, pathways typically associated with the progeroid phenotype such as altered fatty acid metabolism, insulin and mTOR signaling, P53 activation, ROS defense or hypoxia response were partially reversed. In addition, bile acid metabolism, which has been recently proposed as a therapeutic target for progeria interventions, is also upregulated by NR supplementation. Finally, using changes in the expression of major urinary proteins (MUPs) as a representative alteration in mouse models of accelerated aging, there is clear evidence of a significant recovery of the progeroid transcriptomic pattern in *Zmpste24<sup>-/-</sup>* mice. Strikingly, despite the connections described in the literature between NAD<sup>+</sup> and mitochondrial biology <sup>87</sup>, there is no clear contribution of mitochondrial pathways to the recovery of the phenotype, which seems to correspond more to a general recovery of the gene expression profile rather than alterations in specific pathways. In the next months, we will perform an RNAseq analysis of the mice supplemented with niacin and, comparing it with the NR intervention, we hope to obtain more answers about the specific

mechanism responsible for the improvement of the phenotype and the differences in the supplementation with one or the other precursor.

To examine whether increasing NAD<sup>+</sup> levels also improve the phenotype of the canonical progeria model, we supplemented *Lmna*<sup>G609G/G609G</sup> mice with NR. In contrast to what was observed in the *Zmpste24*<sup>-/-</sup> model, surprisingly, survival was unchanged compared to control *Lmna*<sup>G609G/G609G</sup> animals. Moreover, the alterations present in *Lmna*<sup>G609G/G609G</sup> mice in blood cells, especially in the red line, as well as the metabolic drift evidenced in Oxymax, appeared to be aggravated. Furthermore, hypoglycemia and hypothermia of mice present in *Lmna*<sup>G609G/G609G</sup> mice were exacerbated, whereas NR supplementation in the *Zmpste24*<sup>-/-</sup> model only reduced glycemia. Niacin supplementation also did not seem to improve the phenotype of *Lmna*<sup>G609G/G609G</sup> mice, as no changes in body weight or lifespan were evidenced. As in the *Zmpste24*<sup>-/-</sup> model, niacin raised body temperature, but no further significant metabolic changes were observed. Therefore, it seems that the use of NAD<sup>+</sup> precursors in *Lmna*<sup>G609G/G609G</sup> mice does not provide health benefits and could even be potentially detrimental.

As discussed above, testing in future experiments whether supplementation is actually increasing NAD<sup>+</sup> levels is critical in both models. The failure of this intervention in *Lmna*<sup>G609G/G609G</sup> mice could have multiple causes, such as a model-specific deleterious effect of NAD<sup>+</sup> restoration by secondary effects on other metabolic pathways. The contrasting results between the two models highlight the need to further study the particular differences between *Zmpste24*<sup>-/-</sup> and *Lmna*<sup>G609G/G609G</sup> mice despite the similarities in their phenotype. Perhaps, the success of NAD<sup>+</sup> supplementation is dependent on a particular metabolic context and thus, the *Zmpste24*<sup>-/-</sup>-specific metabolic phenotype facilitates these benefits. Aging metabolism is very complex and interconnected, and perhaps expecting NAD<sup>+</sup> supplementation to be beneficial *per se* in any physiological context is naïve, given the involvement of this metabolite in such diverse cellular pathways<sup>246–248</sup>. Finally, despite the increased lifespan in the *Zmpste24*<sup>-/-</sup> model with both precursors, the divergent physiological consequences on glycemia, body temperature, and energy metabolism demand further study of how the molecular pathways by which NAD<sup>+</sup> is increased influence health beyond the mere concentration increase itself (Figure 27).

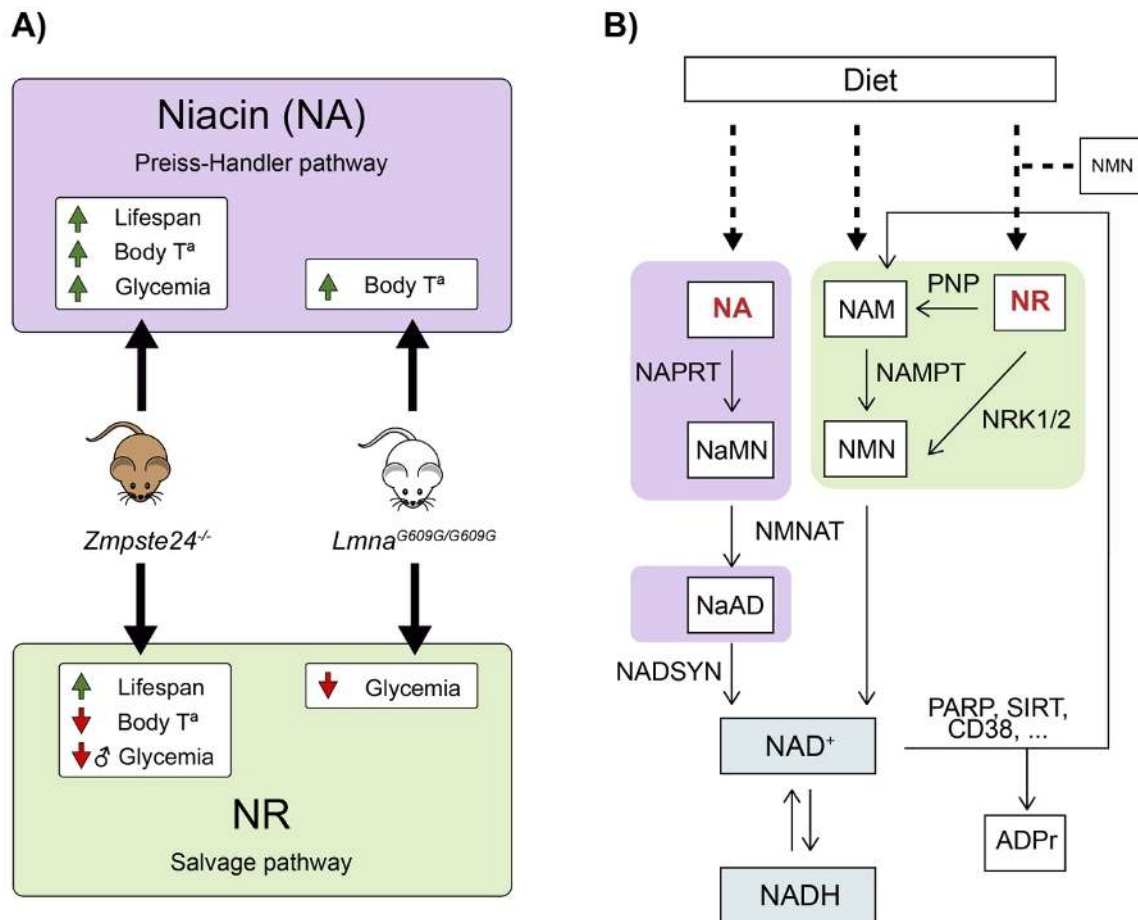


**Figure 27. Review of the two strategies used in *Zmpste24<sup>-/-</sup>* and *Lmna<sup>G609G/G609G</sup>* mice to induce NAD<sup>+</sup> boost, based on NR or niacin supplementation. A) Diagram of the physiological adaptations induced by NR and niacin in both progeroid mouse models. B) Illustration of mammalian NAD<sup>+</sup> biosynthesis pathways with exogenous precursors supplementation. Purple boxes represent Preiss-Handler pathway while green boxes represent salvage pathway. Red font indicates NAD<sup>+</sup> precursors.**

Although the lifespan extension obtained by NAD<sup>+</sup> supplementation does not appear to be caused by a major switch in mitochondrial pathways, mitochondria play an active role in the regulation of aging metabolism through their role in cellular bioenergetics, communication with the nucleus, and control of proteostasis<sup>124,249,250</sup>. Thus, it has emerged as a potential therapeutic target to regulate cellular metabolic activity and delay aging and the onset of aging-associated diseases<sup>120,251</sup>. LONP1 is a central protease in mitochondrial biology, with a multitude of functions such as degradation of damaged proteins, gene regulation or DNA maintenance and replication<sup>146,148,150–152,160–162,252</sup>. The LONP1 heterozygous mice show an OXPHOS complex reprogramming that alters their mitochondrial functionality and reduces their susceptibility to the development of colon tumors and papillomas<sup>165</sup>. Remarkably, the increased expression of LONP1 also seems to alter the organization of OXPHOS

complexes and has a relevant role in certain types of cancers<sup>165</sup>. In order to further deep in the study of this protease, in the **third objective of this Doctoral Thesis** we decided to generate a transgenic mouse model of LONP1 overexpression and to perform its physiological, metabolic and mitochondrial characterization.

The strategy to generate the transgenic lines was designed for the consecutive insertion of several copies of *Lonp1* but did not control the insertion locus. We generated four different colonies of which transcriptional and protein expression analysis determined that two of the lines had 2 extra copies of *Lonp1* while the other two had 6 extra copies. As all four colonies were viable and showed no apparent differences in their phenotype, we decided to work with the two lines with the highest expression. However, as we verified later, one of the selected lines seemed to present the transgenic cassette inserted in close linkage to the *Trp53* locus, so we excluded it for the majority of the work to prevent possible interferences in the results and to avoid erroneous conclusions.

*Lonp1<sup>TG</sup>* mice were indistinguishable from their control littermates, with no change in body weight or appearance, and showed only minor differences at the histological level that do not seem to alter significantly their physiology. Although LONP1 is required for the control of proteostasis and the correct function of the mitochondrial machinery, *Lonp1<sup>TG</sup>* mice did not exhibit any differences compared to control mice under proteostatic or inflammatory stress. The lack of differences in these proteostatic stress conditions could be explained by many factors. On the one hand, it might be necessary to optimize drug doses to assess the consequences of LONP1 overexpression in chronic conditions, in contrast to the acute stress experiments conducted. On the other hand, it is possible that these toxics generate a systemic physiological response that overshadows the differences at the mitochondrial level, so it would be necessary to repeat these experiments at the cellular level to reduce the variability and to have a clearer view of what is happening in the mitochondria.

In relation to tumor development, we observed an increased mortality of transgenic mice in the context of TP53 deficiency after crossing them with *Trp53<sup>-/-</sup>* mice. However, the absence of differences after chemical induction of colon tumors led us to speculate that the favoring of tumor development by LONP1 overexpression may be dependent on the tumor type and environment, maybe determined by the specific bioenergetic requirements of cancer cells.

At the metabolic level, no major alterations were observed in *Lonp1<sup>TG</sup>* mice neither in serum metabolites, with few sex-dependent and very modest changes, nor in glucose metabolism or in circulating cholesterol or aldosterone, despite the relationship of LONP1 with StAR and cholesterol metabolism. These negative results led us to hypothesize that perhaps the effects of LONP1 overexpression were not observable under basal conditions and were only measurable under conditions of metabolic stress. Therefore, we fed our mice with a high-fat and a high-sucrose diet, widely validated in the literature to simulate western-like diets. However, no changes were detected at body weight gain, insulin and glucose response tests, histological level, thermogenic response by cold shock nor Oxymax analysis. In summary, *Lonp1<sup>TG</sup>* mice show no histological or systemic metabolic alterations, even under conditions of metabolic stress, which is surprising as we would expect LONP1 to have a relevant role in resistance to chronic mitochondrial stresses.

Given the above, we wondered whether the overexpression of LONP1 would lead to any alteration in the mitochondria that was not reflected at the physiological level. The mitochondrial genome varies in the number of copies and in the stability of its genes between individuals and with age, being transcriptionally regulated by proteins such as POLRMT or TFAM. Since TFAM is a substrate of LONP1, we hypothesized that there should be differences at the level the mtDNA biology of TG mice, but we did not observe changes in the ratio of nuclear to mitochondrial genomes, nor did we see an increase in ND4 deletions or changes in protein levels of POLRMT or TFAM. Furthermore, mitochondria from *Lonp1<sup>TG</sup>* animals did not show any changes in protein levels of OXPHOS subunits, complexes or supercomplexes. Functional characterization of the mitochondria from transgenic mice was completed by a Seahorse system analysis under basal and fatty acid enrichment conditions, which revealed reduced respiration in the basal and proton leak phase and a reduction of the extracellular acidification rate only under basal conditions. These results are shocking and evidence that mitochondrial fitness is much more affected by decreasing than increasing LONP1 levels. Perhaps, the fact that we have performed most of our experiments in murine models may make us lose clarity on what happens specifically at the mitochondrial level, but it also makes it clear that whether or not there are changes in mitochondria, they are not of great relevance at the physiological level.

An early hypothesis when we generated the transgenic mouse was that overexpression of LONP1 would alter the energetic and physiological balance

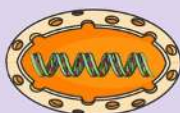
between mitochondrial fitness and tumor malignancy. We speculated that increasing LONP1 would somehow generate mitochondria with higher energetic potential and thus delay the physiological decline of aging and extend lifespan, in turn increasing the risk of developing cancer in *Lonp1<sup>TG</sup>* mice. The absence of changes in lifespan of *Lonp1<sup>TG</sup>* mice could be explained by the trade-off of mitochondrial optimization with increased cancer mortality, attending to the increased tumor incidence at least in the context of TP53 deficiency. However, validating this hypothesis would require a survival analysis of tumor-free animals and the results did not suggest any lifespan extension, as neither maximal survival nor telomere length varied between the two experimental groups. Nevertheless, TG animals might exhibit the same lifespan but reaching advanced ages in better health.

To evaluate the potential mitochondrial optimization, we performed a health characterization on aspects such as muscular endurance, motor coordination or animal appearance at advanced ages. First, we performed a muscular endurance test on the treadmill that revealed a higher endurance of females under basal conditions. Then, we decided to train these mice for two weeks at 50-60% of maximal intensity and test them with the same treadmill running test to evaluate the potential improvement in mitochondrial health mediated by exercise<sup>253–255</sup>. We expected that TG mice would increase their endurance to a greater extent, but instead we observed that the initial differences in females were lost. To analyze if LONP1 overexpression mitigates the aging-derived sarcopenia<sup>256–258</sup>, we performed a hanging wire test in 2-year-old mice, which revealed that the *Lonp1<sup>TG</sup>* animals were able to resist longer and with fewer falls while hanging. This improvement in their abilities appeared to derive from a muscle strength gain rather than an improvement in coordination, as these aged mice exhibited no differences in the Rotarod test. We then developed a score of aging based on a subset of features of their appearance. Although most of these showed no change from the control animals, there were some features classically associated with mouse aging such as loss of whiskers, alopecia, or corneal opacity that showed improvement in the TG mice.

Overall, *Lonp1<sup>TG</sup>* mice show very limited changes relative to WT littermates that are summarized as increased incidence of tumors in TP53 deficiency, reduced mitochondrial respiration at specific energetic phases, and health improvements in muscular endurance and appearance in aged individuals. Thus, considering the observations made in the heterozygous *Lonp1<sup>+/-</sup>* mice<sup>165</sup>, mitochondria are more

sensitive to decreased than increased LONP1 levels. Despite the accumulation of negative results, the crucial role of LONP1 in mitochondria raises the possibility that the design of the transgenic colony in the BL6 murine background may be masking some of the effects of LONP1 overexpression. The literature describes how some specific mitochondrial mutations in the murine background can influence and determine the phenotype of a model. To explore this possibility, in the coming months we will generate a cohort of *Lonp1*<sup>TG</sup> mice in CD1 background, and we will detail their basic physiology and lifespan.

To summarize, in the present Doctoral Thesis we have contributed to the study of aging by generating and characterizing new murine models of premature aging, as well as testing new metabolic interventions to delay the functional decline. First, we generated a new murine model of NGPS and characterized its bone alterations to validate it as a useful tool for the study of progeria and bone aging. Next, we explored a metabolic intervention to delay physiological decline in progeria, based on the increase of NAD<sup>+</sup> with NR and niacin supplementation in the two most robust progeria mouse models. Supplementation with both precursors delays aging only in the *Zmpste24*<sup>-/-</sup> model and opens the possibility of NAD<sup>+</sup> treatment for some progeroid pathologies, although it also highlights the complexity of progeroid biology and aging metabolism. Finally, due to the involvement of mitochondria in most metabolic interventions, we have studied the effects of LONP1 overexpression on mitochondrial physiology and biology through the generation of a transgenic murine model of *Lonp1* (Figure 28). In this PhD Thesis, the objectives addressed range from the translation of clinical challenges to biological research with the development of the new murine model of NGPS, to applied science with the development of new metabolic interventions, as well as basic science experimentation with the study of the role of LONP1 in mitochondria.

	NGPS mouse model	LONP1 overexpression mouse model	NAD <sup>+</sup> boost in accelerated aging
Mouse model	Banf1 <sup>A12T/A12T</sup>	Lonp1 <sup>+TG</sup>	Zmpste24 <sup>-/-</sup> Lmna <sup>G609G/G609G</sup>
Hallmarks implicated	  Genomic instability    Cellular senescence	  Loss of proteostasis    Mitochondrial dysfunction	  Deregulated nutrient-sensing    Altered cellular communication
Physiological target	 Genome - Nucleus	 Mitochondria	 Metabolism Complex level
Physiological consequences			

**Figure 28. Summary of the three main objectives addressed in this doctoral thesis, specifying the murine model used, the main hallmarks of aging addressed and the physiological targets and consequences.** The first column shows the study of the p.Ala12Thr mutation in the nuclear protein BAF and how the generation of the new murine model of NGPS recapitulates the bone alterations present in human patients. The second column shows the generation of a transgenic murine model of overexpression of LONP1, an essential protease in mitochondria. The third column illustrates the testing of a metabolic intervention based on NAD<sup>+</sup> boost with NR precursors and niacin in accelerated aging models, reflecting improvement of the progeroid phenotype and increased longevity at least in the *Zmpste24*<sup>-/-</sup> model.





# CONCLUSIONS



1. Complete absence of BAF is lethal in mice, whereas its heterozygous deletion or the presence of the c.34G>A mutation of *Banf1* in homozygosis or hemizygosis does not affect their longevity.
2. *Banf1*<sup>A12T/A12T</sup> mice present bone alterations in aged individuals, in *Lmna*<sup>G609G/G609G</sup> progeroid background and under conditions of bone stress such as osteoporosis induction by ovariectomy or iron overdose.
3. *Banf1*<sup>A12T/A12T</sup> mice exhibit a gene expression pattern in tibia similar to that of Osteogenesis Imperfecta.
4. Supplementation with NR or niacin extends lifespan and ameliorates the accelerated aging phenotype of the *Zmpste24*<sup>-/-</sup> mice through a partial recovery of the alterations in gene expression classically associated with progeria.
5. Supplementation with NR or niacin does not delay premature aging in the *Lmna*<sup>G609G/G609G</sup> mouse model.
6. Overexpression of LONP1 in the *Lonp1*<sup>TG</sup> transgenic mouse model does not produce alterations in mitochondrial biology, metabolism, health or longevity.







# **CONCLUSIONES**



2. La ausencia completa de BAF es letal en ratones, mientras que su delección en heterocigosis o la presencia de la mutación c.34G>A de *Banf1* en homocigosis o hemicigosis no afecta a su longevidad.
3. Los ratones *Banf1*<sup>A12T/A12T</sup> presentan alteraciones óseas en individuos envejecidos, en fondo progeroide *Lmna*<sup>G609G/G609G</sup> y en condiciones de estrés óseo por inducción de osteoporosis mediante ovariectomía o sobredosis de hierro.
4. Los ratones *Banf1*<sup>A12T/A12T</sup> presentan un patrón de expresión génica en tibia similar al característico de Osteogénesis Imperfecta.
5. La suplementación con NR o niacina extiende la supervivencia y rescata parcialmente el fenotipo de envejecimiento acelerado de los ratones *Zmpste24*<sup>-/-</sup> a través de una recuperación parcial de las alteraciones en la expresión génica clásicamente asociadas a la progeria.
6. La suplementación con NR o niacina no retrasa el envejecimiento prematuro en el modelo murino *Lmna*<sup>G609G/G609G</sup>.
7. La sobreexpresión de LONP1 en el modelo murino transgénico *Lonp1*<sup>TG</sup> no produce alteraciones en la biología mitocondrial, el metabolismo, la salud o la longevidad.







# REFERENCES



1. Wollman, A. J. M., Nudd, R., Hedlund, E. G. & Leake, M. C. From Animaculum to single molecules: 300 years of the light microscope. *Open Biol.* **5**, 150019 (2015).
2. Shendure, J. *et al.* DNA sequencing at 40: past, present and future. *Nature* **550**, 345–353 (2017).
3. López-Otín, C. & Kroemer, G. Hallmarks of Health. *Cell* **184**, 33–63 (2021).
4. Schumacher, B., Pothof, J., Vijg, J. & Hoeijmakers, J. H. J. The central role of DNA damage in the ageing process. *Nature* **592**, 695–703 (2021).
5. Ma, S. & Gladyshev, V. N. Molecular signatures of longevity: Insights from cross-species comparative studies. *Semin. Cell Dev. Biol.* **70**, 190–203 (2017).
6. Tacutu, R. *et al.* Human Ageing Genomic Resources: integrated databases and tools for the biology and genetics of ageing. *Nucleic Acids Res.* **41**, D1027-1033 (2013).
7. Austad, S. N. & Fischer, K. E. Sex Differences in Lifespan. *Cell Metab.* **23**, 1022–1033 (2016).
8. Sampathkumar, N. K. *et al.* Widespread sex dimorphism in aging and age-related diseases. *Hum. Genet.* **139**, 333–356 (2020).
9. Morris, B. J., Willcox, B. J. & Donlon, T. A. Genetic and epigenetic regulation of human aging and longevity. *Biochim. Biophys. Acta Mol. Basis Dis.* **1865**, 1718–1744 (2019).
10. Brooks-Wilson, A. R. Genetics of healthy aging and longevity. *Hum. Genet.* **132**, 1323–1338 (2013).
11. Fontana, L. & Partridge, L. Promoting health and longevity through diet: from model organisms to humans. *Cell* **161**, 106–118 (2015).
12. Longo, V. D. & Panda, S. Fasting, Circadian Rhythms, and Time-Restricted Feeding in Healthy Lifespan. *Cell Metab.* **23**, 1048–1059 (2016).
13. Bah, T. M., Goodman, J. & Iliff, J. J. Sleep as a Therapeutic Target in the Aging Brain. *Neurother. J. Am. Soc. Exp. Neurother.* **16**, 554–568 (2019).
14. Mattis, J. & Sehgal, A. Circadian Rhythms, Sleep, and Disorders of Aging. *Trends Endocrinol. Metab. TEM* **27**, 192–203 (2016).
15. Carapeto, P. V. & Aguayo-Mazzucato, C. Effects of exercise on cellular and tissue aging. *Aging* **13**, 14522–14543 (2021).
16. Weyh, C., Krüger, K. & Strasser, B. Physical Activity and Diet Shape the Immune System during Aging. *Nutrients* **12**, E622 (2020).

17. Strasser, B., Wolters, M., Weyh, C., Krüger, K. & Ticinesi, A. The Effects of Lifestyle and Diet on Gut Microbiota Composition, Inflammation and Muscle Performance in Our Aging Society. *Nutrients* **13**, 2045 (2021).
18. Furrer, R. & Handschin, C. Lifestyle vs. pharmacological interventions for healthy aging. *Aging* **12**, 5–7 (2020).
19. Klimova, B., Valis, M. & Kuca, K. Cognitive decline in normal aging and its prevention: a review on non-pharmacological lifestyle strategies. *Clin. Interv. Aging* **12**, 903–910 (2017).
20. Madore, C., Yin, Z., Leibowitz, J. & Butovsky, O. Microglia, Lifestyle Stress, and Neurodegeneration. *Immunity* **52**, 222–240 (2020).
21. da Costa, J. P. *et al.* A synopsis on aging-Theories, mechanisms and future prospects. *Ageing Res. Rev.* **29**, 90–112 (2016).
22. López-Otín, C., Blasco, M. A., Partridge, L., Serrano, M. & Kroemer, G. The hallmarks of aging. *Cell* **153**, 1194–1217 (2013).
23. North, B. J. & Sinclair, D. A. The intersection between aging and cardiovascular disease. *Circ. Res.* **110**, 1097–1108 (2012).
24. Palmer, A. K., Gustafson, B., Kirkland, J. L. & Smith, U. Cellular senescence: at the nexus between ageing and diabetes. *Diabetologia* **62**, 1835–1841 (2019).
25. Liu, R.-M. Aging, Cellular Senescence, and Alzheimer’s Disease. *Int. J. Mol. Sci.* **23**, 1989 (2022).
26. Hou, Y. *et al.* Ageing as a risk factor for neurodegenerative disease. *Nat. Rev. Neurol.* **15**, 565–581 (2019).
27. Collado, M., Blasco, M. A. & Serrano, M. Cellular senescence in cancer and aging. *Cell* **130**, 223–233 (2007).
28. Tarride, J.-E. *et al.* A review of the cost of cardiovascular disease. *Can. J. Cardiol.* **25**, e195-202 (2009).
29. Heidenreich, P. A. *et al.* Forecasting the future of cardiovascular disease in the United States: a policy statement from the American Heart Association. *Circulation* **123**, 933–944 (2011).
30. Rattan, S. I. S. Aging is not a disease: implications for intervention. *Aging Dis.* **5**, 196–202 (2014).
31. Wang, M.-J. *et al.* Rejuvenating Strategies of Tissue-specific Stem Cells for Healthy Aging. *Aging Dis.* **10**, 871–882 (2019).

32. Kleijer, W. J. *et al.* Incidence of DNA repair deficiency disorders in western Europe: Xeroderma pigmentosum, Cockayne syndrome and trichothiodystrophy. *DNA Repair* **7**, 744–750 (2008).
33. Coppedè, F. The epidemiology of premature aging and associated comorbidities. *Clin. Interv. Aging* **8**, 1023–1032 (2013).
34. Özen, S., Akıncı, B. & Oral, E. A. Current Diagnosis, Treatment and Clinical Challenges in the Management of Lipodystrophy Syndromes in Children and Young People. *J. Clin. Res. Pediatr. Endocrinol.* **12**, 17–28 (2020).
35. Black, M. M. *et al.* Early childhood development coming of age: science through the life course. *Lancet Lond. Engl.* **389**, 77–90 (2017).
36. Kubben, N. & Misteli, T. Shared molecular and cellular mechanisms of premature ageing and ageing-associated diseases. *Nat. Rev. Mol. Cell Biol.* **18**, 595–609 (2017).
37. Ramírez, C. L., Cadiñanos, J., Varela, I., Freije, J. M. P. & López-Otín, C. Human progeroid syndromes, aging and cancer: new genetic and epigenetic insights into old questions. *Cell. Mol. Life Sci. CMLS* **64**, 155–170 (2007).
38. Navarro, C. L., Cau, P. & Lévy, N. Molecular bases of progeroid syndromes. *Hum. Mol. Genet.* **15 Spec No 2**, R151-161 (2006).
39. Oshima, J., Sidorova, J. M. & Monnat, R. J. Werner syndrome: Clinical features, pathogenesis and potential therapeutic interventions. *Ageing Res. Rev.* **33**, 105–114 (2017).
40. Ellis, N. A., Sander, M., Harris, C. C. & Bohr, V. A. Bloom's syndrome workshop focuses on the functional specificities of RecQ helicases. *Mech. Ageing Dev.* **129**, 681–691 (2008).
41. Karikkineth, A. C., Scheibye-Knudsen, M., Fivenson, E., Croteau, D. L. & Bohr, V. A. Cockayne syndrome: Clinical features, model systems and pathways. *Ageing Res. Rev.* **33**, 3–17 (2017).
42. Crabbe, L., Jauch, A., Naeger, C. M., Holtgreve-Grez, H. & Karlseder, J. Telomere dysfunction as a cause of genomic instability in Werner syndrome. *Proc. Natl. Acad. Sci. U. S. A.* **104**, 2205–2210 (2007).
43. Butin-Israeli, V., Adam, S. A., Goldman, A. E. & Goldman, R. D. Nuclear lamin functions and disease. *Trends Genet. TIG* **28**, 464–471 (2012).
44. Schreiber, K. H. & Kennedy, B. K. When lamins go bad: nuclear structure and disease. *Cell* **152**, 1365–1375 (2013).

45. Merideth, M. A. *et al.* Phenotype and course of Hutchinson-Gilford progeria syndrome. *N. Engl. J. Med.* **358**, 592–604 (2008).
46. De Sandre-Giovannoli, A. *et al.* Lamin a truncation in Hutchinson-Gilford progeria. *Science* **300**, 2055 (2003).
47. Eriksson, M. *et al.* Recurrent de novo point mutations in lamin A cause Hutchinson-Gilford progeria syndrome. *Nature* **423**, 293–298 (2003).
48. Cadiñanos, J., Varela, I., López-Otín, C. & Freije, J. M. P. From immature lamin to premature aging: molecular pathways and therapeutic opportunities. *Cell Cycle Georget. Tex* **4**, 1732–1735 (2005).
49. Rusiñol, A. E. & Sinensky, M. S. Farnesylated lamins, progeroid syndromes and farnesyl transferase inhibitors. *J. Cell Sci.* **119**, 3265–3272 (2006).
50. Gordon, L. B., Rothman, F. G., López-Otín, C. & Misteli, T. Progeria: a paradigm for translational medicine. *Cell* **156**, 400–407 (2014).
51. Cabanillas, R. *et al.* Néstor-Guillermo progeria syndrome: a novel premature aging condition with early onset and chronic development caused by BANF1 mutations. *Am. J. Med. Genet. A.* **155A**, 2617–2625 (2011).
52. Puente, X. S. *et al.* Exome sequencing and functional analysis identifies BANF1 mutation as the cause of a hereditary progeroid syndrome. *Am. J. Hum. Genet.* **88**, 650–656 (2011).
53. Fisher, H. G., Patni, N. & Scheuerle, A. E. An additional case of Néstor-Guillermo progeria syndrome diagnosed in early childhood. *Am. J. Med. Genet. A.* **182**, 2399–2402 (2020).
54. Montes de Oca, R., Shoemaker, C. J., Gucek, M., Cole, R. N. & Wilson, K. L. Barrier-to-autointegration factor proteome reveals chromatin-regulatory partners. *PloS One* **4**, e7050 (2009).
55. Lee, K. K. *et al.* Distinct functional domains in emerin bind lamin A and DNA-bridging protein BAF. *J. Cell Sci.* **114**, 4567–4573 (2001).
56. Paquet, N. *et al.* Néstor-Guillermo Progeria Syndrome: a biochemical insight into Barrier-to-Autointegration Factor 1, alanine 12 threonine mutation. *BMC Mol. Biol.* **15**, 27 (2014).
57. Samson, C. *et al.* Structural analysis of the ternary complex between lamin A/C, BAF and emerin identifies an interface disrupted in autosomal recessive progeroid diseases. *Nucleic Acids Res.* **46**, 10460–10473 (2018).

58. Capanni, C. *et al.* Lamin A precursor induces barrier-to-autointegration factor nuclear localization. *Cell Cycle Georget. Tex* **9**, 2600–2610 (2010).
59. Halfmann, C. T. *et al.* Repair of nuclear ruptures requires barrier-to-autointegration factor. *J. Cell Biol.* **218**, 2136–2149 (2019).
60. Young, A. M., Gunn, A. L. & Hatch, E. M. BAF facilitates interphase nuclear membrane repair through recruitment of nuclear transmembrane proteins. *Mol. Biol. Cell* **31**, 1551–1560 (2020).
61. Kono, Y. *et al.* Nucleoplasmic lamin C rapidly accumulates at sites of nuclear envelope rupture with BAF and cGAS. *J. Cell Biol.* **221**, e202201024 (2022).
62. Bolderson, E. *et al.* Barrier-to-autointegration factor 1 (Banf1) regulates poly [ADP-ribose] polymerase 1 (PARP1) activity following oxidative DNA damage. *Nat. Commun.* **10**, 5501 (2019).
63. Burgess, J. T. *et al.* Barrier-to-autointegration-factor (Banf1) modulates DNA double-strand break repair pathway choice via regulation of DNA-dependent kinase (DNA-PK) activity. *Nucleic Acids Res.* **49**, 3294–3307 (2021).
64. Haraguchi, T. *et al.* Nuclear localization of barrier-to-autointegration factor is correlated with progression of S phase in human cells. *J. Cell Sci.* **120**, 1967–1977 (2007).
65. Marcelot, A. *et al.* Di-phosphorylated BAF shows altered structural dynamics and binding to DNA, but interacts with its nuclear envelope partners. *Nucleic Acids Res.* **49**, 3841–3855 (2021).
66. Rose, M. *et al.* The Impact of Rare Human Variants on Barrier-To-Auto-Integration Factor 1 (Banf1) Structure and Function. *Front. Cell Dev. Biol.* **9**, 775441 (2021).
67. Torras-Llort, M. *et al.* A fraction of barrier-to-autointegration factor (BAF) associates with centromeres and controls mitosis progression. *Commun. Biol.* **3**, 454 (2020).
68. Haraguchi, T. *et al.* Live cell imaging and electron microscopy reveal dynamic processes of BAF-directed nuclear envelope assembly. *J. Cell Sci.* **121**, 2540–2554 (2008).
69. Janssen, A. *et al.* The BAF A12T mutation disrupts lamin A/C interaction, impairing robust repair of nuclear envelope ruptures in Nestor-Guillermo progeria syndrome cells. *Nucleic Acids Res.* **50**, 9260–9278 (2022).

70. Gillooly, J. F., Brown, J. H., West, G. B., Savage, V. M. & Charnov, E. L. Effects of size and temperature on metabolic rate. *Science* **293**, 2248–2251 (2001).
71. Van Voorhies, W. A. The influence of metabolic rate on longevity in the nematode *Caenorhabditis elegans*. *Aging Cell* **1**, 91–101 (2002).
72. Barzilai, N., Huffman, D. M., Muzumdar, R. H. & Bartke, A. The critical role of metabolic pathways in aging. *Diabetes* **61**, 1315–1322 (2012).
73. Houtkooper, R. H. *et al.* The metabolic footprint of aging in mice. *Sci. Rep.* **1**, 134 (2011).
74. Pendás, A. M. *et al.* Defective prelamin A processing and muscular and adipocyte alterations in Zmpste24 metalloproteinase-deficient mice. *Nat. Genet.* **31**, 94–99 (2002).
75. Osorio, F. G. *et al.* Splicing-directed therapy in a new mouse model of human accelerated aging. *Sci. Transl. Med.* **3**, 106ra107 (2011).
76. Bárcena, C. *et al.* Methionine Restriction Extends Lifespan in Progeroid Mice and Alters Lipid and Bile Acid Metabolism. *Cell Rep.* **24**, 2392–2403 (2018).
77. López-Otín, C., Galluzzi, L., Freije, J. M. P., Madeo, F. & Kroemer, G. Metabolic Control of Longevity. *Cell* **166**, 802–821 (2016).
78. Osorio, F. G. *et al.* Nuclear lamina defects cause ATM-dependent NF- $\kappa$ B activation and link accelerated aging to a systemic inflammatory response. *Genes Dev.* **26**, 2311–2324 (2012).
79. Franceschi, C., Garagnani, P., Vitale, G., Capri, M. & Salvioli, S. Inflammaging and ‘Garb-aging’. *Trends Endocrinol. Metab. TEM* **28**, 199–212 (2017).
80. Zoncu, R., Efeyan, A. & Sabatini, D. M. mTOR: from growth signal integration to cancer, diabetes and ageing. *Nat. Rev. Mol. Cell Biol.* **12**, 21–35 (2011).
81. Longo, V. D., Di Tano, M., Mattson, M. P. & Guidi, N. Intermittent and periodic fasting, longevity and disease. *Nat. Aging* **1**, 47–59 (2021).
82. Kroemer, G., López-Otín, C., Madeo, F. & de Cabo, R. Carbotoxicity-Noxious Effects of Carbohydrates. *Cell* **175**, 605–614 (2018).
83. Green, C. L., Lamming, D. W. & Fontana, L. Molecular mechanisms of dietary restriction promoting health and longevity. *Nat. Rev. Mol. Cell Biol.* **23**, 56–73 (2022).
84. Mariño, G. *et al.* Insulin-like growth factor 1 treatment extends longevity in a mouse model of human premature aging by restoring somatotroph axis function. *Proc. Natl. Acad. Sci. U. S. A.* **107**, 16268–16273 (2010).

85. Katsyuba, E., Romani, M., Hofer, D. & Auwerx, J. NAD<sup>+</sup> homeostasis in health and disease. *Nat. Metab.* **2**, 9–31 (2020).
86. Amjad, S. *et al.* Role of NAD<sup>+</sup> in regulating cellular and metabolic signaling pathways. *Mol. Metab.* **49**, 101195 (2021).
87. Covarrubias, A. J., Perrone, R., Grozio, A. & Verdin, E. NAD<sup>+</sup> metabolism and its roles in cellular processes during ageing. *Nat. Rev. Mol. Cell Biol.* **22**, 119–141 (2021).
88. Gomes, A. P. *et al.* Declining NAD(+) induces a pseudohypoxic state disrupting nuclear-mitochondrial communication during aging. *Cell* **155**, 1624–1638 (2013).
89. Guarente, L. Linking DNA damage, NAD(+)/SIRT1, and aging. *Cell Metab.* **20**, 706–707 (2014).
90. Rajman, L., Chwalek, K. & Sinclair, D. A. Therapeutic Potential of NAD-Boosting Molecules: The In Vivo Evidence. *Cell Metab.* **27**, 529–547 (2018).
91. Zapata-Pérez, R., Wanders, R. J. A., van Karnebeek, C. D. M. & Houtkooper, R. H. NAD<sup>+</sup> homeostasis in human health and disease. *EMBO Mol. Med.* **13**, e13943 (2021).
92. Bai, P. *et al.* PARP-1 Inhibition Increases Mitochondrial Metabolism through SIRT1 Activation. *Cell Metab.* **13**, 461–468 (2011).
93. Barbosa, M. T. P. *et al.* The enzyme CD38 (a NAD glycohydrolase, EC 3.2.2.5) is necessary for the development of diet-induced obesity. *FASEB J. Off. Publ. Fed. Am. Soc. Exp. Biol.* **21**, 3629–3639 (2007).
94. Camacho-Pereira, J. *et al.* CD38 Dictates Age-Related NAD Decline and Mitochondrial Dysfunction through an SIRT3-Dependent Mechanism. *Cell Metab.* **23**, 1127–1139 (2016).
95. Bordone, L. *et al.* SIRT1 transgenic mice show phenotypes resembling calorie restriction. *Aging Cell* **6**, 759–767 (2007).
96. Satoh, A. *et al.* Sirt1 extends life span and delays aging in mice through the regulation of Nk2 homeobox 1 in the DMH and LH. *Cell Metab.* **18**, 416–430 (2013).
97. Imai, S. & Guarente, L. NAD<sup>+</sup> and sirtuins in aging and disease. *Trends Cell Biol.* **24**, 464–471 (2014).
98. Bonkowski, M. S. & Sinclair, D. A. Slowing ageing by design: the rise of NAD<sup>+</sup> and sirtuin-activating compounds. *Nat. Rev. Mol. Cell Biol.* **17**, 679–690 (2016).

99. Kane, A. E. & Sinclair, D. A. Sirtuins and NAD<sup>+</sup> in the Development and Treatment of Metabolic and Cardiovascular Diseases. *Circ. Res.* **123**, 868–885 (2018).
100. Gulshan, M. *et al.* Overexpression of Nmnat3 efficiently increases NAD and NGD levels and ameliorates age-associated insulin resistance. *Aging Cell* **17**, e12798 (2018).
101. Yoshida, M. *et al.* Extracellular Vesicle-Contained eNAMPT Delays Aging and Extends Lifespan in Mice. *Cell Metab.* **30**, 329–342.e5 (2019).
102. Wang, G. *et al.* P7C3 neuroprotective chemicals function by activating the rate-limiting enzyme in NAD salvage. *Cell* **158**, 1324–1334 (2014).
103. LaFargue, C. J., Dal Molin, G. Z., Sood, A. K. & Coleman, R. L. Exploring and comparing adverse events between PARP inhibitors. *Lancet Oncol.* **20**, e15–e28 (2019).
104. Garten, A. *et al.* Physiological and pathophysiological roles of NAMPT and NAD metabolism. *Nat. Rev. Endocrinol.* **11**, 535–546 (2015).
105. Abdellatif, M. *et al.* Nicotinamide for the treatment of heart failure with preserved ejection fraction. *Sci. Transl. Med.* **13**, eabd7064 (2021).
106. Kiss, T. *et al.* Nicotinamide mononucleotide (NMN) supplementation promotes anti-aging miRNA expression profile in the aorta of aged mice, predicting epigenetic rejuvenation and anti-atherogenic effects. *GeroScience* **41**, 419–439 (2019).
107. de Picciotto, N. E. *et al.* Nicotinamide mononucleotide supplementation reverses vascular dysfunction and oxidative stress with aging in mice. *Aging Cell* **15**, 522–530 (2016).
108. Diguët, N. *et al.* Nicotinamide Riboside Preserves Cardiac Function in a Mouse Model of Dilated Cardiomyopathy. *Circulation* **137**, 2256–2273 (2018).
109. Hou, Y. *et al.* NAD<sup>+</sup> supplementation normalizes key Alzheimer's features and DNA damage responses in a new AD mouse model with introduced DNA repair deficiency. *Proc. Natl. Acad. Sci. U. S. A.* **115**, E1876–E1885 (2018).
110. Hou, Y. *et al.* NAD<sup>+</sup> supplementation reduces neuroinflammation and cell senescence in a transgenic mouse model of Alzheimer's disease via cGAS-STING. *Proc. Natl. Acad. Sci. U. S. A.* **118**, e2011226118 (2021).
111. Yoshino, M. *et al.* Nicotinamide mononucleotide increases muscle insulin sensitivity in prediabetic women. *Science* **372**, 1224–1229 (2021).

112. Sun, C. *et al.* Re-equilibration of imbalanced NAD metabolism ameliorates the impact of telomere dysfunction. *EMBO J.* **39**, e103420 (2020).
113. Cantó, C. *et al.* The NAD(+) precursor nicotinamide riboside enhances oxidative metabolism and protects against high-fat diet-induced obesity. *Cell Metab.* **15**, 838–847 (2012).
114. Trammell, S. A. J. *et al.* Nicotinamide riboside is uniquely and orally bioavailable in mice and humans. *Nat. Commun.* **7**, 12948 (2016).
115. Martens, C. R. *et al.* Chronic nicotinamide riboside supplementation is well-tolerated and elevates NAD+ in healthy middle-aged and older adults. *Nat. Commun.* **9**, 1286 (2018).
116. Airhart, S. E. *et al.* An open-label, non-randomized study of the pharmacokinetics of the nutritional supplement nicotinamide riboside (NR) and its effects on blood NAD+ levels in healthy volunteers. *PloS One* **12**, e0186459 (2017).
117. Okabe, K. *et al.* Oral Administration of Nicotinamide Mononucleotide Is Safe and Efficiently Increases Blood Nicotinamide Adenine Dinucleotide Levels in Healthy Subjects. *Front. Nutr.* **9**, 868640 (2022).
118. Fang, E. F. *et al.* NAD+ augmentation restores mitophagy and limits accelerated aging in Werner syndrome. *Nat. Commun.* **10**, 5284 (2019).
119. Scheibye-Knudsen, M. *et al.* A high-fat diet and NAD(+) activate Sirt1 to rescue premature aging in cockayne syndrome. *Cell Metab.* **20**, 840–855 (2014).
120. Amorim, J. A. *et al.* Mitochondrial and metabolic dysfunction in ageing and age-related diseases. *Nat. Rev. Endocrinol.* **18**, 243–258 (2022).
121. Chakrabarty, R. P. & Chandel, N. S. Mitochondria as Signaling Organelles Control Mammalian Stem Cell Fate. *Cell Stem Cell* **28**, 394–408 (2021).
122. Sun, N., Youle, R. J. & Finkel, T. The Mitochondrial Basis of Aging. *Mol. Cell* **61**, 654–666 (2016).
123. Zimmermann, A., Madreiter-Sokolowski, C., Stryeck, S. & Abdellatif, M. Targeting the Mitochondria-Proteostasis Axis to Delay Aging. *Front. Cell Dev. Biol.* **9**, 656201 (2021).
124. Jang, J. Y., Blum, A., Liu, J. & Finkel, T. The role of mitochondria in aging. *J. Clin. Invest.* **128**, 3662–3670 (2018).
125. Trifunovic, A. *et al.* Premature ageing in mice expressing defective mitochondrial DNA polymerase. *Nature* **429**, 417–423 (2004).

126. Yu, T. *et al.* Premature aging is associated with higher levels of 8-oxoguanine and increased DNA damage in the Polg mutator mouse. *Aging Cell* **21**, e13669 (2022).
127. Yang, L. *et al.* Mitochondrial DNA mutation exacerbates female reproductive aging via impairment of the NADH/NAD<sup>+</sup> redox. *Aging Cell* **19**, e13206 (2020).
128. Chen, A. *et al.* Nicotinamide Riboside and Metformin Ameliorate Mitophagy Defect in Induced Pluripotent Stem Cell-Derived Astrocytes With POLG Mutations. *Front. Cell Dev. Biol.* **9**, 737304 (2021).
129. Quirós, P. M., Mottis, A. & Auwerx, J. Mitonuclear communication in homeostasis and stress. *Nat. Rev. Mol. Cell Biol.* **17**, 213–226 (2016).
130. Melber, A. & Haynes, C. M. UPRmt regulation and output: a stress response mediated by mitochondrial-nuclear communication. *Cell Res.* **28**, 281–295 (2018).
131. Markaki, M., Palikaras, K. & Tavernarakis, N. Novel Insights Into the Anti-aging Role of Mitophagy. *Int. Rev. Cell Mol. Biol.* **340**, 169–208 (2018).
132. Onishi, M., Yamano, K., Sato, M., Matsuda, N. & Okamoto, K. Molecular mechanisms and physiological functions of mitophagy. *EMBO J.* **40**, e104705 (2021).
133. Killackey, S. A., Philpott, D. J. & Girardin, S. E. Mitophagy pathways in health and disease. *J. Cell Biol.* **219**, e202004029 (2020).
134. Bravo-San Pedro, J. M., Kroemer, G. & Galluzzi, L. Autophagy and Mitophagy in Cardiovascular Disease. *Circ. Res.* **120**, 1812–1824 (2017).
135. Leduc-Gaudet, J.-P., Hussain, S. N. A., Barreiro, E. & Gousspillou, G. Mitochondrial Dynamics and Mitophagy in Skeletal Muscle Health and Aging. *Int. J. Mol. Sci.* **22**, 8179 (2021).
136. Kerr, J. S. *et al.* Mitophagy and Alzheimer's Disease: Cellular and Molecular Mechanisms. *Trends Neurosci.* **40**, 151–166 (2017).
137. Geng, L., Lam, K. S. L. & Xu, A. The therapeutic potential of FGF21 in metabolic diseases: from bench to clinic. *Nat. Rev. Endocrinol.* **16**, 654–667 (2020).
138. Gimeno, R. E. & Moller, D. E. FGF21-based pharmacotherapy--potential utility for metabolic disorders. *Trends Endocrinol. Metab. TEM* **25**, 303–311 (2014).
139. Kaur, N. *et al.* Multi-organ FGF21-FGFR1 signaling in metabolic health and disease. *Front. Cardiovasc. Med.* **9**, 962561 (2022).

140. Wang, D. *et al.* GDF15: emerging biology and therapeutic applications for obesity and cardiometabolic disease. *Nat. Rev. Endocrinol.* **17**, 592–607 (2021).
141. Johann, K., Kleinert, M. & Klaus, S. The Role of GDF15 as a Myomitokine. *Cells* **10**, 2990 (2021).
142. Baker, B. M. & Haynes, C. M. Mitochondrial protein quality control during biogenesis and aging. *Trends Biochem. Sci.* **36**, 254–261 (2011).
143. Lionaki, E. & Tavernarakis, N. Oxidative stress and mitochondrial protein quality control in aging. *J. Proteomics* **92**, 181–194 (2013).
144. Ngo, J. K. & Davies, K. J. A. Importance of the Lon protease in mitochondrial maintenance and the significance of declining Lon in aging. *Ann. N. Y. Acad. Sci.* **1119**, 78–87 (2007).
145. Ngo, J. K., Pomatto, L. C. D. & Davies, K. J. A. Upregulation of the mitochondrial Lon Protease allows adaptation to acute oxidative stress but dysregulation is associated with chronic stress, disease, and aging. *Redox Biol.* **1**, 258–264 (2013).
146. Quirós, P. M., Bárcena, C. & López-Otín, C. Lon protease: A key enzyme controlling mitochondrial bioenergetics in cancer. *Mol. Cell. Oncol.* **1**, e968505 (2014).
147. Gibellini, L. *et al.* Evidence for mitochondrial Lonp1 expression in the nucleus. *Sci. Rep.* **12**, 10877 (2022).
148. Lu, B. *et al.* The ATP-dependent Lon protease of *Mus musculus* is a DNA-binding protein that is functionally conserved between yeast and mammals. *Gene* **306**, 45–55 (2003).
149. Szczepanowska, K. & Trifunovic, A. Mitochondrial matrix proteases: quality control and beyond. *FEBS J.* (2021) doi:10.1111/febs.15964.
150. Pinti, M. *et al.* Mitochondrial Lon protease at the crossroads of oxidative stress, ageing and cancer. *Cell. Mol. Life Sci. CMLS* **72**, 4807–4824 (2015).
151. Gibellini, L. *et al.* The biology of Lonp1: More than a mitochondrial protease. *Int. Rev. Cell Mol. Biol.* **354**, 1–61 (2020).
152. Venkatesh, S., Lee, J., Singh, K., Lee, I. & Suzuki, C. K. Multitasking in the mitochondrion by the ATP-dependent Lon protease. *Biochim. Biophys. Acta* **1823**, 56–66 (2012).
153. Fukuda, R. *et al.* HIF-1 regulates cytochrome oxidase subunits to optimize efficiency of respiration in hypoxic cells. *Cell* **129**, 111–122 (2007).

154. Quirós, P. M. Determination of Aconitase Activity: A Substrate of the Mitochondrial Lon Protease. *Methods Mol. Biol. Clifton NJ* **1731**, 49–56 (2018).
155. Bota, D. A. & Davies, K. J. A. Lon protease preferentially degrades oxidized mitochondrial aconitase by an ATP-stimulated mechanism. *Nat. Cell Biol.* **4**, 674–680 (2002).
156. Tian, Q. *et al.* Lon peptidase 1 (LONP1)-dependent breakdown of mitochondrial 5-aminolevulinic acid synthase protein by heme in human liver cells. *J. Biol. Chem.* **286**, 26424–26430 (2011).
157. Granot, Z. *et al.* Turnover of mitochondrial steroidogenic acute regulatory (StAR) protein by Lon protease: the unexpected effect of proteasome inhibitors. *Mol. Endocrinol. Baltim. Md* **21**, 2164–2177 (2007).
158. Bahat, A. *et al.* Transcriptional activation of LON Gene by a new form of mitochondrial stress: A role for the nuclear respiratory factor 2 in StAR overload response (SOR). *Mol. Cell. Endocrinol.* **408**, 62–72 (2015).
159. Liu, T. *et al.* DNA and RNA binding by the mitochondrial lon protease is regulated by nucleotide and protein substrate. *J Biol Chem* vol. 279 13902–10 (2004).
160. Yang, Q. *et al.* LONP-1 and ATFS-1 sustain deleterious heteroplasmy by promoting mtDNA replication in dysfunctional mitochondria. *Nat. Cell Biol.* **24**, 181–193 (2022).
161. Matsushima, Y., Goto, Y. & Kaguni, L. S. Mitochondrial Lon protease regulates mitochondrial DNA copy number and transcription by selective degradation of mitochondrial transcription factor A (TFAM). *Proc. Natl. Acad. Sci. U. S. A.* **107**, 18410–18415 (2010).
162. Lu, B. *et al.* Phosphorylation of human TFAM in mitochondria impairs DNA binding and promotes degradation by the AAA+ Lon protease. *Mol. Cell* **49**, 121–132 (2013).
163. Lu, B. Mitochondrial Lon Protease and Cancer. *Adv. Exp. Med. Biol.* **1038**, 173–182 (2017).
164. Quirós, P. M. *et al.* ATP-dependent Lon protease controls tumor bioenergetics by reprogramming mitochondrial activity. *Cell Rep.* **8**, 542–556 (2014).
165. Quirós, P. M. *et al.* ATP-dependent Lon protease controls tumor bioenergetics by reprogramming mitochondrial activity. *Cell Rep.* **8**, 542–556 (2014).

166. Quirós, P. M. *et al.* ATP-dependent Lon protease controls tumor bioenergetics by reprogramming mitochondrial activity. *Cell Rep.* **8**, 542–556 (2014).
167. Liu, P., Jenkins, N. A. & Copeland, N. G. A highly efficient recombineering-based method for generating conditional knockout mutations. *Genome Res.* **13**, 476–484 (2003).
168. Osorio, F. G. *et al.* Splicing-directed therapy in a new mouse model of human accelerated aging. *Sci. Transl. Med.* **3**, 106ra107 (2011).
169. Tsay, J. *et al.* Bone loss caused by iron overload in a murine model: importance of oxidative stress. *Blood* **116**, 2582–2589 (2010).
170. Parfitt, A. M. Bone histomorphometry: standardization of nomenclature, symbols and units. Summary of proposed system. *Bone Miner.* **4**, 1–5 (1988).
171. Fraile, J. M., Campos-Iglesias, D., Rodríguez, F., Español, Y. & Freije, J. M. P. The deubiquitinase USP54 is overexpressed in colorectal cancer stem cells and promotes intestinal tumorigenesis. *Oncotarget* **7**, 74427–74434 (2016).
172. Folgueras, A. R., Freitas-Rodríguez, S., Español, Y. & Velasco, G. Cancer Susceptibility Models in Protease-Deficient Mice. *Methods Mol. Biol. Clifton NJ* **1731**, 235–245 (2018).
173. Lira, V. A. *et al.* Autophagy is required for exercise training-induced skeletal muscle adaptation and improvement of physical performance. *FASEB J. Off. Publ. Fed. Am. Soc. Exp. Biol.* **27**, 4184–4193 (2013).
174. Codina-Martínez, H. *et al.* Autophagy is required for performance adaptive response to resistance training and exercise-induced adult neurogenesis. *Scand. J. Med. Sci. Sports* **30**, 238–253 (2020).
175. Whitehead, J. C. *et al.* A clinical frailty index in aging mice: comparisons with frailty index data in humans. *J. Gerontol. A. Biol. Sci. Med. Sci.* **69**, 621–632 (2014).
176. Dobin, A. *et al.* STAR: ultrafast universal RNA-seq aligner. *Bioinforma. Oxf. Engl.* **29**, 15–21 (2013).
177. Love, M. I., Huber, W. & Anders, S. Moderated estimation of fold change and dispersion for RNA-seq data with DESeq2. *Genome Biol.* **15**, 550 (2014).
178. Korotkevich, G. *et al.* Fast gene set enrichment analysis. 060012 Preprint at <https://doi.org/10.1101/060012> (2021).

179. Cabanillas, R. *et al.* Néstor-Guillermo progeria syndrome: a novel premature aging condition with early onset and chronic development caused by BANF1 mutations. *Am. J. Med. Genet. A.* **155A**, 2617–2625 (2011).
180. Puente, X. S. *et al.* Exome sequencing and functional analysis identifies BANF1 mutation as the cause of a hereditary progeroid syndrome. *Am. J. Hum. Genet.* **88**, 650–656 (2011).
181. Furukawa, K. *et al.* Barrier-to-autointegration factor plays crucial roles in cell cycle progression and nuclear organization in *Drosophila*. *J. Cell Sci.* **116**, 3811–3823 (2003).
182. Segura-Totten, M. & Wilson, K. L. BAF: roles in chromatin, nuclear structure and retrovirus integration. *Trends Cell Biol.* **14**, 261–266 (2004).
183. Bolderson, E. *et al.* Barrier-to-autointegration factor 1 (Banf1) regulates poly [ADP-ribose] polymerase 1 (PARP1) activity following oxidative DNA damage. *Nat. Commun.* **10**, 5501 (2019).
184. Robin, J. D. & Magdinier, F. Physiological and Pathological Aging Affects Chromatin Dynamics, Structure and Function at the Nuclear Edge. *Front. Genet.* **7**, 153 (2016).
185. Martins, F., Sousa, J., Pereira, C. D., da Cruz E Silva, O. A. B. & Rebelo, S. Nuclear envelope dysfunction and its contribution to the aging process. *Aging Cell* **19**, e13143 (2020).
186. Lombard, D. B. *et al.* Mutations in the WRN gene in mice accelerate mortality in a p53-null background. *Mol. Cell. Biol.* **20**, 3286–3291 (2000).
187. Chang, S. *et al.* Essential role of limiting telomeres in the pathogenesis of Werner syndrome. *Nat. Genet.* **36**, 877–882 (2004).
188. Hockemeyer, D., Palm, W., Wang, R. C., Couto, S. S. & de Lange, T. Engineered telomere degradation models dyskeratosis congenita. *Genes Dev.* **22**, 1773–1785 (2008).
189. Murga, M. *et al.* A mouse model of ATR-Seckel shows embryonic replicative stress and accelerated aging. *Nat. Genet.* **41**, 891–898 (2009).
190. Villa-Bellosta, R. *et al.* Defective extracellular pyrophosphate metabolism promotes vascular calcification in a mouse model of Hutchinson-Gilford progeria syndrome that is ameliorated on pyrophosphate treatment. *Circulation* **127**, 2442–2451 (2013).

191. Lee, S.-J. *et al.* Interruption of progerin-lamin A/C binding ameliorates Hutchinson-Gilford progeria syndrome phenotype. *J. Clin. Invest.* **126**, 3879–3893 (2016).
192. Hamczyk, M. R. *et al.* Vascular Smooth Muscle-Specific Progerin Expression Accelerates Atherosclerosis and Death in a Mouse Model of Hutchinson-Gilford Progeria Syndrome. *Circulation* **138**, 266–282 (2018).
193. Ovadya, Y. *et al.* Impaired immune surveillance accelerates accumulation of senescent cells and aging. *Nat. Commun.* **9**, 5435 (2018).
194. Hamczyk, M. R. *et al.* Progerin accelerates atherosclerosis by inducing endoplasmic reticulum stress in vascular smooth muscle cells. *EMBO Mol. Med.* **11**, e9736 (2019).
195. Loi, M. *et al.* Barrier-to-Autointegration Factor (BAF) involvement in prelamin A-related chromatin organization changes. *Oncotarget* **7**, 15662–15677 (2016).
196. Osorio, F. G. *et al.* Nuclear lamina defects cause ATM-dependent NF- $\kappa$ B activation and link accelerated aging to a systemic inflammatory response. *Genes Dev.* **26**, 2311–2324 (2012).
197. Bárcena, C. *et al.* Methionine Restriction Extends Lifespan in Progeroid Mice and Alters Lipid and Bile Acid Metabolism. *Cell Rep.* **24**, 2392–2403 (2018).
198. Gao, Y. & Ge, W. The histone methyltransferase DOT1L inhibits osteoclastogenesis and protects against osteoporosis. *Cell Death Dis.* **9**, 33 (2018).
199. Rauch, F. & Glorieux, F. H. Osteogenesis imperfecta. *Lancet Lond. Engl.* **363**, 1377–1385 (2004).
200. Tournis, S. & Dede, A. D. Osteogenesis imperfecta - A clinical update. *Metabolism.* **80**, 27–37 (2018).
201. Van Dijk, F. S. & Sillence, D. O. Osteogenesis imperfecta: clinical diagnosis, nomenclature and severity assessment. *Am. J. Med. Genet. A.* **164A**, 1470–1481 (2014).
202. Moffatt, P., Boraschi-Diaz, I., Marulanda, J., Bardai, G. & Rauch, F. Calvaria Bone Transcriptome in Mouse Models of Osteogenesis Imperfecta. *Int. J. Mol. Sci.* **22**, 5290 (2021).
203. Gomes, A. P. *et al.* Declining NAD(+) induces a pseudohypoxic state disrupting nuclear-mitochondrial communication during aging. *Cell* **155**, 1624–1638 (2013).

204. Guarente, L. Linking DNA damage, NAD(+)/SIRT1, and aging. *Cell Metab.* **20**, 706–707 (2014).
205. Rajman, L., Chwalek, K. & Sinclair, D. A. Therapeutic Potential of NAD-Boosting Molecules: The In Vivo Evidence. *Cell Metab.* **27**, 529–547 (2018).
206. Zapata-Pérez, R., Wanders, R. J. A., van Karnebeek, C. D. M. & Houtkooper, R. H. NAD<sup>+</sup> homeostasis in human health and disease. *EMBO Mol. Med.* **13**, e13943 (2021).
207. Trammell, S. A. J. *et al.* Nicotinamide riboside is uniquely and orally bioavailable in mice and humans. *Nat. Commun.* **7**, 12948 (2016).
208. Martens, C. R. *et al.* Chronic nicotinamide riboside supplementation is well-tolerated and elevates NAD<sup>+</sup> in healthy middle-aged and older adults. *Nat. Commun.* **9**, 1286 (2018).
209. Airhart, S. E. *et al.* An open-label, non-randomized study of the pharmacokinetics of the nutritional supplement nicotinamide riboside (NR) and its effects on blood NAD<sup>+</sup> levels in healthy volunteers. *PLoS One* **12**, e0186459 (2017).
210. Okabe, K. *et al.* Oral Administration of Nicotinamide Mononucleotide Is Safe and Efficiently Increases Blood Nicotinamide Adenine Dinucleotide Levels in Healthy Subjects. *Front. Nutr.* **9**, 868640 (2022).
211. Morais, P. *et al.* Restrictive dermopathy--a lethal congenital laminopathy. Case report and review of the literature. *Eur. J. Pediatr.* **168**, 1007–1012 (2009).
212. Osorio, F. G., Obaya, A. J., López-Otín, C. & Freije, J. M. P. Accelerated ageing: from mechanism to therapy through animal models. *Transgenic Res.* **18**, 7–15 (2009).
213. Pendás, A. M. *et al.* Defective prelamin A processing and muscular and adipocyte alterations in Zmpste24 metalloproteinase-deficient mice. *Nat. Genet.* **31**, 94–99 (2002).
214. Bárcena, C. *et al.* Methionine Restriction Extends Lifespan in Progeroid Mice and Alters Lipid and Bile Acid Metabolism. *Cell Rep.* **24**, 2392–2403 (2018).
215. Bárcena, C. *et al.* Healthspan and lifespan extension by fecal microbiota transplantation into progeroid mice. *Nat. Med.* **25**, 1234–1242 (2019).
216. Wu, B. *et al.* Metabonomic study on ageing: NMR-based investigation into rat urinary metabolites and the effect of the total flavone of Epimedium. *Mol. Biosyst.* **4**, 855–861 (2008).

217. Garratt, M., Stockley, P., Armstrong, S. D., Beynon, R. J. & Hurst, J. L. The scent of senescence: sexual signalling and female preference in house mice. *J. Evol. Biol.* **24**, 2398–2409 (2011).
218. Chowdhury, A. R. *et al.* Mitochondria-targeted paraquat and metformin mediate ROS production to induce multiple pathways of retrograde signaling: A dose-dependent phenomenon. *Redox Biol.* **36**, 101606 (2020).
219. Liao, P.-C., Wolken, D. M. A., Serrano, E., Srivastava, P. & Pon, L. A. Mitochondria-Associated Degradation Pathway (MAD) Function beyond the Outer Membrane. *Cell Rep.* **32**, 107902 (2020).
220. Harland, M., Torres, S., Liu, J. & Wang, X. Neuronal Mitochondria Modulation of LPS-Induced Neuroinflammation. *J. Neurosci. Off. J. Soc. Neurosci.* **40**, 1756–1765 (2020).
221. Pintado, C., Macías, S., Domínguez-Martín, H., Castaño, A. & Ruano, D. Neuroinflammation alters cellular proteostasis by producing endoplasmic reticulum stress, autophagy activation and disrupting ERAD activation. *Sci. Rep.* **7**, 8100 (2017).
222. Cocetta, V., Ragazzi, E. & Montopoli, M. Mitochondrial Involvement in Cisplatin Resistance. *Int. J. Mol. Sci.* **20**, E3384 (2019).
223. Zhang, Y. & Maurizi, M. R. Mitochondrial ClpP activity is required for cisplatin resistance in human cells. *Biochim. Biophys. Acta* **1862**, 252–264 (2016).
224. Fang, H.-Y. *et al.* Overexpression of optic atrophy 1 protein increases cisplatin resistance via inactivation of caspase-dependent apoptosis in lung adenocarcinoma cells. *Hum. Pathol.* **43**, 105–114 (2012).
225. Dong, T. *et al.* Opa1 Prevents Apoptosis and Cisplatin-Induced Ototoxicity in Murine Cochleae. *Front. Cell Dev. Biol.* **9**, 744838 (2021).
226. Zhang, W.-W. *et al.* Steroidogenic acute regulatory protein/aldosterone synthase mediates angiotensin II-induced cardiac fibrosis and hypertrophy. *Mol. Biol. Rep.* **47**, 1207–1222 (2020).
227. Quiros, P. M., Goyal, A., Jha, P. & Auwerx, J. Analysis of mtDNA/nDNA Ratio in Mice. *Curr. Protoc. Mouse Biol.* **7**, 47–54 (2017).
228. Madeo, F., Carmona-Gutierrez, D., Hofer, S. J. & Kroemer, G. Caloric Restriction Mimetics against Age-Associated Disease: Targets, Mechanisms, and Therapeutic Potential. *Cell Metab.* **29**, 592–610 (2019).

229. Gordon, L. B., Rothman, F. G., López-Otín, C. & Misteli, T. Progeria: a paradigm for translational medicine. *Cell* **156**, 400–407 (2014).
230. Koboldt, D. C., Steinberg, K. M., Larson, D. E., Wilson, R. K. & Mardis, E. R. The next-generation sequencing revolution and its impact on genomics. *Cell* **155**, 27–38 (2013).
231. Vera, E., Bernardes de Jesus, B., Foronda, M., Flores, J. M. & Blasco, M. A. The rate of increase of short telomeres predicts longevity in mammals. *Cell Rep.* **2**, 732–737 (2012).
232. Hockemeyer, D., Palm, W., Wang, R. C., Couto, S. S. & de Lange, T. Engineered telomere degradation models dyskeratosis congenita. *Genes Dev.* **22**, 1773–1785 (2008).
233. Chang, S. *et al.* Essential role of limiting telomeres in the pathogenesis of Werner syndrome. *Nat. Genet.* **36**, 877–882 (2004).
234. Almeida, M. *et al.* Estrogens and Androgens in Skeletal Physiology and Pathophysiology. *Physiol. Rev.* **97**, 135–187 (2017).
235. Khosla, S. & Monroe, D. G. Regulation of Bone Metabolism by Sex Steroids. *Cold Spring Harb. Perspect. Med.* **8**, a031211 (2018).
236. Moffatt, P., Boraschi-Diaz, I., Marulanda, J., Bardai, G. & Rauch, F. Calvaria Bone Transcriptome in Mouse Models of Osteogenesis Imperfecta. *Int. J. Mol. Sci.* **22**, 5290 (2021).
237. Burla, R. *et al.* Interplay of the nuclear envelope with chromatin in physiology and pathology. *Nucl. Austin Tex* **11**, 205–218 (2020).
238. Sears, R. M. & Roux, K. J. Diverse cellular functions of barrier-to-autointegration factor and its roles in disease. *J. Cell Sci.* **133**, jcs246546 (2020).
239. Fang, E. F. *et al.* NAD<sup>+</sup> in Aging: Molecular Mechanisms and Translational Implications. *Trends Mol. Med.* **23**, 899–916 (2017).
240. Ji, L. L. & Yeo, D. Maintenance of NAD<sup>+</sup> Homeostasis in Skeletal Muscle during Aging and Exercise. *Cells* **11**, 710 (2022).
241. White, A. T. & Schenk, S. NAD(+)/NADH and skeletal muscle mitochondrial adaptations to exercise. *Am. J. Physiol. Endocrinol. Metab.* **303**, E308-321 (2012).
242. Fang, E. F. *et al.* NAD<sup>+</sup> augmentation restores mitophagy and limits accelerated aging in Werner syndrome. *Nat. Commun.* **10**, 5284 (2019).

243. Fang, E. F. *et al.* NAD<sup>+</sup> Replenishment Improves Lifespan and Healthspan in Ataxia Telangiectasia Models via Mitophagy and DNA Repair. *Cell Metab.* **24**, 566–581 (2016).
244. Okur, M. N. *et al.* Cockayne syndrome proteins CSA and CSB maintain mitochondrial homeostasis through NAD<sup>+</sup> signaling. *Aging Cell* **19**, e13268 (2020).
245. Verdin, E. NAD<sup>+</sup> in aging, metabolism, and neurodegeneration. *Science* **350**, 1208–1213 (2015).
246. Hwang, E. S. & Song, S. B. Possible Adverse Effects of High-Dose Nicotinamide: Mechanisms and Safety Assessment. *Biomolecules* **10**, E687 (2020).
247. Poljšak, B., Kovač, V. & Milisav, I. Current Uncertainties and Future Challenges Regarding NAD<sup>+</sup> Boosting Strategies. *Antioxid. Basel Switz.* **11**, 1637 (2022).
248. Cercillieux, A., Ciarlo, E. & Canto, C. Balancing NAD<sup>+</sup> deficits with nicotinamide riboside: therapeutic possibilities and limitations. *Cell. Mol. Life Sci. CMLS* **79**, 463 (2022).
249. Kauppila, T. E. S., Kauppila, J. H. K. & Larsson, N.-G. Mammalian Mitochondria and Aging: An Update. *Cell Metab.* **25**, 57–71 (2017).
250. Vernier, M. & Giguère, V. Aging, senescence and mitochondria: the PGC-1/ERR axis. *J. Mol. Endocrinol.* **66**, R1–R14 (2021).
251. López-Lluch, G., Hernández-Camacho, J. D., Fernández-Ayala, D. J. M. & Navas, P. Mitochondrial dysfunction in metabolism and ageing: shared mechanisms and outcomes? *Biogerontology* **19**, 461–480 (2018).
252. Liu, T. *et al.* DNA and RNA binding by the mitochondrial Ion protease is regulated by nucleotide and protein substrate. *J. Biol. Chem.* **279**, 13902–13910 (2004).
253. Gan, Z., Fu, T., Kelly, D. P. & Vega, R. B. Skeletal muscle mitochondrial remodeling in exercise and diseases. *Cell Res.* **28**, 969–980 (2018).
254. Hood, D. A., Memme, J. M., Oliveira, A. N. & Triolo, M. Maintenance of Skeletal Muscle Mitochondria in Health, Exercise, and Aging. *Annu. Rev. Physiol.* **81**, 19–41 (2019).
255. Memme, J. M., Erlich, A. T., Phukan, G. & Hood, D. A. Exercise and mitochondrial health. *J. Physiol.* **599**, 803–817 (2021).
256. Johnson, M. L., Robinson, M. M. & Nair, K. S. Skeletal muscle aging and the mitochondrion. *Trends Endocrinol. Metab. TEM* **24**, 247–256 (2013).

257. Coen, P. M., Musci, R. V., Hinkley, J. M. & Miller, B. F. Mitochondria as a Target for Mitigating Sarcopenia. *Front. Physiol.* **9**, 1883 (2018).
258. Wiedmer, P. *et al.* Sarcopenia - Molecular mechanisms and open questions. *Ageing Res. Rev.* **65**, 101200 (2021).





# **APPENDIX: PUBLICATIONS**



## List of publications related to the Thesis

### Journal publications:

- Bárcena C, Valdés-Mas R, **Mayoral P**, Garabaya C, Durand S, Rodríguez F, Fernández-García MT, Salazar N, Nogacka AM, Garatachea N, Bossut N, Aprahamian F, Lucia A, Kroemer G, Freije JMP, Quirós PM, López-Otín C. (2019). *Healthspan and lifespan extension by fecal microbiota transplantation into progeroid mice*. Nat Med. 25(8):1234-1242
- Bárcena C, **Mayoral P**, Quirós PM (2018). *Mitohormesis, an Antiaging Paradigm*. Int Rev Cell Mol Biol. 340:35-77
- Bárcena C, Quirós PM, Durand S, **Mayoral P**, Rodríguez F, Caravia XM, Mariño G, Garabaya C, Fernández-García MT, Kroemer G, Freije JMP, López-Otín C. (2018). *Methionine Restriction Extends Lifespan in Progeroid Mice and Alters Lipid and Bile Acid Metabolism*. Cell Rep. 24(9):2392-2403
- Quesada V, Freitas-Rodríguez S, Miller J, Pérez-Silva JG, Jiang ZF, Tapia W, Santiago-Fernández O, Campos-Iglesias D, Kuderna LFK, Quinzin M, Álvarez MG, Carrero D, Beheregaray LB, Gibbs JP, Chiari Y, Glaberman S, Ciofi C, Araujo-Voces M, **Mayoral P**, Arango JR, Tamargo-Gómez I, Roiz-Valle D, Pascual-Torner M, Evans BR, Edwards DL, Garrick RC, Russello MA, Poulakakis N, Gaughran SJ, Rueda DO, Bretones G, Marquès-Bonet T, White KP, Caccone A, López-Otín C. (2018) *Giant tortoise genomes provide insights into longevity and age-related disease*. Nat Ecol Evol. 3(1):87-95

**Chapters in books:**

- **Mayoral P**, Bárcena C & López-Otín C (2018). *Progeria mouse models. Conn's Handbook of Models for Human Aging 2nd Edition*. Elsevier. Editors: Jeffrey Ram P. Michael Conn.
- Bárcena C, **Mayoral P**, Quirós PM, López-Otín C (2017). *Physiological and Pathological Functions of Mitochondrial Proteases. Proteases in Physiology and Pathology*. Springer. Editors: Sajal Chakraborti, Naranjan S. Dhalla

**Congresses:**

- **Mayoral P**, Bárcena C, Quirós PM, Rodríguez F, Maeso D, Freije JMP and López-Otín C. A mouse model for the Néstor-Guillermo Progeria Syndrome phenocopies bone alterations associated with aging. Molecular, Cellular and Organismal Drivers of Aging. CNIO - "La Caixa" Foundation Frontiers Meeting. Madrid (Spain), 9-10 May 2022. Poster.
- Campos-Iglesias D, Álvarez MG, Pérez-Silva JM, Freitas-Rodríguez S, Santiago-Fernández O, Bretones G, Carrero D, **Mayoral P**, Arango JR, Araujo-Voces M, Roiz-Valle D, Quesada V, Caccone A, López-Otín C. *Genomic analysis suggests that moderate IGF signaling can be involved in the longevity of giant tortoises*. 45<sup>th</sup> FEBS Congress. Ljubljana (Slovenia), 3-8 July 2021. Poster
- **Mayoral P**. III Young Researchers Meeting. CIBERONC (Centro de Investigación Biomédica en Red), Online, 14-15 December 2020.
- **Mayoral P**. XVII ASEICA International Congress. Online, 4-6 November 2020.
- Bárcena C, Quirós PM, **Mayoral P**, Durand S, Rodríguez F, Caravia XM, Mariño G, Garabaya C, Kroemer G, Freije JMP and López-Otín C. *Methionine restriction extends lifespan in a mouse model of premature aging by modulating*

*bile acid signaling*. Keystone Symposia: Aging and Mechanisms of Aging Related Disease. Yokohama (Japan), 15 May 2017. Poster and oral communication

- Bárcena C, de la Rosa J, **Mayoral P**, Cadiñanos J, Freije JMP and López-Otín C. *Cancer susceptibility in premature aging*. XV Aseica International Congress. Sevilla (Spain), 21 October 2015. Poster.



# Healthspan and lifespan extension by fecal microbiota transplantation into progeroid mice

Clea Bárcena<sup>1</sup>, Rafael Valdés-Mas<sup>1</sup>, Pablo Mayoral<sup>1</sup>, Cecilia Garabaya<sup>1</sup>, Sylvère Durand<sup>2,3,4,5</sup>, Francisco Rodríguez<sup>1</sup>, María Teresa Fernández-García<sup>6</sup>, Nuria Salazar<sup>7,8</sup>, Alicja M. Nogacka<sup>7,8</sup>, Nuria Garatachea<sup>9,10</sup>, Noélie Bossut<sup>2,3,4,5</sup>, Fanny Aprahamian<sup>2,3,4,5</sup>, Alejandro Lucia<sup>11,12</sup>, Guido Kroemer<sup>13,14,15,16</sup>, José M. P. Freije<sup>13,16</sup>, Pedro M. Quirós<sup>13,16\*</sup> and Carlos López-Otín<sup>13,16\*</sup>

**The gut microbiome is emerging as a key regulator of several metabolic, immune and neuroendocrine pathways<sup>1,2</sup>. Gut microbiome deregulation has been implicated in major conditions such as obesity, type 2 diabetes, cardiovascular disease, non-alcoholic fatty acid liver disease and cancer<sup>3–6</sup>, but its precise role in aging remains to be elucidated. Here, we find that two different mouse models of progeria are characterized by intestinal dysbiosis with alterations that include an increase in the abundance of Proteobacteria and Cyanobacteria, and a decrease in the abundance of Verrucomicrobia. Consistent with these findings, we found that human progeria patients also display intestinal dysbiosis and that long-lived humans (that is, centenarians) exhibit a substantial increase in Verrucomicrobia and a reduction in Proteobacteria. Fecal microbiota transplantation from wild-type mice enhanced healthspan and lifespan in both progeroid mouse models, and transplantation with the verrucomicrobia *Akkermansia muciniphila* was sufficient to exert beneficial effects. Moreover, metabolomic analysis of ileal content points to the restoration of secondary bile acids as a possible mechanism for the beneficial effects of reestablishing a healthy microbiome. Our results demonstrate that correction of the accelerated aging-associated intestinal dysbiosis is beneficial, suggesting the existence of a link between aging and the gut microbiota that provides a rationale for microbiome-based interventions against age-related diseases.**

Traditionally seen as detrimental, the pathophysiological implications of the microbiota have expanded considerably in recent years. It is now known that the microbiota has essential metabolic and immunological functions that are conserved from worms<sup>7</sup> to humans<sup>1,2</sup>. In mammals, the gut microbiota is involved in food processing, activation of satiety pathways, protection against pathogens and production of metabolites including vitamins, short-chain fatty acids and secondary bile acids<sup>8–10</sup>. The gut microbiota also signals

to distant organs, contributing to the maintenance of host physiology<sup>11</sup>. Intestinal microbiota alterations are associated with major conditions like obesity, type 2 diabetes, cardiovascular disease, non-alcoholic fatty acid liver disease, cancer and the response to antineoplastic therapy<sup>3–6</sup>.

Although some works have explored the microbiome profile of long-lived humans<sup>12,13</sup>, no alterations have been described in accelerated aging syndromes. In this work, we study the gut microbiome of two mouse models of Hutchinson–Gilford progeria syndrome (HGPS), patients with HGPS<sup>14</sup> and Nestor–Guillermo progeria syndrome (NGPS)<sup>15</sup>, as well as human centenarians and their controls. We found intestinal dysbiosis in both mouse models and progeria patients. In turn, the microbiota of centenarians is characterized by the presence of both pathological and health-associated bacterial genera. We show that fecal microbiota transplantation (FMT) from wild-type (WT) donors to progeroid recipients attenuates the accelerated-aging phenotype and increases survival, whereas FMT from progeroid donors to WT recipients induces metabolic alterations. Analysis of centenarians and progeria mouse models points to a beneficial role for the genus *Akkermansia*, as oral gavage of *Akkermansia muciniphila* extends the lifespan of progeroid mice.

To explore the relevance of the microbiome in progeria, we first studied the gut metagenome profile of the *Lmna*<sup>G609G/G609G</sup> mouse model of HGPS<sup>16</sup>, by comparing WT and *Lmna*<sup>G609G/G609G</sup> mice at three different ages: 1 month (WT 1mo and *Lmna*<sup>G609G/G609G</sup> 1mo), 4 months (when *Lmna*<sup>G609G/G609G</sup> mice exhibit a progeroid phenotype; WT 4mo and *Lmna*<sup>G609G/G609G</sup> 4mo) and 22 months (for WT mice only; WT 22mo; Extended Data Fig. 1a). To assess how progeria affects the gut microbial community structure, we studied the alpha- and beta-diversity associated with each genotype and compared the microbial diversity within and between communities. Alpha-diversity was analyzed by calculating the Chao1 (a proxy for community richness) and Shannon's index (a proxy for diversity, taking into account both richness and evenness). We did not observe differences in bacterial

<sup>1</sup>Departamento de Bioquímica y Biología Molecular, Facultad de Medicina, Instituto Universitario de Oncología (IUOPA), Universidad de Oviedo, Oviedo, Spain. <sup>2</sup>Cell Biology and Metabolomics Platforms, Gustave Roussy Cancer Campus, Villejuif, France. <sup>3</sup>Equipe 11 labellisée par la Ligue contre le Cancer, Centre de Recherche des Cordeliers, Paris, France. <sup>4</sup>INSERM, U1138, Paris, France. <sup>5</sup>Université Paris Descartes, Sorbonne Paris Cité, Paris, France. <sup>6</sup>Unidad de histopatología molecular, IUOPA, Universidad de Oviedo, Oviedo, Spain. <sup>7</sup>Department of Microbiology and Biochemistry of Dairy Products, Instituto de Productos Lácteos de Asturias, Consejo Superior de Investigaciones Científicas (IPLA-CSIC), Villaviciosa, Spain. <sup>8</sup>Diet, Microbiota and Health Group, Instituto de Investigación Sanitaria del Principado de Asturias (ISPA), Oviedo, Spain. <sup>9</sup>Faculty of Health and Sport Sciences, Department of Psychiatry and Nursing, University of Zaragoza, Huesca, Spain. <sup>10</sup>GENUD (Growth, Exercise, NUtrition and Development) Research Group, University of Zaragoza, Zaragoza, Spain. <sup>11</sup>Faculty of Sport Science, Universidad Europea de Madrid, Madrid, Spain. <sup>12</sup>Instituto de Investigación Hospital 12 de Octubre (i+12) y Centro de Investigación Biomédica en Red de Fragilidad y Envejecimiento Saludable (CIBERFES), Madrid, Spain. <sup>13</sup>Université Pierre et Marie Curie, Paris, France. <sup>14</sup>Pôle de Biologie, Hôpital Européen Georges Pompidou, AP-HP, Paris, France. <sup>15</sup>Karolinska Institute, Department of Women's and Children's Health, Karolinska University Hospital, Stockholm, Sweden. <sup>16</sup>Centro de Investigación Biomédica en Red de Cáncer (CIBERONC), Madrid, Spain.

\*e-mail: [pmquiros@gmail.com](mailto:pmquiros@gmail.com); [clo@uniovi.es](mailto:clo@uniovi.es)



# Giant tortoise genomes provide insights into longevity and age-related disease

Víctor Quesada <sup>1,19</sup>, Sandra Freitas-Rodríguez<sup>1,19</sup>, Joshua Miller <sup>2,19</sup>, José G. Pérez-Silva <sup>1,19</sup>, Zi-Feng Jiang<sup>3</sup>, Washington Tapia<sup>4,5</sup>, Olaya Santiago-Fernández<sup>1</sup>, Diana Campos-Iglesias<sup>1</sup>, Lukas F. K. Kuderna <sup>6,7</sup>, Maud Quinzin<sup>2</sup>, Miguel G. Álvarez<sup>1</sup>, Dido Carrero<sup>1</sup>, Luciano B. Beheregaray<sup>8</sup>, James P. Gibbs<sup>9</sup>, Ylenia Chiari <sup>10</sup>, Scott Glaberman <sup>10</sup>, Claudio Ciofi <sup>11</sup>, Miguel Araujo-Voces<sup>1</sup>, Pablo Mayoral<sup>1</sup>, Javier R. Arango<sup>1</sup>, Isaac Tamargo-Gómez<sup>1</sup>, David Roiz-Valle<sup>1</sup>, María Pascual-Torner<sup>1</sup>, Benjamin R. Evans <sup>2</sup>, Danielle L. Edwards<sup>12</sup>, Ryan C. Garrick<sup>13</sup>, Michael A. Russello <sup>14</sup>, Nikos Poulakakis<sup>15,16</sup>, Stephen J. Gaughran<sup>2</sup>, Danny O. Rueda<sup>4</sup>, Gabriel Bretones<sup>1</sup>, Tomàs Marquès-Bonet <sup>6,7,17,18</sup>, Kevin P. White<sup>3</sup>, Adalgisa Caccone <sup>2\*</sup> and Carlos López-Otín <sup>1\*</sup>

**Giant tortoises are among the longest-lived vertebrate animals and, as such, provide an excellent model to study traits like longevity and age-related diseases. However, genomic and molecular evolutionary information on giant tortoises is scarce. Here, we describe a global analysis of the genomes of Lonesome George—the iconic last member of *Chelonoidis abingdonii*—and the Aldabra giant tortoise (*Aldabrachelys gigantea*). Comparison of these genomes with those of related species, using both unsupervised and supervised analyses, led us to detect lineage-specific variants affecting DNA repair genes, inflammatory mediators and genes related to cancer development. Our study also hints at specific evolutionary strategies linked to increased lifespan, and expands our understanding of the genomic determinants of ageing. These new genome sequences also provide important resources to help the efforts for restoration of giant tortoise populations.**

Comparative genomic analyses leverage the mechanisms of natural selection to find genes and biochemical pathways related to complex traits and processes. Multiple works have used these techniques with the genomes of long-lived mammals to shed light on the signalling and metabolic networks that might play a role in regulating age-related conditions<sup>1,2</sup>. Similar studies on unrelated longevous organisms might unveil novel evolutionary strategies and genetic determinants of ageing in different environments. In this regard, giant tortoises constitute one of the few groups of vertebrates with an exceptional longevity: in excess of 100 years according to some estimates.

In this manuscript, we report the genomic sequencing and comparative genomic analysis of two long-lived giant tortoises: Lonesome George—the last representative of *Chelonoidis abingdonii*<sup>3</sup>, endemic to the island of Pinta (Galapagos Islands, Ecuador)—and an individual of *Aldabrachelys gigantea*, endemic to the Aldabra Atoll and the only extant species of giant tortoises in the Indian Ocean<sup>4</sup> (Fig. 1a). Unsupervised and supervised comparative analyses of these genomic sequences add new genetic information on the

evolution of turtles, and provide novel candidate genes that might underlie the extraordinary characteristics of giant tortoises, including their gigantism and longevity.

## Results and discussion

The genome of Lonesome George was sequenced using a combination of Illumina and PacBio platforms (Supplementary Section 1.1). The assembled genome (CheloAbing 1.0) has a genomic size of 2.3 gigabases and contains 10,623 scaffolds with an N50 of 1.27 megabases (Supplementary Section 1.1 and Supplementary Tables 1–3). We also sequenced, with the Illumina platform, the closely related tortoise *A. gigantea* at an average read depth of 28X. These genomic sequences were aligned to CheloAbing 1.0.

TimeTree database estimations (<http://www.timetree.org>) indicate that Galapagos and Aldabra giant tortoises shared a last common ancestor about 40 million years ago, while both diverged from the human lineage more than 300 million years ago (Supplementary Section 1.4). A preliminary analysis of demographic history using the pairwise sequentially Markovian coalescent (PSMC)<sup>5</sup> model

<sup>1</sup>Departamento de Bioquímica y Biología Molecular, Instituto Universitario de Oncología del Principado de Asturias, CIBERONC, Universidad de Oviedo, Oviedo, Spain. <sup>2</sup>Department of Ecology and Evolutionary Biology, Yale University, New Haven, CT, USA. <sup>3</sup>Institute for Genomics and Systems Biology, The University of Chicago, Chicago, IL, USA. <sup>4</sup>Galapagos National Park Directorate, Galapagos Islands, Ecuador. <sup>5</sup>Galapagos Conservancy, Fairfax, VA, USA. <sup>6</sup>Institute of Evolutionary Biology (UPF-CSIC), Barcelona, Spain. <sup>7</sup>CNAG-CRG, Centre for Genomic Regulation, Barcelona Institute of Science and Technology, Barcelona, Spain. <sup>8</sup>College of Science and Engineering, Flinders University, Adelaide, South Australia, Australia. <sup>9</sup>College of Environmental Science and Forestry, State University of New York, Syracuse, NY, USA. <sup>10</sup>Department of Biology, University of South Alabama, Mobile, AL, USA.

<sup>11</sup>Department of Biology, University of Florence, Florence, Italy. <sup>12</sup>School of Natural Sciences, University of California, Merced, CA, USA. <sup>13</sup>Department of Biology, University of Mississippi, Oxford, MS, USA. <sup>14</sup>Department of Biology, The University of British Columbia, Kelowna, British Columbia, Canada.

<sup>15</sup>Department of Biology, School of Sciences and Engineering, University of Crete, Heraklion, Greece. <sup>16</sup>Natural History Museum of Crete, Heraklion, Greece.

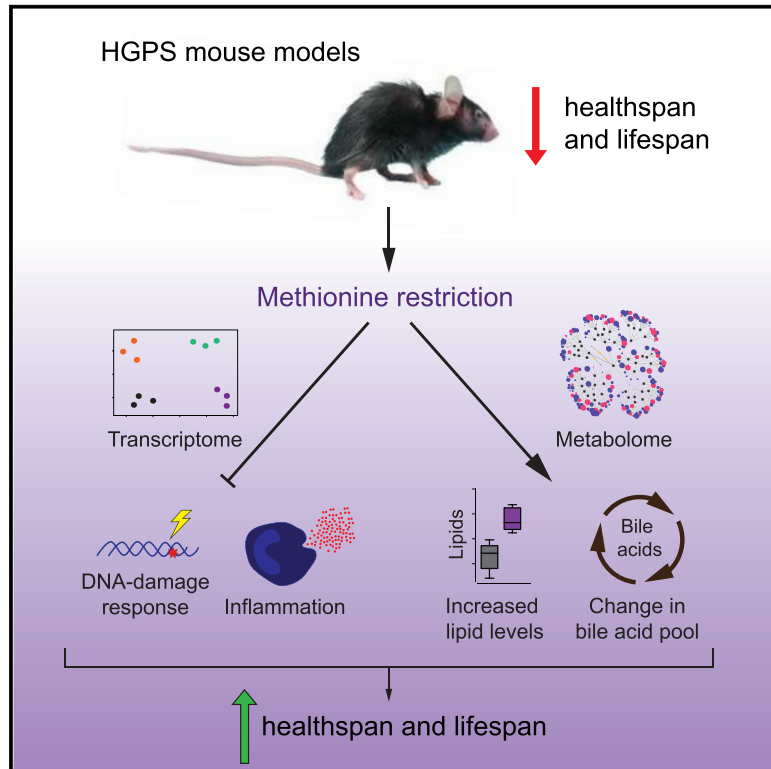
<sup>17</sup>Catalan Institution of Research and Advanced Studies, Barcelona, Spain. <sup>18</sup>Institut Català de Paleontologia Miquel Crusafont, Universitat Autònoma de Barcelona, Barcelona, Spain. <sup>19</sup>These authors contributed equally: Víctor Quesada, Sandra Freitas-Rodríguez, Joshua Miller, José G. Pérez-Silva.

\*e-mail: [adalgisa.caccone@yale.edu](mailto:adalgisa.caccone@yale.edu); [clo@uniovi.es](mailto:clo@uniovi.es)



## Methionine Restriction Extends Lifespan in Progeroid Mice and Alters Lipid and Bile Acid Metabolism

### Graphical Abstract



### Authors

Clea Bárcena, Pedro M. Quirós, Sylvère Durand, ..., Guido Kroemer, José M.P. Freije, Carlos López-Otín

### Correspondence

jmpf@uniovi.es (J.M.P.F.),  
clo@uniovi.es (C.L.-O.)

### In Brief

Barcena et al. demonstrate that methionine restriction (MR) extends health span and lifespan in two mouse models of Hutchinson-Gilford progeria syndrome. MR attenuates transcriptional alterations in inflammation and DNA-damage response pathways and restores metabolomic dysregulation in the lipid and bile acid pool.

### Highlights

- Methionine restriction (MR) extends health span and lifespan in progeroid mice
- MR reverts transcriptional alterations in inflammation and DNA-damage response pathways
- MR modifies the lipid and bile acid pool in *Lmna*<sup>G609G</sup> mutant mice
- Diet enriched in cholic acid enhances health span and lifespan of progeria mice

### Data and Software Availability

GSE117188







# Mitohormesis, an Antiaging Paradigm

Clea Bárcena\*, Pablo Mayoral\* and Pedro M. Quirós\*,<sup>§,1</sup>

\*Departamento de Bioquímica y Biología Molecular, Facultad de Medicina, Instituto Universitario de Oncología (IUOPA), Universidad de Oviedo, 33006-Oviedo, Spain

<sup>§</sup>Centro de Investigación Biomédica en Red de Cáncer (CIBERONC), Spain

<sup>1</sup>Corresponding author: E-mail: pmquiros@gmail.com

## Contents

1. Introduction	2
2. Mitonuclear Communication	3
3. Mitohormesis Signaling	4
3.1 Reactive Oxygen Species	5
3.2 Mitochondrial Ions and Metabolites	6
3.3 Proteotoxic Signals	7
3.4 Mitochondria—Cytosol Stress Responses	10
3.4.1 Translational Stress Response	10
3.4.2 Post-translational Stress Responses	11
3.5 Mitokines	12
4. Mitohormesis and Lifespan	13
5. Mitohormesis and Healthspan	21
6. Concluding Remarks and Future Outlook	27
References	30

## Abstract

Mitohormesis is a term used to define a biological response where the induction of a reduced amount of mitochondrial stress leads to an increment in health and viability within a cell, tissue, or organism. The mitochondrial stress response activated by a potentially damaging stimulus requires a coordinated dialogue with the cellular nucleus, known as mitonuclear communication. This interplay induced by the hormetic response in mitochondria relies in a variety of signals among which the most relevant ones are reactive oxygen species (ROS), mitochondrial metabolites, proteotoxic signals, the mitochondria—cytosol stress response, and the release of mitokines. The activation of the mitohormetic response increases lifespan in different animal models, from worms to mammals. Further, mitohormesis also enhances healthspan, particularly improving metabolism and immune system. Although multiple mediators and stress signals have been proposed to activate this protective mechanism, beneficial outcomes of mitohormesis are most probably due to an increase in mitochondrial ROS.



# Progeria Mouse Models

Pablo Mayoral, Clea Bárcena, Carlos López-Otín

Universidad de Oviedo, Oviedo, Spain

## INTRODUCTION

Aging is a physiological process common to most animal species. During lifetime, our genome and cellular machinery are damaged by several factors such as radiations, spontaneous DNA breaks and mutations, replication and transcription errors, pathogens and different kinds of stresses such as reactive oxygen species damage, nutrient deprivation, or inflammation (Lopez-Otin et al., 2013). There are cellular repair systems specifically responsible for restoring the cellular harmony but, eventually, these alterations accumulate driving aging. Traditionally, aging was defined as an unalterable process with no escape for almost every living being. Nowadays, multiple studies are beginning to decipher the molecular basis of aging, thus opening the possibility to develop strategies aimed at delaying the physiological decline or even reverting it in a future.

There is a group of human diseases characterized by an early onset of an aged appearance, named segmental progeroid syndromes. Although luckily uncommon, these syndromes possess several characteristics that resemble physiological aging, conferring their study the potential of providing information about the nature of accelerated aging, and expanding our knowledge of physiological aging (Ramirez et al., 2007). Among them, laminopathies are a group of diseases characterized by mutations in the nuclear lamina genes or those involving lamin maturation. These alterations lead to the deleterious accumulation of certain proteins in the nuclear envelope, inducing changes in nuclear structure and premature aging (Carrero et al., 2016).

Progeria, also called Hutchinson–Gilford progeria syndrome (HGPS), is a rare human disorder that belongs to the group of laminopathies. Children born with HGPS suffer an accelerated aging that causes a dramatic reduction in health and life span, with a short life expectancy of 14 years. This disease recapitulates several aspects of physiological aging such as weight loss, alopecia, bone fragility, and heart disease, which is the most common cause of death in these patients (Merideth et al., 2008).

HGPS syndrome is caused by the accumulation of an aberrant lamin A nuclear protein, called progerin, owing to defects in lamin A processing. Prelamin A maturation begins with the binding of a farnesyl group at the C-terminal CAAX motif. It continues with a first cleavage of AAX residues, which can be exerted by ZMPSTE24 or RCE1, and the subsequent addition of a carboxymethyl group. Finally, ZMPSTE24 cleaves again prelamina A at the RSY-LLG motif, generating a modified C-terminal peptide and the mature lamin A (Cadinanos et al., 2005). If ZMPSTE24 is not present or is not functional, as in *Zmpste24*<sup>-/-</sup> mice, prelamina A cannot undergo the final catalytic processing and accumulates in the nuclear envelope (Pendas et al., 2002). Likewise, mutations in the *LMNA* gene that alter the physiological splicing of exons 10 to 11 generate a -modified prelamina A protein with a deletion in the cleavage domain of the ZMPSTE24 protease. Hence, this aberrant form of prelamina A, named progerin, accumulates causing nuclear assembly defects and eventually leading to a progeroid state (Sinensky et al., 1994) (Fig. 51.1). To further investigate this syndrome, several mouse models have been generated carrying mutations in the *Lmna* gene, including those present in HGPS patients (Tables 51.1 and 51.2). In fact, as the accumulation of progerin is a physiological process also seen in regular aging, these models constitute an extraordinary tool to study the pathways of normal aging (Burtner and Kennedy, 2010; Scaffidi and Misteli, 2006).

It is also remarkable that there are additional disorders that resemble the progeria phenotype due to mutations in *LMNA* different from the ones associated with HGPS (Soria-Valles et al., 2016). In some cases, the cryptic splicing site is activated but in minor intensity. Thus, lower levels of progerin are produced and a milder form of progeria is established, eventually developing atherosclerosis (Hisama et al., 2011). Beside *LMNA* mutations, changes in nuclear envelope genes (Puente et al., 2011) or in genes that participate in DNA repair machinery (Carrero et al., 2016; Navarro et al., 2006) can also trigger premature aging. In this chapter, we discuss the mouse models available for the study of progeria and present a detailed description of their anatomical and molecular characteristics. Also, we briefly portray other murine models that have been generated in the context of progeria-like disorders. Finally, we highlight the main treatment strategies for progeria that have been assayed in the available mouse models for this syndrome.



---

# Physiological and Pathological Functions of Mitochondrial Proteases

# 1

Clea Bárcena, Pablo Mayoral, Pedro M. Quirós,  
and Carlos López-Otín

---

## Abstract

Mitoproteases display an essential role in the preservation of mitochondrial homeostasis under regular and stress conditions. These enzymes perform tightly regulated proteolytic reactions by which they participate in mitochondrial protein trafficking, processing and activation of proteins, protein quality control, regulation of mitochondrial biogenesis, control of mitochondrial dynamics, mitophagy, and apoptosis. In this chapter, we have revised the physiological functions of the intrinsic mitochondrial proteases, analyzing their roles in the different compartments of this organelle and their connection to human pathology, primarily cancer, neurodegenerative disorders, and multisystemic diseases.

---

## Keywords

Mitochondria • Mitoproteases • Mitochondrial dynamics • Cancer • Aging • Neurodegenerative disorders

---

## 1.1 Introduction

Due to their prokaryotic origin, mitochondria possess some structural characteristics that make them remarkably different from other organelles of eukaryotic cells. They have a double membrane with an intermembrane space, being the inner membrane expanded by the formation of numerous foldings named *cristae*. Enclosed among these *cristae*, we can find the mitochondrial matrix, where several copies of mitochondrial DNA genome are contained. Mitochondria play essential biological

---

C. Bárcena • P. Mayoral • P.M. Quirós • C. López-Otín (✉)  
Departamento de Bioquímica y Biología Molecular, Facultad de Medicina, Instituto  
Universitario de Oncología (IUOPA), Universidad de Oviedo, 33006 Oviedo, Spain  
e-mail: [clo@uniovi.es](mailto:clo@uniovi.es)





